

Universität
Rostock



Traditio et Innovatio

Tetracyanidoborates with triply charged rare earth metal cations and their optical properties

Dissertation

zur Erlangung des Grades

doctor rerum naturalium (Dr. rer. nat.)

am Institut für Chemie

der Mathematisch-Naturwissenschaftlichen Fakultät

der Universität Rostock

Rostock, 2015

vorgelegt von

Liisa Hackbarth

geboren am 15.04.1984 in Kirkkonummi (Finnland)

aus Rostock

Gutachter:

1. Gutachter:

Prof. Dr. Martin Köckerling

Institut für Chemie, Universität Rostock

2. Gutachter:

Prof. Dr. Stefan Lochbrunner

Institut für Physik, Universität Rostock

Datum der Einreichung: 29. Mai 2015

Datum der Verteidigung: 24. November 2015

Acknowledgement

I would like to thank Prof. Dr. Martin Köckerling from the Institute of Chemistry at the University of Rostock for offering me an interesting research topic and for the opportunity to work on this dissertation. I would like to thank Dr. Torsten Küppers for the crystal structure of cerium tetracyanidoborate hydrate. The current and former members of the group of Solid State Chemistry (Antje, Arne B., Arne P., Christian, Daniel, Dominik, Elias, Fanni, Jessica, Jonas J., Jonas K. Philipp, Swantje und Tao) I would like to thank for the wise advices and help along with the nice working atmosphere.

I would like to thank the scientific staff of the Institute of Chemistry at the University of Rostock (Dr. Michalik, Dr. Villinger, Frau Berndt, Frau Duncker, Frau Goronzi, Frau Schicht and Frau Weihs) for the analyses and advices for measurements.

I would also like thank Prof. Dr. Stephan Lochbrunner and Dr. Henning Marciniak of the Institute of Physics at the University of Rostock for the opportunity to use their spectrofluorometer, UV-Vis spectrometer and streak camera system and for the luminescence, absorption and luminescence lifetime measurements.

Last, but not least, I would like to thank my family, my dear Björn and his family, and my friends, especially Timo, for proofreading and for supporting me during this time.

Declaration

I hereby declare that this work was written by myself independently without any help from others and that I used only the aids and sources mentioned in this work.

Rostock, 2015

Liisa Hackbarth

Erklärung

Ich versichere hiermit an Eides statt, dass ich die vorliegende Arbeit selbstständig angefertigt und ohne fremde Hilfe verfasst habe, keine außer den von mir angegebenen Hilfsmitteln und Quellen dazu verwendet habe und die den benutzten Werken inhaltlich und wörtlich entnommenen Stellen als solche kenntlich gemacht habe.

Rostock, 2015

Liisa Hackbarth

Abstract

The aim of this thesis is the description of the synthesis and characterization of a new group of tetracyanidoborates: tetracyanidoborates with trivalent rare earth metal cations. Their optical properties in the ultraviolet and visible range are also discussed. Common synthetic routes for tetracyanidoborates are adapted and applied to the preparation of the rare earth tetracyanidoborate hydrates. They are accessible with high yields and high purity through a reaction between the tetracyanidoboronic acid and rare earth hydroxides.

It is shown that the rare earth tetracyanidoborates form isostructural groups, like the $[\text{LRE}(\text{H}_2\text{O})_5][\text{B}(\text{CN})_4]_3 \cdot 0.5 \text{ H}_2\text{O}$, where LRE^{3+} is La, Ce, Pr, Nd, Sm, Eu and Gd, the $[\text{HRE}(\text{H}_2\text{O})_7][\text{B}(\text{CN})_4]_3$ and the $[\text{HRE}(\text{H}_2\text{O})_8][\text{B}(\text{CN})_4]_3 \cdot 3 \text{ H}_2\text{O}$, where HRE^{3+} is Tb, Dy, Ho, Er, Tm, Yb, Lu and Y. Furthermore, the coordination number 9 is noticed to be common among the light rare earth cations, whereas the minor coordination number 8 is prevalent for the heavy rare earth cations in their tetracyanidoborates. This different construction of the coordination spheres between light and heavy rare earth cations leads to different structures depending on the energetic efficiency of the structural arrangement. Generally, the rare earth tetracyanidoborate hydrates are found to crystallize in the monoclinic crystal system. Moreover, other different crystal structures are observed depending on the crystallization temperature and the type of coordinated ligands and co-crystallized solvent molecules.

The tetracyanidoborate hydrates with triply charged rare earth cations are characterized comprehensively by X-ray diffraction, vibrational spectroscopy, NMR-spectroscopy as well as by thermal analysis. Furthermore, the optical properties of some dehydrated rare earth tetracyanidoborates are investigated by UV-spectroscopy and luminescence measurements. The results of the optical measurements indicate that the tetracyanidoborates with rare earth metal cations exhibit rare earth cation specific luminescence properties which are apparently improved by the tetracyanidoborate anion. Therefore, the tetracyanidoborates with trivalent rare earth metal cations could have possible applications in phosphors.

Zusammenfassung

Das Thema dieser Arbeit ist die Synthese und Charakterisierung einer neuen Klasse der Tetracyanidoborate: Tetracyanidoborate mit dreiwertigen Seltenerdmetall-Kationen. Außerdem werden ihre optischen Eigenschaften im ultravioletten und sichtbaren Bereich diskutiert. Die bereits bekannten Synthesewege der Tetracyanidoborate wurden für die Darstellung der hydratisierten Seltenerdmetall-Tetracyanidoborate angepasst und verwendet. Die Seltenerdmetall-Tetracyanidoborate konnten durch eine Reaktion zwischen Tetracyanidoborsäure und Seltenerdmetall-Hydroxiden in guten Ausbeuten und mit hoher Reinheit gewonnen werden.

Die Seltenerdmetall-Tetracyanidoborat-Hydrate bilden isostrukturelle Gruppen, wie $[\text{LRE}(\text{H}_2\text{O})_5][\text{B}(\text{CN})_4]_3 \cdot 0.5 \text{ H}_2\text{O}$ ($\text{LRE}^{3+} = \text{La, Ce, Pr, Nd, Sm, Eu, Gd}$), $[\text{HRE}(\text{H}_2\text{O})_7][\text{B}(\text{CN})_4]_3$ und $[\text{HRE}(\text{H}_2\text{O})_8][\text{B}(\text{CN})_4]_3 \cdot 3 \text{ H}_2\text{O}$ ($\text{HRE}^{3+} = \text{Tb, Dy, Ho, Er, Tm, Yb, Lu, Y}$). Des Weiteren kommt die Koordinationszahl 9 unter den leichten Seltenerdmetall-Kationen häufig vor, während die Koordinationszahl 8 für die schweren Seltenerdmetall-Kationen üblich ist. Dieser unterschiedliche Aufbau der Koordinationssphären zwischen leichten und schweren Seltenerdmetall-Kationen führt zu unterschiedlichen Strukturen. Im Allgemeinen kristallisieren die Seltenerdmetall-Tetracyanidoborat-Hydrate in monoklinen Kristallsystemen. Außerdem wurden, abhängig von der Kristallisationstemperatur und der Anwesenheit anderer Liganden und co-kristallisierter Lösungsmittelmoleküle, auch andere Kristallstrukturen gefunden.

Die Tetracyanidoborate mit dreiwertigen, hydratisierten Seltenerdmetall-Kationen wurden umfassend durch Einkristallstrukturanalysen, Pulverdiffraktometrie, Schwingungsspektroskopie, NMR-Spektroskopie sowie durch thermische Analysen charakterisiert. Außerdem wurden optische Eigenschaften einiger dehydratisierten Seltenerdmetall-Tetracyanidoborate durch UV-Spektroskopie und Lumineszenzmessungen untersucht. Die Ergebnisse der optischen Messungen zeigen, dass die Seltenerdmetall-Tetracyanidoborate typische Lumineszenzeigenschaften der Seltenerdmetall-Kationen aufweisen. Diese Eigenschaften werden durch das Tetracyanidoborat-Anion offenbar verbessert. Deshalb könnten die Tetracyanidoborate mit dreiwertigen Seltenerdmetall-Kationen Anwendung in Leuchtstoffen finden.

Contents

1	Introduction.....	1
1.1	History of the tetracyanidoborat anion	1
1.2	Characterized tetracyanidoborates.....	3
1.3	Rare earth elements and their compounds.....	4
1.4	Properties and applications of rare earth compounds.....	5
2	Goals	8
3	Results and discussion	11
3.1	Syntheses	11
3.2	Single crystal structure analysis	13
3.3	Powder diffraction	30
3.4	Vibrational spectroscopy	36
3.5	Nuclear magnetic resonance spectroscopy	46
3.6	Thermochemical properties	49
3.7	Solubilities	52
3.8	Optical absorption and emission properties.....	53
3.8.1	Preface.....	53
3.8.2	Preparation of the samples: Dehydration	56
3.8.3	Properties of the dehydrated samples.....	57
3.8.4	UV–Vis absorbance measurements.....	58
3.8.5	Excitation with ultraviolet lamp.....	60
3.8.6	Luminescence measurements	64
3.9	Experimental section	74
4	Conclusions.....	76
5	Outlook	79
6	Analytical Methods.....	81
7	Bibliography	84
8	Appendix.....	89
8.1	Hydrogen bonds in tetracyanidoborates with rare earth metal cations.....	89

List of abbreviations

Å	Ångström (1 Ångström = $1.0 \cdot 10^{-10}$ meter)
aq	aqueous
as	asymmetric
BMI	1-butyl-3-methylimidazolium
br.	broad (IR, NMR)
δ	chemical shift
CN	cyanido group
Δ	delta, difference
DMF	dimethylformamide
DMSO	dimethyl sulfoxide
DSC	Differential Scanning Calorimetry
ED	electric dipole
EMI	1-ethyl-3-methylimidazolium
et al.	et alii
H	Enthalpy
h	hour
HRE	heavy rare earth metal cation
HRETCB	heavy rare earth tetracyanidoborate
ICP-OES	inductively coupled plasma optical emission spectrometry
IR	infrared
λ	lambda, wavelength
LMCT	ligand-to-metal charge-transfer
LRE	light rare earth metal cation
LRETCB	light rare earth tetracyanidoborate

M	metal
MA	maleic anhydride
MLCT	metal- to-ligand charge-transfer
MMA	methyl methacrylate
phen	1,10-phenanthroline
QBS	quinine bisulphate
RE	rare earth
REE	rare earth element
RETCB	rare earth tetracyanidoborate
SMM	single molecule magnets
TCB	tetracyanidoborate
THF	tetrahydrofuran
TMS	tetramethylsilane
TTA	α - thenoyltrifluoroacetone
UV	ultraviolet
Vis	visible
ν	wavenumber

1 Introduction

In this thesis the syntheses of new tetracyanidoborates (TCB) with triply charged rare earth metal cations are presented. In addition, the spectroscopic and structural study of these compounds is described and furthermore, the thermal stability and luminescence properties of some of these new salts are discussed. The luminescence properties are also compared with common rare earth based phosphors.

1.1 History of the tetracyanidoborat anion

The history of tetracyanidoborates started already in the 1950s when the first attempts to prepare the $[\text{B}(\text{CN})_4]^-$ anion took place. Back then, G. Wittig and P. Raff tried to synthesize $\text{Li}[\text{B}(\text{CN})_4]$ by reaction of $\text{Li}[\text{BH}_4]$ with HCN , but the reaction led to $\text{Li}[\text{BH}_3(\text{CN})]$ instead.¹ Since then, several cyanidoboron compounds were synthesized. However, the products were in many cases polymeric and the consistency of the products was indefinite.² Nonetheless, the $[\text{B}(\text{CN})_4]^-$ ion was successfully discovered from the solution of BCl_3 in nitrobenzene in the presence of KCN in 1960. With the aid of ^{11}B nuclear magnetic resonance, the formation of $[\text{B}(\text{CN})_4]^-$ through slow ligand exchange in the solution could be observed.³ Furthermore, in 1967 E. Bessler published a successful preparation of stable monomeric cyanidoboron compounds through reactions of various BCl derivatives with monocyanoanions. However, instead of tetracyanidoborates these compounds were only mono- and dicyanidoborates.² Ten years later, in 1977, it was believed that the first crystalline tetracyanidoborate compounds had been finally synthesized by reaction of BCl_3 with AgCN and CuCN , and the new compounds were characterized by IR spectroscopy.⁴ However, these results differ from others published in 2000⁵. It therefore seems plausible that the compounds synthesized in 1977 were isocyanido complexes, $\text{M}[\text{B}(\text{NC})_4]$ ($\text{M} = \text{Ag}, \text{Cu}$).

Meanwhile, tetracyanidoborate related cyanidohydroborates with two and three cyanide groups were synthesized in the 1980s. The reaction of $\text{Na}[\text{BH}_3\text{CN}]$ with HCl in THF gave $(\text{BH}_2\text{CN})_n$, which was also isolated in solid form and identified by IR and ^1H NMR spectroscopy. Furthermore, the lithium dicyanidodihydroborate, $\text{Li}[\text{BH}_2(\text{CN})_2]$, was synthesized from $(\text{BH}_2\text{CN})_n$. In addition, a formation of silver isocyanidohydroborates,

$\text{Ag}[\text{BH}_n(\text{NC})_{4-n}]$, was successful. The silver salts were also transformed into the corresponding sodium salts, which were isolated as triisocyanidohydroborate and diisocyanidodihydroborate. The corresponding cyanidoborates were additionally received by isomerization.⁶

Almost half a century after the first attempts to synthesize the tetracyanidoborate anion, Bernhardt et al.⁵ finally succeeded in the preparation of this very desired anion. They produced the anion (Fig. 1.) in form of the tetrabutylammonium salt, $[\text{Bu}_4\text{N}][\text{B}(\text{CN})_4]$, by the reaction of $[\text{Bu}_4\text{N}][\text{BX}_4]$ ($\text{X} = \text{Br}, \text{Cl}$) in toluene with KCN. The silver tetracyanidoborate was received after metathesis with AgNO_3 , and successively the metathesis reaction with KBr brought the potassium salt. The new tetracyanidoborate anion was comprehensively characterized structurally and spectroscopically and the first X-ray crystal structures of tetracyanidoborates, $\text{M}[\text{B}(\text{CN})_4]$, where $\text{M} = [\text{Bu}_4\text{N}]^+, \text{Ag}^+, \text{K}^+$, were published.⁵ An improved synthetic procedure was found in 2003, which allowed a production of potassium tetracyanidoborate in multigram amounts. The improved method was a molten flux reaction of KBF_4 with LiCl and KCN, where LiCl and KCN at a molar ratio of 1:1 form a eutectic mixture, which melts under 300°C .⁷ After this improvement, the chemistry of tetracyanidoborates developed rapidly.⁸

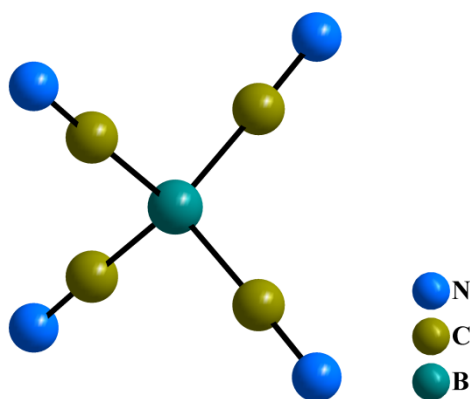


Figure 1. An isolated tetracyanidoborate ion

1.2 Characterized tetracyanidoborates

Besides the potassium compound, tetracyanidoborates with other alkali metal cations have been synthesized and characterized extensively.⁹ The potassium tetracyanidoborate acts as a precursor for other alkali metal tetracyanidoborates, which are available through conversion via the tripropylammonium or the triethylammonium salt. The tetracyanidoborates with the smallest alkali metals, lithium and sodium, form cubic structures, whereas potassium, rubidium and cesium tetracyanidoborate form tetragonal crystals.⁹ A salt metathesis reaction is a further possible synthesis route for different monovalent and divalent tetracyanidoborates from the alkali metal compounds.^{7,10,11} Furthermore, when the discovery of the stable tetracyanidoboronic acid was published in 2007, a new and usable method for preparation of tetracyanidoborates became available.¹² Many tetracyanidoborates with divalent metal cations, and also the first tetracyanidoborate with a triply charged metal cation, have been synthesized this way.^{8, 11, 13-15}

Tetracyanidoborates are very applicable to ionic liquids for the reason that the tetracyanidoborate anion is chemically robust and weakly coordinating.¹⁶ The $[\text{B}(\text{CN})_4]^-$ anion forms ionic liquids with different kinds of organic cations. These liquids have high chemical or electrochemical stability and low viscosity. There are known tetracyanidoborate compounds with sterically demanding phosphonium cations, like $[\text{Ph}_4\text{P}][\text{B}(\text{CN})_4]$, $[\text{nBu}_4\text{P}][\text{B}(\text{CN})_4]$, $[\text{EtPh}_3\text{P}][\text{B}(\text{CN})_4]$ and $[\text{nBuPh}_3\text{P}][\text{B}(\text{CN})_4]$. With exception of the first compound, these salts cannot be considered as ionic liquids, due to their melting points above 100°C.¹⁷ Other known tetracyanidoborates with large organic cations are tetrapropylammonium tetracyanidoborate, $[(\text{C}_3\text{H}_7)_4\text{N}][\text{B}(\text{CN})_4]$ ¹⁸, 1-butyl-3-methylimidazolium (BMI) tetracyanidoborate and 1-ethyl-3-methylimidazolium (EMI) tetracyanidoborate.¹⁹ They usually have melting points below 100°C.

Because of the excellent properties of the $[\text{B}(\text{CN})_4]^-$ anion, there are a lot of applications for the tetracyanidoborates. The suitability of lithium, potassium and sodium salts as battery electrolytes and also the applicability of the $\text{EMI}[\text{B}(\text{CN})_4]$ as solvent for the electrolytes have been investigated.²⁰ $\text{EMI}[\text{B}(\text{CN})_4]$ is also suitable for electrolytes used in dye-sensitized solar cells, because of its low viscosity and high thermal stability.²¹ Furthermore, this tetracyanidoborate is convenient in comparison with other low-viscosity melts of 1-Ethyl-3-methylimidazolium compounds, due to its stability under prolonged thermal stress and light

soaking.²² Moreover, another tetracyanidoborate salt, $[(C_3H_7)_4N][B(CN)_4]$, is used for the modification of membranes in pervaporation membrane separation processes.^{18, 23, 24}

1.3 Rare earth elements and their compounds

The rare earth elements (REEs) include the 15 lanthanides ($Z = 57$ through 71) and the transition metal elements scandium and yttrium ($Z = 21$ and 39). The name “rare earth” derives from the rare earth minerals from which these metals were originally isolated in the 18th and 19th centuries. Actually, most of the REEs are rather abundant in nature. The Earth’s crust even contains more cerium, the most abundant REE, than copper or lead.²⁵ In spite of the very similar physicochemical properties of all REEs, they are traditionally divided into two groups: the light REEs and the heavy REEs. The light REEs are the lanthanide elements with lower atomic numbers and are generally more abundant in the Earth crust’s than the heavy REEs with higher atomic numbers. Even though yttrium has the second lowest atomic number of all REEs, it is generally classified into the heavy REEs because of the chemical and physical similarities. REEs can furthermore be separated into three groups corresponding to their solubility: the insoluble cerium group or “light REEs” (La, Ce, Pr, Nd, Sm); the slightly soluble terbium group or “middle REEs” (Eu, Gd, Tb, Dy); and the soluble ytterbium group or “heavy REEs” (Ho, Er, Tm, Yb, Lu, Y). However, if the separation takes place in aqueous-organic biphasic extraction processes, rare earth ions with different extraction behaviors can presumably be separated into different groups.^{25, 26}

The REEs have been found in soils²⁷, river waters²⁸, seawater²⁹ and even in the deep-sea mud in the Pacific Ocean³⁰. They are never found as pure elements, but in various minerals like phosphorites³¹ and silicates³². Because rare earth metals react very easily with oxygen of the ambient atmosphere, the most stable rare earth compounds are the oxides. Usually, the rare earth ions in oxides have a trivalent state, but in the case of Ce, Pr and Tb, divalent or tetravalent states are also known.³³ Further known rare earth compounds are among others their borides³⁴, halides³⁵, carbonates³⁶, sulfates³⁷, hydrides³⁸ and alloys³⁹.

1.4 Properties and applications of rare earth compounds

The coordination chemistry of rare earth metal cations can be compared with that of the d-type transition metal ions. Formerly, this coordination chemistry was of interest only for separation of rare earth metal cations from each other. Later, the interest in other aspects of coordination chemistry has developed and grown together with a substantial increase in investigative efforts and theoretical interpretations in the area of coordination compounds. The coordination number six is common in some compounds of rare earth metal cations. Nevertheless, there are many evidences that the true coordination number of these cations is larger than six. For example, many rare earth salts contain more than six water molecules per cation. Furthermore, there are complex rare earth species which indicate coordination numbers larger than six. Additionally, rare earth metal cations are most commonly associated with 7–12 nearest donor neighbors in many of their crystal structures.⁴⁰

Most of the REEs have the ground state electron configuration $[\text{Xe}]4f^x6s^2$ ($x = \text{atomic number of REE} - 56$ (atomic number of Xe+2)). Only four of them (La, Ce, Gd and Lu) have the ground state configuration $[\text{Xe}]4f^{x-1}5d^16s^2$. Except for lutetium, all lanthanides are classified as f-block elements. The other REEs, scandium and yttrium, are members of group 3 of the periodic table.⁴¹ For the lanthanide series, a very regular trend has been observed: the ionic radius decreases with the increasing atomic number.^{42,43} This phenomenon is known as the lanthanide contraction and is caused by the addition of electrons to the poorly shielding 4f orbitals which leads to an increase in effective nuclear charge and, respectively, a decrease in ionic radius.⁴⁴

The magnetic, optical and other properties of different REE compounds depend on the 4f electrons of the RE ions. In comparison with other REE applications, the use in permanent magnets is a quite recent implementation. The first RE-cobalt magnets were developed by Strnat around 1970. The development of permanent magnets based on REE-Iron-Boron compounds took place in Japan in 1984 with several precursors and parallel developments in Europe and in the USA. Whereas traditional magnets, like alnico and hexagonal ferrites, are still widely used in the mass production of magnets, most of the high performance permanent magnets are nowadays made from RE-intermetallics.⁴⁵ Other known types of RE-magnets are i.e. hybrid magnets⁴⁶, molecular magnets⁴⁷ and single molecule magnets (SMM)⁴⁸.

Rare earth permanent magnets are desired, because of their high magnetocrystalline anisotropy, i.e. the constancy of magnetization direction against the crystal axes.⁴⁵ Compared with isotropic magnets, the anisotropic magnets have high coercivity and can be used in devices, in which a specific magnetic field orientation is needed. Moreover, hybrid bonded magnets have been developed in order to improve the magnetic properties. REE containing magnets with higher density and decreasing content of organic binder were obtained in the same way.⁴⁶ Furthermore, rare earth coordination complexes can act as single-molecule-magnets as a consequence of their large magnetic anisotropy.⁴⁸

Nowadays many luminescent materials, also called phosphors, are based on rare earth metal cations. These phosphors often improve the devices, in which they are applied. Optical emissions of rare earth ions are usually due to the transitions within the $4f^n$ configuration. Because the f-electrons are well shielded from the chemical environment by the $5s^25p^6$ filled sub-shells, they almost retain their atomic character. The f-f-emission spectrum is therefore composed of sharp lines. Furthermore, f-f-transitions are partially forbidden and many of them are also spin forbidden. For that reason, these transitions are commonly very slow with durations from microseconds to milliseconds.^{49, 50}

All trivalent rare earth ions, except for Sc^{III} , Y^{III} , La^{III} and Lu^{III} are luminescent. Gd^{III} has ultraviolet luminescence (312–315 nm), Pr^{III} , Sm^{III} , Eu^{III} , Tb^{III} , Dy^{III} and Tm^{III} typically exhibit visible luminescence and Nd^{III} , Ho^{III} , Er^{III} and Yb^{III} emit in the near-infrared range. Some of them show fluorescence, others phosphorescence. Laporte-forbidden f-f-transitions, which cause rare earth luminescence, have weak oscillator strengths. They are not able to absorb electromagnetic radiation well. The excited states can be easily quenched by high energy vibrations such as O-H, N-H or C-H oscillators located both in the inner and outer coordination spheres. Therefore, a lanthanide ($\text{Ln}(\text{III})$) ion needs an adequate environment including ligands with suitable chromophoric groups to harvest light and afterwards populate the metal-ion excited states through energy transfer, while simultaneously providing a rigid and protective coordination shell to minimize non-radiative de-activation.⁵⁰ The chromophoric group absorbs the optical energy, which is transferred to a triplet state of the ligand by the intersystem crossing and is after that intramolecularly shifted to the $\text{Ln}(\text{III})$ ion.⁵¹

A ligand adequate for rare earth metal cations in high luminous phosphors should have high molar absorptivity and efficient intersystem crossing from singlet to triplet state. The intramolecular energy transfer from the triplet state of the ligand to the resonance level of the

Ln(III) ion is one of the most important processes influencing luminescence quantum yields of the Ln(III) chelates. The quantum yield is maximized, when the transfer takes place from the lowest triplet state of the ligand directly to the lowest excited level of Ln(III). Nevertheless, the luminescence of rare earth ions can be easily degraded by quenching mechanisms. Inorganic rare earth phosphors with quantum yields close to the unity were described as well as REE based luminescent materials with quantum yields even larger than unity.^{49, 50, 51}

2 Goals

Since 2000, five main methods have been developed for the synthesis of the tetracyanidoborate anion:⁵²

1. The reaction of $[\text{Bu}_4\text{N}][\text{BX}_4]$ ($\text{X} = \text{Br}, \text{Cl}$) with KCN at 120–180°C.⁵²
2. The reaction of $\text{Et}_2\text{O}\cdot\text{BF}_3$ with Me_3SiCN at room temperature under formation of an intermediate, $\text{Me}_3\text{SiNCB}(\text{CN})_3$, and subsequent hydrolysis to $[\text{B}(\text{CN})_4]^-$.⁵³
3. The reaction of $\text{M}[\text{BF}_4]$ ($\text{M} = \text{Li}, \text{K}$) with Me_3SiCN under formation of $[\text{BF}_2(\text{CN})_2]^-$ or $[\text{BF}(\text{CN})_3]^-$ depending on the reaction conditions and subsequent thermal conversion to $[\text{B}(\text{CN})_4]^-$.^{53, 54}
4. The reaction of $\text{BF}_3\cdot\text{OEt}_2$ with KCN in CH_3CN to $[\text{BF}_3\text{CN}]^-$ or $[\text{BF}_2(\text{CN})_2]^-$ depending on the reaction conditions followed by a thermal conversion to $[\text{B}(\text{CN})_4]^-$.⁷
5. A molten flux reaction of KCN with KBF_4 in LiCl at 300°C.⁷

The first method is relatively slow (with a duration of one to three weeks) and it is not always reproducible. In addition, it produces tetrabutylammonium tetracyanidoborate, from which the further tetracyanidoborates can only be converted via the silver salt. The tetracyanidoborates prepared according to the methods 2–4 contain variable amounts of impurities. Furthermore, the yields of these methods are not very satisfying. Contrary to the other methods, method 5 enables the preparation of tetracyanidoborates in large amounts with high purity and proper yields within a day. Therefore, the molten flux reaction of KCN with KBF_4 in LiCl has superior characteristics and is the most promising method for synthesis of tetracyanidoborates.⁵²

The product of the method 5, the potassium tetracyanidoborate, works as a precursor for other alkali metal tetracyanidoborates.⁹ By treating $\text{K}[\text{B}(\text{CN})_4]$ with tri-*n*-propylamine and concentrated hydrochloric acid, tri-*n*-propylammonium tetracyanidoborate can be formed. This ionic liquid reacts with LiOH, NaOH or CsOH and the corresponding alkali metal tetracyanidoborates are received. The synthesis of the fourth alkalimetal tetracyanidoborate, $[\text{Rb}(\text{CN})_4]$, is very similar to the previous synthesis. Hereby, the sodium salt is the precursor instead of the potassium salt and triethylamine is used in place of tri-*n*-propylamine to form a

triethylammonium tetracyanidoborate. This in turn reacts with hydrous RbOH and the reaction leads to the formation of rubidium tetracyanidoborate.⁹

A salt metathesis reaction is another possibility to prepare different tetracyanidoborates from the potassium tetracyanidoborate. For example, a reaction of $\text{K}[\text{B}(\text{CN})_4]$ with CuCl in water leads to the precipitation of $\text{Cu}[\text{B}(\text{CN})_4]$ and KCl solution.⁷ The reaction also occurs between $\text{K}[\text{B}(\text{CN})_4]$ and $\text{Hg}(\text{NO}_3)_2$, whereby a poorly water-soluble $\text{Hg}[\text{B}(\text{CN})_4]_2$ is formed.¹⁰ Along with the mercury compound, further tetracyanidoborates with divalent cations can similarly be prepared through salt metathesis.¹¹ In these reactions it is generally important to find a solvent in which the starting materials are soluble and from which the product precipitates or is otherwise separable.

The third alternative synthesis of tetracyanidoborates is a reaction of a metal oxide, hydroxide or carbonate with the strong tetracyanidoboric acid, $\text{H}[\text{B}(\text{CN})_4]$. The acid is received by treatment of an aqueous solution of alkali metal tetracyanidoborate with an acidic cation exchange resin.¹² Among others, the tetracyanidoborate compounds with divalent copper, zinc, cobalt, magnesium and calcium have been synthesized this way.^{11,13,14,15} Furthermore, the first tetracyanidoborate with a triply charged metal cation, the iron(III) tetracyanidoborate, was prepared by the reaction between metal hydroxide and $\text{H}[\text{B}(\text{CN})_4]$.⁸

The tetracyanidoborate anion has been found to be very stable chemically and thermally.^{5,7} It can be heated in boiling water or in boiling concentrated hydrochloric acid for hours without decomposition. Similarly, in anhydrous HF at 50°C the anion stays mostly undecomposed for about one hour.⁵ The tetracyanidoborates with alkali metal cations are thermally stable up to 500°C, where the anion starts to decompose. The lower decomposition temperatures of the tetracyanidoborates are caused by the decomposition of the countercations, for example organic cations in some ionic liquids.⁹ Compounds with chemically robust anions, like $[\text{B}(\text{CN})_4]^-$, are generally of scientific and economic interest because of their possible applications in ionic liquids, in electrolytes and as stabilizers of unusual cations.

Because of the superior properties of the $[\text{B}(\text{CN})_4]^-$ anion, the tetracyanidoborates have further applications as precursors for other borates. For example, through fluorination of tetracyanidoborate in anhydrous HF solution with an excess of ClF_3 , the chemically rather inert tetrakis(trifluoridomethyl)borate anion, $[\text{B}(\text{CF}_3)_4]^-$, is accessible.⁵⁵ In contrast, related reactions of nitriles with chlorine fluorides most often lead to simple addition reactions to the $\text{R}-\text{C}\equiv\text{N}$ triple bond, resulting in $\text{R}-\text{CF}_2-\text{NCl}_2$ or $\text{R}-\text{CF}_2-\text{NFCl}$ compounds.⁵⁶ Moreover, the

corresponding carboxylate anion, $[\text{B}(\text{CO}_2\text{H})_4]^-$, was for the first time prepared from $[\text{nBu}_4\text{N}][\text{B}(\text{CN})_4]$ by ethylation and subsequent hydrolysis.⁵⁷ The three anions $[\text{B}(\text{CN})_4]^-$, $[\text{B}(\text{CO}_2\text{H})_4]^-$, and $[\text{B}(\text{CF}_3)_4]^-$ with electron-poor ligands coordinated to the boron atom are homoleptic among one another, and they are furthermore promising precursors for other homoleptic boron complexes with four ligands bounded to boron through carbon.

During the preparation of $\text{Cu}[\text{B}(\text{CN})_4]$ it was accidentally found that the tetracyanidoborate anion is unstable in the presence of fluoride in aqueous solution, forming tricyanidofluoridoborate species.⁵⁸ Therefore, the $[\text{B}(\text{CN})_4]^-$ anion can also be regarded as a precursor for the $[\text{BF}(\text{CN})_3]^-$ anion, where the lithium salt is an outstandingly well performing conducting salt for lithium ion batteries.⁵⁹ Another modification for the tetracyanidoborate anion was found in 2011, when the tricyanidoborate anion $[\text{B}(\text{CN})_3]^{2-}$ was obtained by reductive B-C bond fission in $[\text{B}(\text{CN})_4]^-$ by alkaline metals in liquid ammonia at -40°C . This unusual dianion contains nucleophilic boron in the formal oxidation state +1 and has an unexpected high stability, because of the extreme acidity of the underlying, uncharged Lewis acid, $\text{B}(\text{CN})_3$. Furthermore, the salts of the reactive tricyanido dianion are nucleophilic reagents with promising chemistry.⁶⁰

The main goal of this work is the description of the preparation of new tetracyanidoborate hydrates with triply charged rare earth metal cations by applying common synthetic routes for tetracyanidoborates mentioned above. After a successful preparation in high yields and purity, the next step is to characterize the new salts comprehensively by X-ray diffraction, vibrational spectroscopy, NMR-spectroscopy as well as by thermal analysis. Due to the optical properties of rare earth cations, their tetracyanidoborates can also be luminescent. Therefore, they have possible applications in phosphors. Thus, another goal is to investigate the optical properties of some dehydrated rare earth tetracyanidoborates by UV-spectroscopy and luminescence measurements. Furthermore, the suitability of the tetracyanidoborate ion as luminescence intensity improving counterion for rare earth cations is to estimate.

3 Results and discussion

Tetracyanidoborates rise common interest due to their superior chemical and physical properties. Furthermore, these compounds with trivalent rare earth metal cations are even more interesting, because of the exceptional character of the cations. The oxidation number +3 is very common among 4f elements. They form compounds and complexes with high coordination numbers, like 8 or 9. In the rare earth series, the decrease in ionic radii of the cations from 1.216 Å (La^{3+}) to 0.997 Å (Lu^{3+}) causes a break between Gd and Tb compounds accompanied by a reduction of the coordination number from nine to eight. With decreasing ionic radii, the coordination space gets smaller which leads to smaller coordination numbers.^{61,62} This trend is also perceivable in the tetracyanidoborates with rare earth metal cations. They are therefore divided into two groups. The fact that these compounds are among $[\text{Fe}(\text{H}_2\text{O})_6]^{8+}$ one of the firsts tetracyanidoborates with triply charge metal cations, makes them even more desirable.

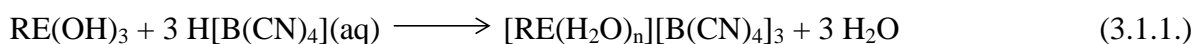
In this section, the tetracyanidoborates with trivalent rare earth metal cations, $[\text{RE}(\text{H}_2\text{O})_x][\text{B}(\text{CN})_4]_3 \cdot y \text{H}_2\text{O}$, ($\text{RE} = \text{La}^{3+}, \text{Ce}^{3+}, \text{Pr}^{3+}, \text{Nd}^{3+}, \text{Sm}^{3+}, \text{Eu}^{3+}, \text{Gd}^{3+}, \text{Tb}^{3+}, \text{Dy}^{3+}, \text{Ho}^{3+}, \text{Er}^{3+}, \text{Tm}^{3+}, \text{Yb}^{3+}, \text{Lu}^{3+}$ and Y^{3+} ; $x = 5, 7, 8$; $y = 0, 0.5, 2, 3$), are described. They were synthesized and characterized for the first time by means of X-ray crystallography, vibrational spectroscopy and nuclear magnetic resonance spectroscopy. Additionally, the thermal stability and solubilities were determined with the ulterior motive to prepare anhydrous compounds. The results of these salts are compared with previously characterized tetracyanidoborates and rare earth compounds.

3.1 Syntheses

The starting material $\text{K}[\text{B}(\text{CN})_4]$ was synthesized as described by E. Bernhardt et al.⁷ utilizing the molten flux reaction of KCN with KBF_4 in LiCl. Some improvements were made for the purification procedures following the reaction according to ref. 63. Some further other improvements were developed to advance the quantity and quality of the product.

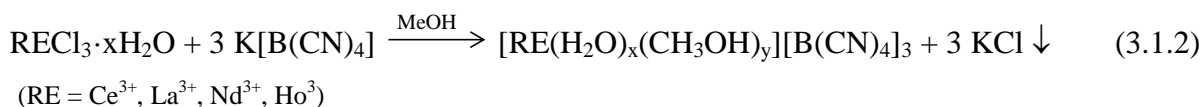
In this study, it was attempted to obtain rare earth tetracyanidoborates through different methods. The first and the best method was the reaction with the strong acid $\text{H}[\text{B}(\text{CN})_4]$

which reacts with metal hydroxides forming the corresponding salt of the metal and water as byproduct. This reaction was carried out with each rare earth compound, whose oxides form in contact to water hydroxides and furthermore react with the strong acid. Only in the case of cerium, praseodymium, holmium and ytterbium salts, the starting materials, $\text{Ce}(\text{OH})_3$, $\text{Pr}(\text{OH})_3$, $\text{Ho}(\text{OH})_3$ and $\text{Yb}(\text{OH})_3$ were precipitated from aqueous solutions of their corresponding metal chlorides with concentrated NH_3 and used directly after precipitation. The reaction with $\text{H}[\text{B}(\text{CN})_4]$ is shown in equation 3.1.1.



($\text{RE} = \text{La}^{3+} - \text{Lu}^{3+}, \text{Y}^{3+}$, except Pm^{3+} ; $n = 5, 7$ or 8 depending on the reaction conditions)

The metathesis reaction between $\text{K}[\text{B}(\text{CN})_4]$ and hydrous rare earth chloride was performed with lanthanum, cerium, neodymium and holmium compounds (equation 3.1.2.) Because of the poor solubility of rare earth chlorides, the reaction was conducted in methanol, where the byproduct potassium chloride is also partly soluble. Furthermore, with the aid of powder X-ray diffraction it was observed that the products contained potassium tetracyanidoborate. This indicates that the metathesis reaction was not complete. Similar results were obtained when the cerium tetracyanidoborate was attempted to be received through an anion-exchange process. Hereby, a solution of CeCl_3 was slowly rinsed through a column filled with $[\text{B}(\text{CN})_4]^-$ anions (equation 3.1.3.). An X-ray diffraction measurement and ICP-OES (inductively coupled plasma optical emission spectrometry) analysis showed that the product contained about 8 wt% potassium cations. This concentration is on the average ten times higher than in the rare earth tetracyanidoborates obtained through the first method. Moreover, the praseodymium, holmium and ytterbium tetracyanidoborates were attempted to be received similarly through the anion-exchange process without better results.



Due to the fact that the metathesis reaction and the ion exchange are improper methods for the preparation of the pure rare earth tetracyanidoborates, the reaction with tetracyanidoboronic

acid has been chosen as the most suitable reaction to form new rare earth salts, $[\text{RE}(\text{H}_2\text{O})_x][\text{B}(\text{CN})_4]_3 \cdot y\text{H}_2\text{O}$ ($x = 5, 7, 8$; $y = 0, 0.5, 2, 3$). The new tetracyanidoborates have been obtained from aqueous solution after evaporating the solvent in high purity.

3.2 Single crystal structure analysis

Suitable crystals for single-crystal X-ray determination are available from aqueous solutions of the cerium (**1**)¹⁶, lanthanum (**2**), gadolinium (**3**), terbium (**4**), dysprosium (**5**), yttrium (**6**), erbium (**7** and **8**) and lutetium (**9**) compounds (Fig. 3.2.1 – 3.2.11). The crystal of the cerium structure (**1**) was grown from aqueous solution and crystallographic characterized by Dr. Küppers. The crystal of the lanthanum structure (**2**) was obtained from aqueous solution, which also contained acetone, acetonitrile and chloroform. Both the crystals of gadolinium compound (**3**) and erbium compound (**8**) were grown from aqueous acetone-chloroform mixture, the crystal of structure **4** from water and the crystals for **5** and **6** from aqueous mixture of acetonitrile and chloroform. The crystal for the erbium structure (**7**) was obtained by MSc. Falk from water solution and the structure **9** was grown from aqueous acetone-acetonitrile-ethanol-chloroform mixture. Different solvents were used to optimize the crystallization time and environment and for the improvement of the crystal quality. The crystals for the structures **2-6**, **8** and **9** were grown at lower temperature than the crystal for the structure **7**. The crystallization occurred by slow evaporation under atmospheric pressure.

Crystallographic data of the cerium (**1**) and the lanthanum (**2**) compound is given in Table 3.2.1.

Table 3.2.1. Crystallographic data of the tetracyanidoborates [Ce(H₂O)₅][B(CN)₄]₃·0.5 H₂O (**1**) and [La(H₂O)₈][B(CN)₄]₃·2 H₂O (**2**).

Compound	1	2
Formula	C ₁₂ H ₁₁ B ₃ CeN ₁₂ O _{5.5}	C ₁₂ H ₂₀ B ₃ LaN ₁₂ O ₁₀
Fw (g mol ⁻¹)	583.84	663.74
<i>T</i> (K)	173	173
Cryst. Syst.	Monoclinic	Monoclinic
Space group	<i>P</i> 2 ₁ / <i>n</i> (no. 14)	<i>P</i> 2 ₁ / <i>c</i> (no. 14)
<i>Z</i>	8	4
<i>a</i> (Å)	15.394(1)	12.5764(2)
<i>b</i> (Å)	10.8138(7)	13.3718(2)
<i>c</i> (Å)	33.341(2)	18.1478(2)
α (°)	90	90
β (°)	103.255(3)	106.151(3)
γ (°)	90	90
<i>V</i> (Å ³)	5402.24(7)	2931.45(6)
$\rho_{\text{calc.}}$ (g cm ⁻³)	1.436	1.504
μ (mm ⁻¹)	1.73	1.52
λ (Å)	0.71073	0.71073
No. of parameters	606	424
GOF on <i>F</i> ²	0.550	1.012
<i>R</i> indices [<i>I</i> > 2σ(<i>I</i>)]	<i>R</i> ₁ = 0.0378	<i>R</i> ₁ = 0.0310
	w <i>R</i> ₂ = 0.0556	w <i>R</i> ₂ = 0.0616
Weighting <i>A/B</i>	0	0.0186/2.2551

Crystals of [Ce(H₂O)₅][B(CN)₄]₃·0.5 H₂O consist of cerium (III) cations, coordinated tetracyanidoborate anions, five coordinated water molecules and half a co-crystallized water molecule per cation. The compound crystallizes in the monoclinic space group *P*2₁/*n* with eight formula units in the primitive cell (Fig. 3.2.1). Each cation is nine-coordinated by five O atoms of water molecules and four N atoms of four different tetracyanidoborate anions in a monocapped square antiprismatic geometry (Fig. 3.2.2). With the Ce-O distances (avg. 2.483 Å) being shorter than Ce-N distances (avg. 2.683), there is a distortion away from the ideal geometry. Bond lengths for [Ce(H₂O)₅][B(CN)₄]₃·0.5 H₂O are given in Table 3.2.2 and bond angles in Table 3.2.3.

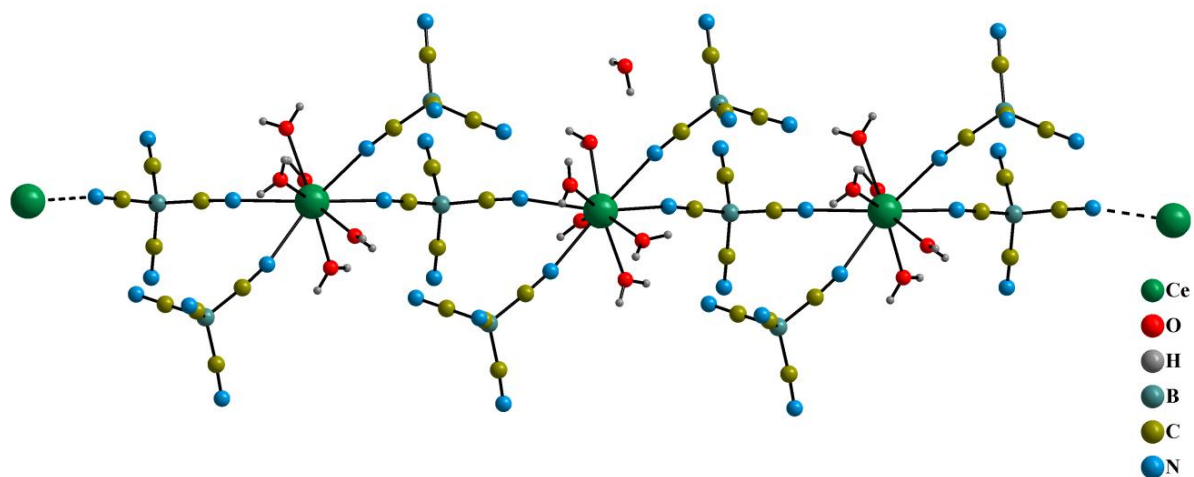


Figure 3.2.1. View of a part of the chain structure of $[\text{Ce}(\text{H}_2\text{O})_5\{\kappa^3\text{N}[\text{B}(\text{CN})_4]\}] \cdot 0.5 \text{H}_2\text{O}$ (**1**).

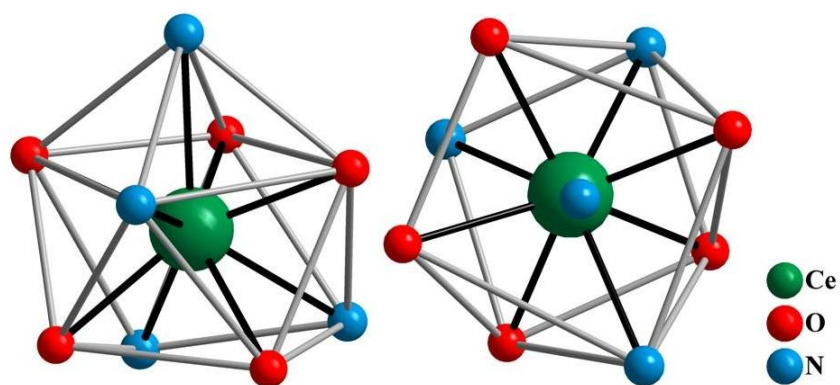


Figure 3.2.2. Side (left) and top (right) view to show the monocapped square antiprismatic coordination environment of Cerium (III) in **1**.

Table 3.2.2. Selected atom distances (Å) within [Ce(H₂O)₅][B(CN)₄]₃·0.5 H₂O (**1**) and [La(H₂O)₈][B(CN)₄]₃·2 H₂O (**2**).

Compound	1	2
Cation:		
RE-O	2.4454(1) – 2.5298(1)	2.5023(2) – 2.5798(2)
Average	2.483	2.537
RE-N _{coord.}	2.6691(2) – 2.7332(2)	2.7424(2)
RE-N _{2.coord.}	2.6288(1) – 2.7017(2)	-
RE-N _{noncoord.}	6.6149(4) – 7.1411(4)	4.1743(4) – 8.7483(1)
Average	4.745	6.435
Anion:		
B-C	1.5759(1) – 1.6104(1)	1.5789(1) – 1.5968(1)
Average	1.591	1.588
C-N _{coord.}	1.1461(1) – 1.1477(1)	1.1361(3)
C-N _{coord.2}	1.1365(1), 1.1402(1)	-
C-N _{noncoord.}	1.1265(1) – 1.1548(1)	1.1287(1) – 1.1381(1)
Average	1.142	1.135

Table 3.2.3. Selected bond angles (°) in [Ce(H₂O)₅][B(CN)₄]₃·0.5 H₂O (**1**) and [La(H₂O)₈][B(CN)₄]₃·2 H₂O (**2**).

Compound	1	2
Cation:		
O-RE-O	71.440(3) – 88.644(3) ^b	66.615(4) – 83.041(3) ^b
O-RE-O	132.566(3) – 147.748(4) ^c	90.532(4) – 140.173(4) ^c
O-RE-N	65.065(3) – 88.253(3) ^{a#1, b}	66.754(4) – 71.737(4) ^b
	97.314(3) – 137.561(5) ^{a#1, c}	110.811(4) – 143.607(5) ^{a#2, c}
N-RE-N	65.808(3) – 67.001(2) ^b	
	126.103(4) – 140.816(3) ^c	
Anion:		
C-B-C	106.516(5) – 111.646(4)	107.066(6) – 112.439(6)
N-C-B	175.481(6) – 179.466(7)	174.930(9) – 179.501(9)

^aSymmetry operations used to generate equivalent atoms: #1: 1+x, -1+y,z; #2: x, 0.5 -y, z + 0.5. ^b Acute angles. ^c Obtuse angles.

Two of the cyanido groups of every third [B(CN)₄]⁻ unit coordinate to two neighbouring Ce³⁺ ions resulting a chain structure in which the tetracyanidoborate anions are bridging the cerium cations. Other [B(CN)₄]⁻ anions are singly coordinated with the cation so that each cation is coordinated by two single coordinated and two twofold coordinated tetracyanidoborate anions. Within the [B(CN)₄]⁻ anion two of the CN groups are bonded to the cerium cation, while the other two are non-coordinating. Consequently, the anion is distorted from an ideal tetrahedron with C-B-C bond angles ranging from 106.516° to 111.646°. This is also

observable in the vibrational spectra where two different C-N absorption frequencies are found. The average C-N and B-C bond distances are comparable to those found in other tetracyanidoborates with singly, divalent or triple charged cations.^{8, 9, 11, 13-15, 17}

The structure of the lanthanum compound (2) (Fig. 3.2.3) contains more water and therefore, the tetracyanidoborate anions do not coordinate with the rare earth metal cation as efficiently as in the cerium structure (Fig. 3.2.1). Crystals of $[\text{La}(\text{H}_2\text{O})_8][\text{B}(\text{CN})_4]_3 \cdot 2 \text{H}_2\text{O}$ consist of lanthanum (III) cations, one third coordinated and two-thirds isolated tetracyanidoborate anions, and also eight coordinated and two co-crystallized water molecules per cation. Each cation is nine-coordinated by eight O atoms of water molecules and one N atom of tetracyanidoborate anion in a tricapped trigonal prismatic geometry (Fig. 3.2.4). It is slightly distorted from ideal tricapped trigonal prism, as it is typical for the UCl_3 type structure.⁶⁴

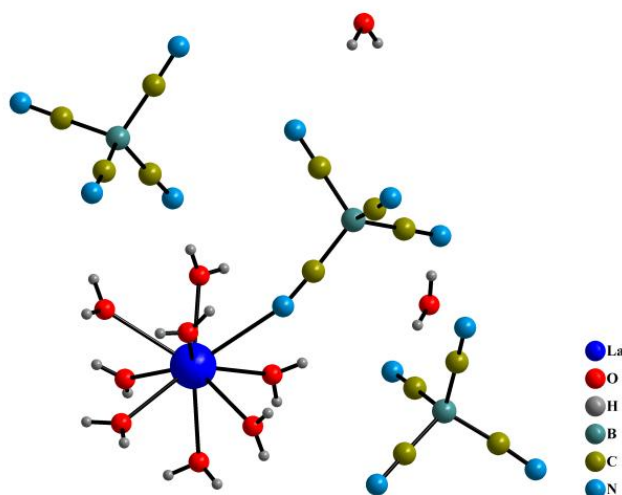


Figure 3.2.3. View of the coordination environment of the La^{3+} ion in $[\text{La}(\text{H}_2\text{O})_8][\text{B}(\text{CN})_4]_3 \cdot 2 \text{H}_2\text{O}$ (2).

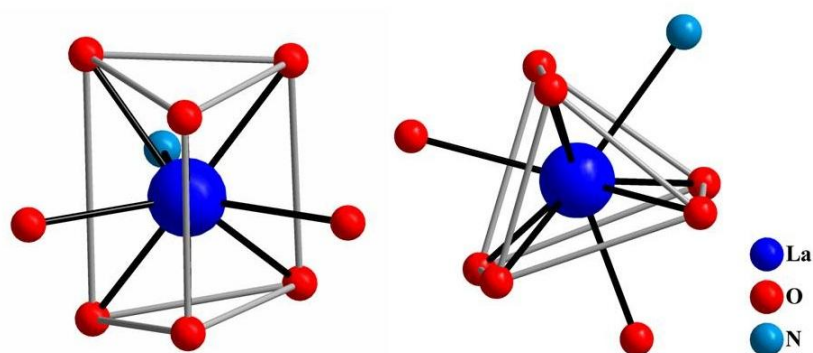


Figure 3.2.4. Side (left) and top (right) view to show the tricapped trigonal prismatic coordination environment of Lanthanum (III) in 2.

In the lanthanum structure (**2**) only one CN group of 12 possible CN groups within three tetracyanidoborate anions coordinates the La^{3+} ion. Due to the coordination of one CN group per La^{3+} ion, the distortion of the tetracyanidoborate anion from an ideal tetrahedron is certainly even larger than of the non-coordinated anions and almost as large as in compound **1** (Table 3.2.3). Hence, the non-coordinated anions are slightly distorted, which indicates considerable interaction between the TCB anions and water molecules (hydrogen bonds presented in the chapter 8.1 in appendix). The average C-N and B-C bond distances (Table 3.2.2) in compound **2** are similar to those in compound **1** and to other tetracyanidoborates.^{8, 9, 11, 13-15, 17}

The isostructural compounds **3-6** contain isolated octa-aqua-rare-earth metal (III) cations, $[\text{RE}(\text{H}_2\text{O})_8]^{3+}$, discrete $[\text{B}(\text{CN})_4]^-$ anions and co-crystallized water molecules with monoclinic symmetry of space group $C2/c$ (Fig. 3.2.5 and 3.2.6). Crystallographic data of the compounds **3-6** are given in Table 3.2.4 and 3.2.5 and bond lengths and bond angles within these compounds in Tables 3.2.6 – 3.2.9.

Table 3.2.4. Crystallographic data of the $[\text{Gd}(\text{H}_2\text{O})_8][\text{B}(\text{CN})_4]_3 \cdot 3 \text{H}_2\text{O}$ (**3**) and $[\text{Tb}(\text{H}_2\text{O})_8][\text{B}(\text{CN})_4]_3 \cdot 3 \text{H}_2\text{O}$ (**4**).

Compound	3	4
Formula	$\text{C}_{12}\text{H}_{22}\text{B}_3\text{GdN}_{12}\text{O}_{11}$	$\text{C}_{12}\text{H}_{22}\text{B}_3\text{TbN}_{12}\text{O}_{11}$
Fw (g mol^{-1})	700.10	701.776
T (K)	173	173
Cryst. Syst.	Monoclinic	Monoclinic
Space group	$C2/c$ (no. 15)	$C2/c$ (no. 15)
Z	8	8
a (Å)	15.9945(1)	15.9786(8)
b (Å)	20.6481(1)	20.5317(8)
c (Å)	21.2210(1)	21.1413(8)
α (°)	90	90
β (°)	112.175(4)	112.226(3)
γ (°)	90	90
V (Å ³)	6489.99(7)	6420.45(5)
$\rho_{\text{calc.}}$ (g cm^{-3})	1.418	1.436
μ (mm^{-1})	2.1	2.26
λ (Å)	0.71073	0.71073
No. of parameters	420	420
GOF on F^2	1.131	0.981
R indices [$I > 2\sigma(I)$]	$R_1 = 0.0290$	$R_1 = 0.0337$
	$wR_2 = 0.0726$	$wR_2 = 0.0762$
Weighting A/B	0.0233/8.2019	0.0263/0

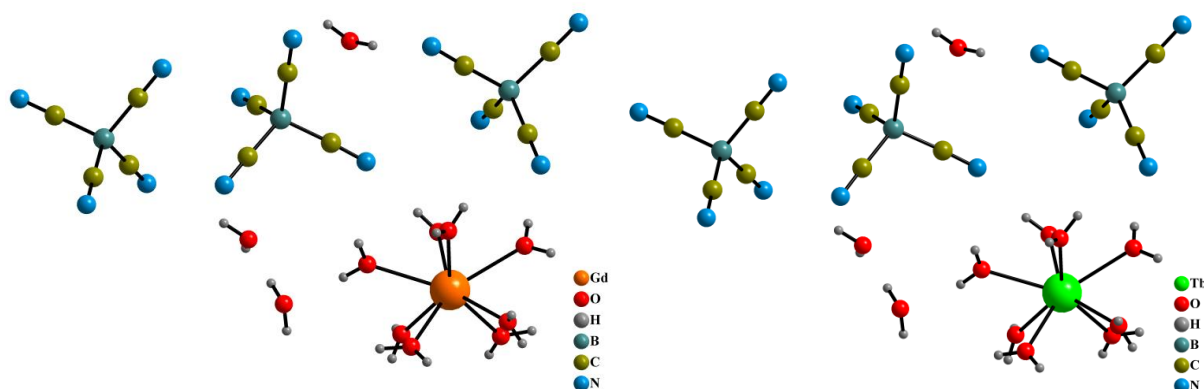


Figure 3.2.5. View of $[\text{RE}(\text{H}_2\text{O})_8]^{3+}$ and $[\text{B}(\text{CN})_4]^-$ ions with co-crystallized water molecules in $[\text{Gd}(\text{H}_2\text{O})_8][\text{B}(\text{CN})_4]_3 \cdot 3\text{H}_2\text{O}$ (**3**) (left) and $[\text{Tb}(\text{H}_2\text{O})_8][\text{B}(\text{CN})_4]_3 \cdot 3\text{H}_2\text{O}$ (**4**) (right).

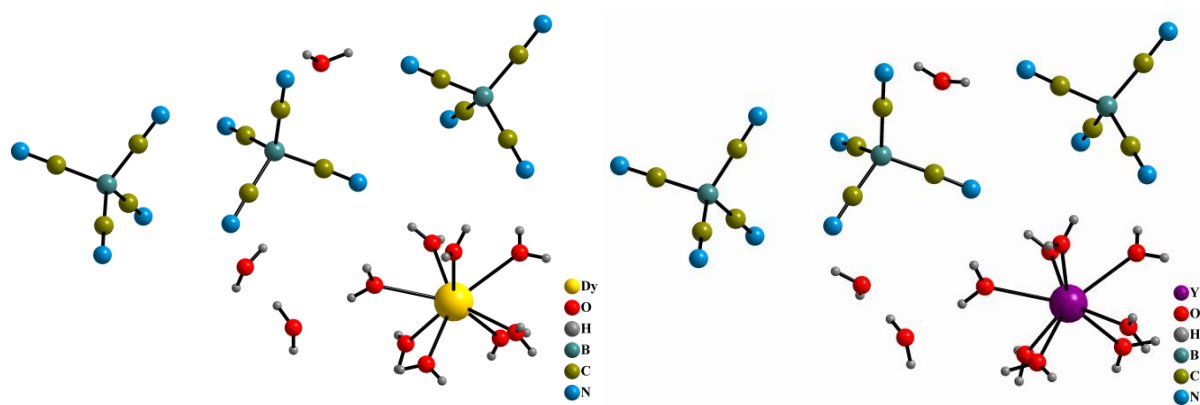


Figure 3.2.6. View of $[\text{RE}(\text{H}_2\text{O})_8]^{3+}$ ion and $[\text{B}(\text{CN})_4]^-$ ions with co-crystallized water molecules in $[\text{Dy}(\text{H}_2\text{O})_8][\text{B}(\text{CN})_4]_3 \cdot 3\text{H}_2\text{O}$ (**5**) (left) and $[\text{Y}(\text{H}_2\text{O})_8][\text{B}(\text{CN})_4]_3 \cdot 3\text{H}_2\text{O}$ (**6**) (right).

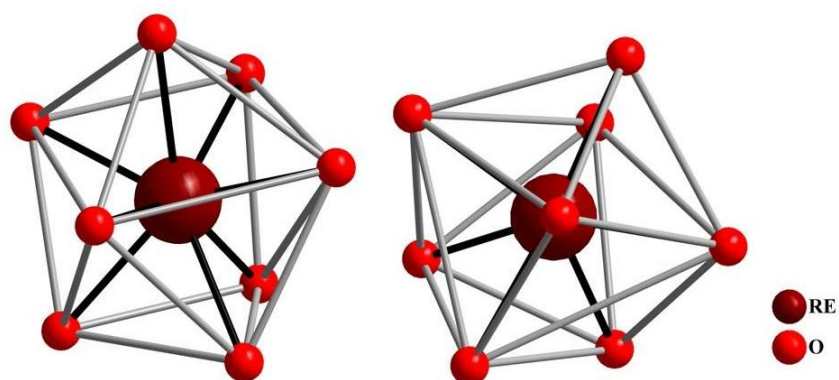


Figure 3.2.7. Side (left) and top (right) view to show the octa-coordinated RE(III) cations in trigonal dodecahedral geometry in compounds **3-6** and **8**.

Table 3.2.5. Crystallographic data of $[\text{Dy}(\text{H}_2\text{O})_8][\text{B}(\text{CN})_4]_3 \cdot 3\text{H}_2\text{O}$ (**5**) and $[\text{Y}(\text{H}_2\text{O})_8][\text{B}(\text{CN})_4]_3 \cdot 3\text{H}_2\text{O}$ (**6**).

Compound	5	6
Formula	$\text{C}_{12}\text{H}_{22}\text{B}_3\text{DyN}_{12}\text{O}_{11}$	$\text{C}_{12}\text{H}_{22}\text{B}_3\text{YN}_{12}\text{O}_{11}$
Fw (g mol^{-1})	705.342	631.756
T (K)	173	173
Cryst. Syst.	Monoclinic	Monoclinic
Space group	$C2/c$ (no. 15)	$C2/c$ (no. 15)
Z	8	8
a (Å)	16.0293(3)	16.0468(7)
b (Å)	20.5472(4)	20.5478(9)
c (Å)	21.1881(4)	21.1799(9)
α (°)	90	90
β (°)	112.234(1)	112.259(2)
γ (°)	90	90
V (Å ³)	6459.58(2)	6463.16(5)
$\rho_{\text{calc.}}$ (g cm^{-3})	1.425	1.273
μ (mm^{-1})	2.37	1.86
λ (Å)	0.71073	0.71073
No. of parameters	420	419
GOF on F^2	1.072	1.015
R indices [$I > 2\sigma(I)$]	$R_1 = 0.0254$	$R_1 = 0.0379$
	$wR_2 = 0.0616$	$wR_2 = 0.0873$
Weighting A/B	0.0225/3.5427	0.0353/1.0334

In the structures of compounds **3–6** eight water molecules are coordinated to the RE^{3+} , whereas all tetracyanidoborate anions exist isolated in the structure, and three co-crystallized water molecules per each RE^{3+} . The non-coordinated, isolated tetracyanidoborate anions usually have ideal tetrahedral C-B-C bond angles about 109.5° . However, the environment around the B atom of the anion is distorted from the ideal tetrahedron in all compounds **3–6** (Tables 3.2.8 and 3.2.9) although direct coordination between the cyanido nitrogen atoms and the rare earth(III) ions is not observed. The distortion in compounds **3–6** is due to the interaction between the cyanido groups and the water molecules. Hydrogen bonds in compounds **3–6** are given in chapter 8.1 in appendix.

Table 3.2.6. Selected atom distances (Å) within and [Gd(H₂O)₈][B(CN)₄]₃ · 3 H₂O (**3**) and [Tb(H₂O)₈][B(CN)₄]₃ · 3 H₂O (**4**).

Compound	3	4
Cation:		
RE-O	2.3546(1) – 2.4311(1)	2.3303(1) – 2.4062(1)
Average	2.386	2.363
RE-N _{noncoord.}	4.5714(2) – 13.2852(5)	4.5476(1) – 13.2261(4)
Average	8.397	8.354
Anion:		
B-C	1.5825(2) – 1.5909(2)	1.5755(1) – 1.5962(1)
Average	1.587	1.585
C-N _{noncoord.}	1.1360(3) – 1.1441(2)	1.1245(1) – 1.1369(1)
Average	1.139	1.131

Table 3.2.7. Selected atom distances (Å) within [Dy(H₂O)₈][B(CN)₄]₃ · 3H₂O (**5**) and [Y(H₂O)₈][B(CN)₄]₃ · 3H₂O (**6**).

Compound	5	6
Cation:		
RE-O	2.3240(0) – 2.4004(0)	2.3093(1) – 2.3910(1)
Average	2.359	2.354
RE-N	4.5352(1) – 13.2585(2)	4.5293(1) – 13.2688(4)
Average	8.368	8.374
Anion:		
B-C	1.5849(0) – 1.5910(0)	1.5812(2) – 1.5935(2)
Average	1.588	1.588
C-N	1.1361(0) – 1.1431(0)	1.1337(2) – 1.1428(2)
Average	1.139	1.137

Table 3.2.8. Selected bond angles (°) in [Gd(H₂O)₈][B(CN)₄]₃ · 3 H₂O (**3**) and [Tb(H₂O)₈][B(CN)₄]₃ · 3 H₂O (**4**).

	3	4
O-RE-O	71.487(2) – 79.842(2) ^{a, b}	71.398(1) – 79.968(1) ^{a, b}
	91.431(2) – 144.593(2) ^{a, c}	92.273(1) – 144.452(2) ^{a, c}
Anion:		
C-B-C	108.077(3) – 110.861(2)	108.027(2) – 111.146(2)
N-C-B	176.568(6) – 179.737(4)	176.372(2) – 179.560(3)

^aSymmetry operation used to generate equivalent atoms: -x,y,0.5-z. ^b Acute angles. ^c Obtuse angles.

Table 3.2.9. Selected bond angles ($^{\circ}$) in $[\text{Dy}(\text{H}_2\text{O})_8][\text{B}(\text{CN})_4]_3 \cdot 3\text{H}_2\text{O}$ (**5**) and $[\text{Y}(\text{H}_2\text{O})_8][\text{B}(\text{CN})_4]_3 \cdot 3\text{H}_2\text{O}$ (**6**).

	5	6
Cation:		
O-RE-O	71.236(1) – 79.873(1) ^{a, b}	71.422(1) – 79.648(1) ^{a, b}
	92.505(1) – 144.589(1) ^{a, c}	92.567(1) – 144.437(2) ^{a, c}
Anion:		
C-B-C	107.988(1) – 111.041(1)	108.211(3) – 110.957(2)
N-C-B	176.570(1) – 179.472(1)	176.480(4) – 179.467(3)

^aSymmetry operation used to generate equivalent atoms: $-x, y, 0.5-z$. ^bAcute angles. ^cObtuse angles.

Crystals of $[\text{Er}(\text{H}_2\text{O})_7][\text{B}(\text{CN})_4]_3$ (**7**) contain erbium (III) cations, which are coordinated trigonal dodecahedrally by seven O atoms of water molecules and one N atom of a tetracyanidoborate anion (Fig. 3.2.8 and 3.2.9). Furthermore, the compound contains two discrete $[\text{B}(\text{CN})_4]^-$ anions per Er^{3+} and has monoclinic symmetry of the space group $P2_1/n$.

Crystallographic data of the erbium compounds are given in Table 3.2.10. Only difference between compounds **3–6** and **8** is the occurrence of co-crystallized solvent molecules (Fig. 3.2.5, 3.2.6 and 3.2.10). Whereas compounds **3–6** contain three co-crystallized water molecules per unit, compound **8** contains only one co-crystallized acetone molecule. As well as in compounds **3–6**, the rare earth metal (III) cations in **8** are coordinated trigonal dodecahedral (Fig. 3.2.7). In compounds **3–8**, the coordination number of the metal cations is eight, which is very typical for the heavy rare earth metal cations.^{40, 65} Furthermore, monoclinic structures are common among other rare earth compounds.^{62, 66} Bond lengths for **7** and **8** are given in Table 3.2.11 and bond angles in Table 3.2.12.

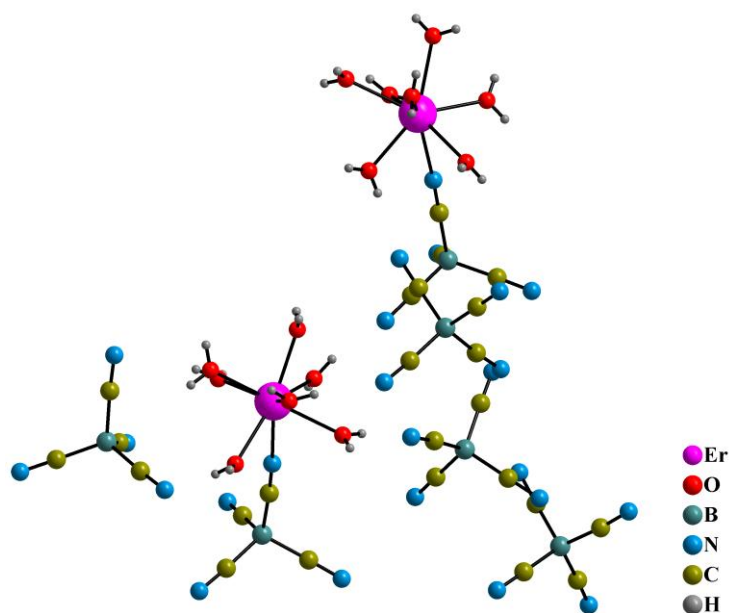


Figure 3.2.8. View of the coordination environment of the Er^{3+} ion in $[\text{Er}(\text{H}_2\text{O})_7][\text{B}(\text{CN})_4]_3$ (**7**).

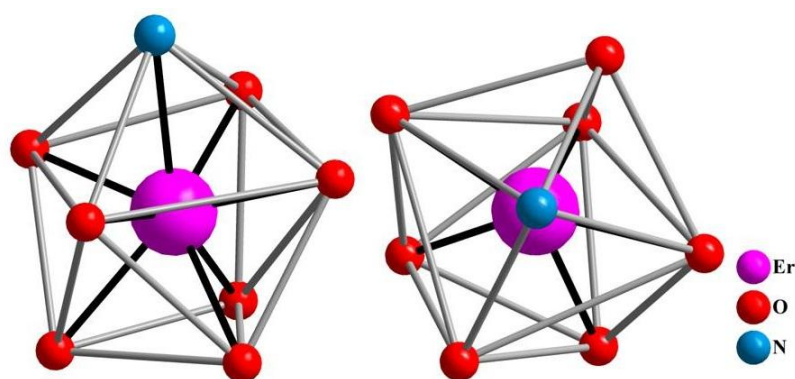


Figure 3.2.9. Side (left) and top (right) view to show the octa-coordinated $\text{Er}(\text{III})$ cations in trigonal dodecahedral geometry in **7**.

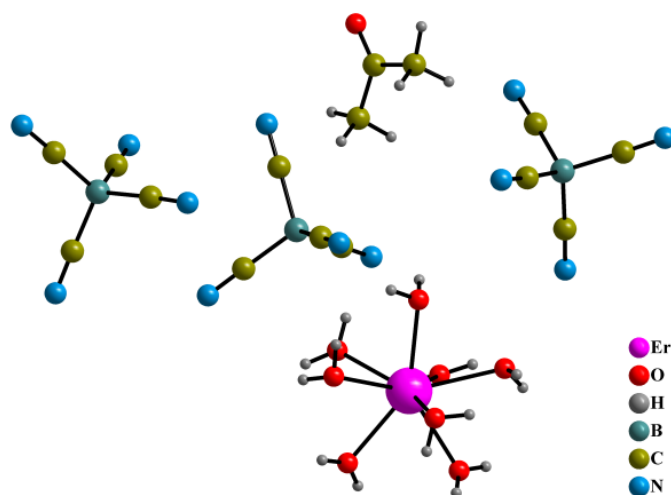


Figure 3.2.10. View of $[\text{Er}(\text{H}_2\text{O})_8]^{3+}$ ion and $[\text{B}(\text{CN})_4]^-$ ions with a co-crystallized acetone molecule in $[\text{Er}(\text{H}_2\text{O})_8][\text{B}(\text{CN})_4]_3 \cdot \text{CH}_3\text{COCH}_3$ (**8**).

Table 3.2.10. Crystallographic data of the tetracyanidoborates [Er(H₂O)₇][B(CN)₄]₃ (**7**) and [Er(H₂O)₈][B(CN)₄]₃·CH₃COCH₃ (**8**)

	7	8
Formula	C ₁₂ H ₁₄ B ₃ ErN ₁₂ O ₇	C ₁₅ H ₂₂ B ₃ ErN ₁₂ O ₉
Fw (g mol ⁻¹)	638.042	714.136
<i>T</i> (K)	173	173
Cryst. Syst.	Monoclinic	Monoclinic
Space group	<i>P</i> 2 ₁ / <i>n</i> (no. 14)	<i>C</i> 2/ <i>c</i> (no. 15)
<i>Z</i>	8	8
<i>a</i> (Å)	13.7705(5)	16.2090(4)
<i>b</i> (Å)	21.2528(7)	20.5676(4)
<i>c</i> (Å)	19.1657(7)	21.2564(4)
α (°)	90	90
β (°)	96.501(2)	112.379(1)
γ (°)	90	90
<i>V</i> (Å ³)	5573.0(3)	6552.75(2)
$\rho_{\text{calc.}}$ (g cm ⁻³)	1.521	1.448
μ (mm ⁻¹)	3.09	2.62
λ (Å)	0.71073	0.71073
No. of parameters	744	363
GOF on <i>F</i> ²	1.049	1.047
<i>R</i> indices [<i>I</i> > 2σ(<i>I</i>)]	<i>R</i> ₁ = 0.0231	<i>R</i> ₁ = 0.0614
	w <i>R</i> ₂ = 0.0718	w <i>R</i> ₂ = 0.1478
Weighting <i>A/B</i>	0.0209/1.6942	0.0705/0

Table 3.2.11. Selected atom distances (Å) within [Er(H₂O)₇][B(CN)₄]₃ (**7**), and [Er(H₂O)₈][B(CN)₄]₃·CH₃COCH₃ (**8**)

	7	8
Cation:		
RE-O	2.2700(1) – 2.3819(1)	2.3092(0) – 2.3822(0)
Average	2.325	2.338
RE-N _{coord.}	2.5062(1) – 2.5283(1)	-
RE-N _{noncoord.}	4.2542(1) – 12.3838(3)	4.5192(1) – 13.3711(2)
Average	4.955	8.426
Anion:		
B-C	1.5796(0) – 1.6034(0)	1.5720(0) – 1.6098(0)
Average	1.591	1.593
C-N _{coord.}	1.1385(0) – 1.1424(0)	-
C-N _{noncoord.}	1.1367(0) – 1.1473(0)	1.1053(0) – 1.1509(0)
Average	1.141	1.1261

Table 3.2.12. Selected bond angles ($^{\circ}$) in $[\text{Er}(\text{H}_2\text{O})_7][\text{B}(\text{CN})_4]_3$ (**7**), and $[\text{Er}(\text{H}_2\text{O})_8][\text{B}(\text{CN})_4]_3 \cdot \text{CH}_3\text{COCH}_3$ (**8**)

	7	8
Cation:		
O-RE-O	69.169(1) – 85.529(1) ^{a #1,b}	71.038(1) – 79.249(1) ^{a #2, b}
	91.981(2) – 148.114(2) ^{a #1,c}	90.029(1) – 145.011(1) ^{a #2, c}
O-RE-N	69.574(2) – 78.043(1)	-
	125.718(2) – 144.278(2)	-
Anion:		
C-B-C	106.544(2) – 112.964(3)	108.296(2) – 111.346(1)
N-C-B	175.214(4) – 179.659(4)	174.868(2) – 179.377(1)

^aSymmetry operations used to generate equivalent atoms: #1: x, y, z; #2: -x, y, 0.5-z. ^b Acute angles. ^c Obtuse angles.

Along with the monoclinic crystal structures, the lutetium compound was found to crystallize in orthorhombic morphology from a solution which contains, besides water, acetone, acetonitrile and ethanol as well. Crystallographic data of the lutetium compound **9** is given in table 3.2.13.

Table 3.2.13. Crystallographic data of $[\text{Lu}(\text{CH}_3\text{CH}_2\text{OH})(\text{H}_2\text{O})_7][\text{B}(\text{CN})_4]_3 \cdot \text{CH}_3\text{CH}_2\text{OH} \cdot 0.5 \text{H}_2\text{O}$ (**9**).

Formula	$\text{C}_{16}\text{H}_{27}\text{B}_3\text{LuN}_{12}\text{O}_{9.5}$
Fw (g mol^{-1})	746.895
<i>T</i> (K)	173
Cryst. Syst.	Orthorhombic
Space group	$P2_12_12_1$ (no. 19)
<i>Z</i>	8
<i>a</i> (Å)	13.2635(3)
<i>b</i> (Å)	19.9227(4)
<i>c</i> (Å)	25.0425(6)
α ($^{\circ}$)	90
β ($^{\circ}$)	90
γ ($^{\circ}$)	90
<i>V</i> (Å ³)	6617.35
$\rho_{\text{calc.}}$ (g cm^{-3})	1.499
μ (mm^{-1})	3.04
λ (Å)	0.71073
No. of parameters	748
GOF on F^2	1.162
<i>R</i> indices [$I > 2\sigma(I)$]	$R_1 = 0.0420$
	$wR_2 = 0.0908$
Weighting <i>A/B</i>	0.0124/21.3788

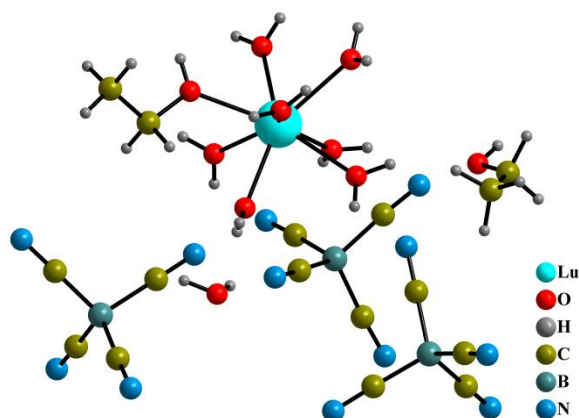


Figure 3.2.11. View of the coordination environment of the Lu^{3+} ion in $[\text{Lu}(\text{CH}_3\text{CH}_2\text{OH})(\text{H}_2\text{O})_7][\text{B}(\text{CN})_4]_3 \cdot \text{CH}_3\text{CH}_2\text{OH}, 0.5 \text{ H}_2\text{O}$ (**9**).

The orthorhombic compound **9** contains isolated hepta-aqua-rare-earth metal (III) cations with a coordinated ethanol molecule, $[\text{B}(\text{CN})_4]^-$ anions and co-crystallized ethanol and water molecules with orthorhombic symmetry of the space group $P2_12_12_1$. With one coordinated ethanol molecule and seven coordinated water molecules (Fig. 3.2.11), the coordination number of the lutetium ion is eight, just like in the coordination number of other rare earth cations in compounds **3–8**. Whereas other eight-coordinated rare earth cations in **3–8** have a trigonal dodecahedral coordination environment, the octa-coordinated lutetium cation is in square antiprismatic geometry in compound **9** (Fig. 3.2.12). Atom distances and bond angles within the lutetium compound are given in Tables 3.2.14 and 3.2.15.

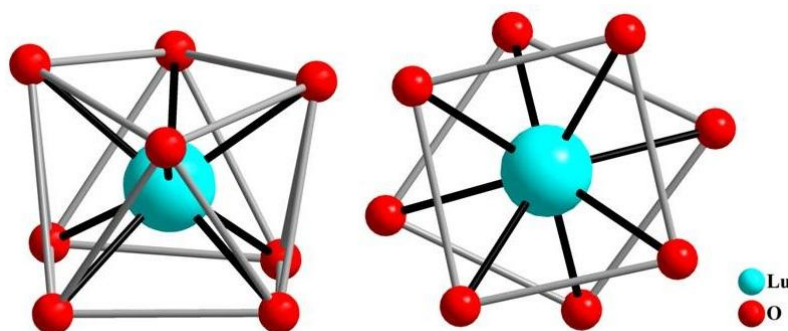


Figure 3.2.12. Side (left) and top (right) view to show the octa-coordinated Lu(III) cations in square antiprismatic geometry in **9**.

Table 3.2.14. Selected atom distances (Å) within **9**.

Cation:	
Lu-O _{H2O}	2.2314(6) – 2.3818(5)
Average	2.307
Lu-O _{EtOH}	2.3385(6), 2.3449(6)
Average	2.342
Lu-N	4.5235(1) – 9.6868(2)
Average	7.296
Anion:	
B-C	1.5557(1) – 1.6268(1)
Average	1.592
C-N	1.1173(1) – 1.1740(1)
Average	1.138

Table 3.2.15. Selected bond angles (°) in **9**.

Cation:	
O-Lu-O	70.881(1) – 86.330(1) ^{a, b}
	99.549(1) – 147.034(1) ^{a, c}
Anion:	
C-B-C	107.243(2) – 111.807(1)
N-C-B	174.646(2) – 179.556(2)

^aSymmetry operation used to generate equivalent atoms: x, y, z. ^b Acute angles. ^c Obtuse angles.

Like in every rare earth tetracyanidoborate analyzed so far, in the compound **9** the environment around the B atom is also distorted. Therefore, the tetracyanidoborate anion is no longer an ideal tetrahedron (C-B-C_{range}: 107.24°–111.81°). The distortion is again due to the remarkable interaction between the cyanido groups and the water molecules (hydrogen bonds in compound **9** are presented in chapter 8.1. in appendix).

The rare earth tetracyanidoborates crystallize in monoclinic crystal system. However, the heaviest rare earth compound also crystallizes with orthorhombic morphology. Similarly, the heavier rare earth bishydroxychlorides have been found to crystallize in the orthorhombic crystal system, as this becomes energetically more favorable.⁶⁷

The RE-O distance seems to get shorter along with the decreasing ionic radii in the rare earth series.^{65, 68, 69} It can be expected from crystallographic evidence that the RE³⁺-H₂O interaction distance is around 2.3–2.4 Å. The distance gets shorter along with decreasing ionic radii in the rare earth tetracyanidoborates (Table. 3.2.16). Due to the lanthanide contraction in the series

of rare earth cations, the ionic radii⁶¹ of the light rare earth cations are greater than the radii of the heavy rare earth cations. The RE³⁺-O distances in the rare earth tetracyanidoborates are similar to the average RE³⁺-O distances observed in aqueous rare earth chloride solutions.⁶⁹ The coordination number of rare earth cations depends also on the ionic radius of the cation. With larger ionic radii, larger coordination numbers are possible. Thus, the coordination number in light rare earth compounds is larger (mostly nine), than in the heavy rare earth tetracyanidoborates, where it is just eight.

With shorter RE³⁺-O distances the interaction between the rare earth cation and water molecules is stronger in the heavy rare earth tetracyanidoborates than in the light rare earth tetracyanidoborates. Therefore, it can be expected that the water molecules are easier to remove from light rare earth compounds than from the heavy ones. This is also observable in the thermal analysis: the dehydration of the light rare earth compound EuTCB occurs at lower temperatures than the dehydration of the heavy rare earth compound ErTCB.

Table 3.2.16. RE³⁺-O distances within compounds **1–9** together with effective ionic radii⁶¹ of RE³⁺.

Compound	RE ³⁺	RE ³⁺ -O distance in Å	Effective ionic radius in Å
2	^{IX} La	2.537	1.216
1	^{IX} Ce	2.483	1.196
3	^{VIII} Gd	2.386	1.053
4	^{VIII} Tb	2.363	1.040
5	^{VIII} Dy	2.359	1.027
6	^{VIII} Y	2.354	1.019
7	^{VIII} Er	2.325	1.004
9	^{VIII} Lu	2.307	0.977

3.3 Powder diffraction

Powder diffraction measurements were performed for each rare earth tetracyanidoborate, RETCB, and the results were compared with the data of single-crystal structures of CeTCB (**1**), LaTCB (**2**), DyTCB (**5**) and ErTCB (**7**). The measurements revealed that light rare earth compounds, LRETCB's, where LRE = La–Gd, except Pm (not investigated), occur in the crystal structure of CeTCB, $[\text{LRE}(\text{H}_2\text{O})_5][\text{B}(\text{CN})_4]_3 \cdot 0.5 \text{H}_2\text{O}$, when investigated in bulk form at room temperature (Figures 3.3.1 and 3.3.2). However, it must be noticed that although it was unsuccessful to measure corresponding powder diffractograms for structure **2**, these findings do not principally exclude the LaTCB structure as another possible structure for all LRETCB compounds. Nonetheless, as the powder diffraction measurements show, the bulk structure for all LRETCB compounds is the CeTCB structure. Therefore, all other characterization measurements for LRETCB's, except the measurements of the dehydrated compounds, were conducted with $[\text{LRE}(\text{H}_2\text{O})_5][\text{B}(\text{CN})_4]_3 \cdot 0.5 \text{H}_2\text{O}$ compounds.

The measurements revealed further that the heavy rare earth tetracyanidoborates, HRETCB's, where HRE = Tb–Lu and Y, occur in the crystal structure of ErTCB, $[\text{HRE}(\text{H}_2\text{O})_7][\text{B}(\text{CN})_4]_3$, when analyzed in bulk form at room temperature (Fig. 3.3.3 and 3.3.4). In addition, the crystal structure of DyTCB, $[\text{HRE}(\text{H}_2\text{O})_8][\text{B}(\text{CN})_4]_3 \cdot 3 \text{H}_2\text{O}$, was also found to occur in all HRETCB compounds, when the samples for the powder diffraction measurement were fine powdered crystals, crystallized at lower temperatures (Fig. 3.3.5 and 3.3.6). Like it is the case for magnesium tetracyanidoborate¹⁵, the crystal structures of HRETCBs seem to depend on the crystallization temperature. The structures, containing more water, occur at lower temperatures. It was also found that the $[\text{HRE}(\text{H}_2\text{O})_8][\text{B}(\text{CN})_4]_3 \cdot 3 \text{H}_2\text{O}$ structure changes to $[\text{HRE}(\text{H}_2\text{O})_7][\text{B}(\text{CN})_4]_3$ when the compound was dried at room temperature. Thus, the common bulk structure for all HRETCB compounds at room temperature is the ErTCB structure (**7**). All other characterization measurements for HRETCB's, except the measurements of dehydrated compounds, were therefore conducted with $[\text{HRE}(\text{H}_2\text{O})_7][\text{B}(\text{CN})_4]_3$ compounds.

The results of the powder diffraction measurements reveal that among rare earth tetracyanidoborate hydrates, there is a division into two isostructural groups dependent on the size of the RE cation. This phenomenon is very typical for many other rare earth compounds. Thus, it can be also expected for the rare earth tetracyanidoborates.

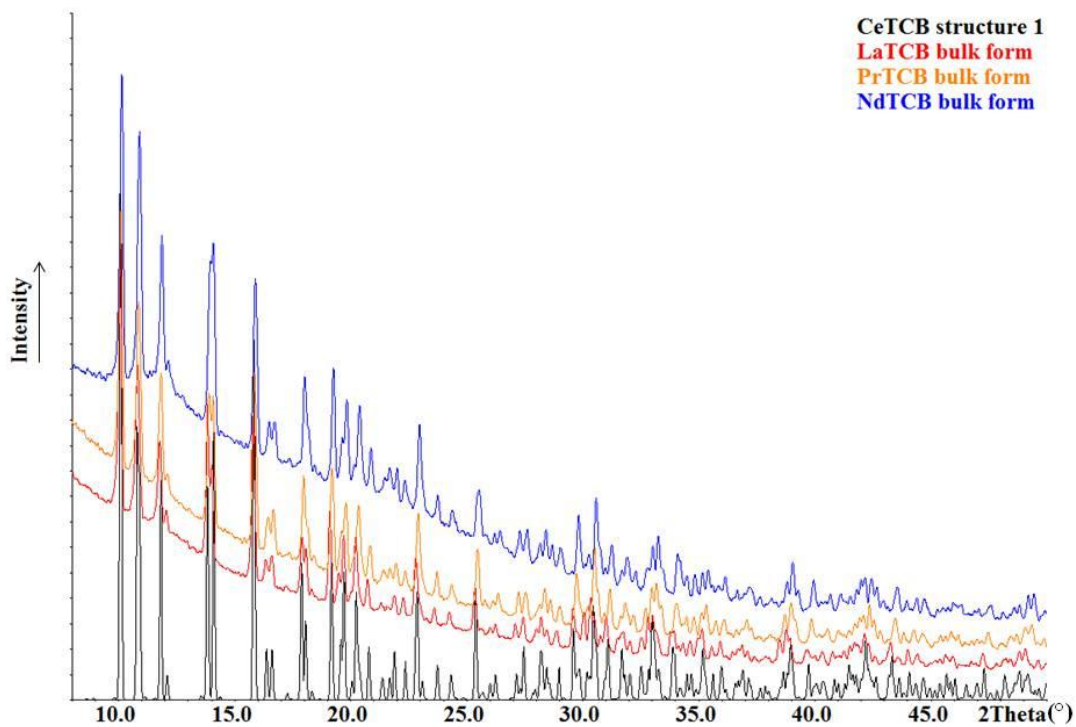


Figure 3.3.1. Powder diffractograms of LaTCB, PrTCB and NdTCB in comparison with the powder diffractogram calculated from single-crystal structure data of CeTCB (1).

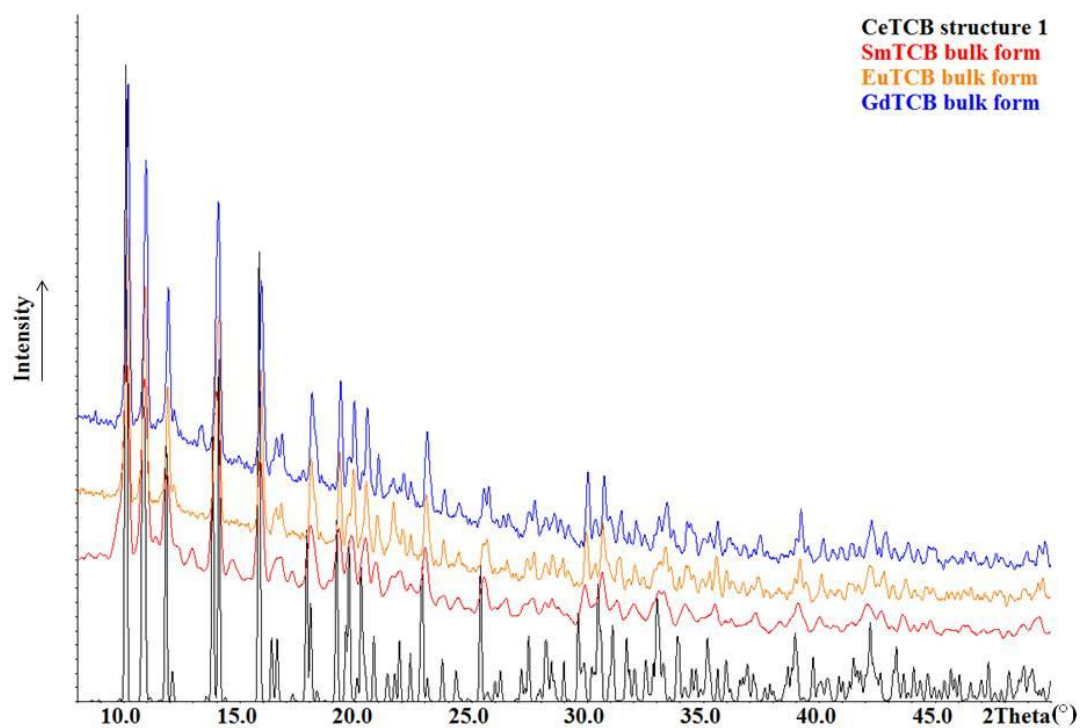


Figure 3.3.2. Powder diffractograms of SmTCB, EuTCB and GdTCB in comparison with the powder diffractogram calculated from single-crystal structure data of CeTCB (1).

The lattice parameters for each light rare earth tetracyanidoborates in bulk form were refined from the peak files created from the powder diagrams. They are presented in the table 3.3.1. A decrease of the lattice parameters could occur with increasing atomic number from the lightest lanthanum compound to the heaviest gadolinium compound due to the lanthanide contraction.⁴⁴ The decrease of the lattice parameters compensates for the decreasing ionic radius and enables the crystallization in the monoclinic crystal system throughout the entire series. This phenomenon is also known in other isostructural series of rare earth compounds, for example in rare earth hydroxysulfates.⁶² However, no serial decrease in the lattice parameter is observed in the light rare earth tetracyanidoborates.

Table 3.3.1. The effective ionic radii (ir)⁶¹ of ${}^{\text{IX}}\text{LRE}^{3+}$ together with the lattice parameters in $[\text{LRE}(\text{H}_2\text{O})_5][\text{B}(\text{CN})_4]_3 \cdot 0.5 \text{H}_2\text{O}$ ($P2_1/n$) refined from the peak files created from the powder diagrams.

Compound	ir (Å)	a (Å)	b (Å)	c (Å)	β (°)	V (Å ³)
LaTCB	1.216	15.393(3)	10.816(1)	33.333(3)	103.243(1)	5402.2(7)
CeTCB	1.196	15.396(2)	10.814(2)	33.338(5)	103.255(1)	5402.5(1)
PrTCB	1.179	15.394(1)	10.814(2)	33.336(4)	103.240(7)	5401.8(7)
NdTCB	1.163	15.396(1)	10.813(2)	33.340(4)	103.261(8)	5402.4(1)
SmTCB	1.132	15.393(1)	10.815(1)	33.341(5)	103.245(2)	5402.3(7)
EuTCB	1.120	15.392(2)	10.818(4)	33.341(5)	103.247(1)	5404.1(2)
GdTCB	1.107	15.393(2)	10.817(4)	33.333(5)	103.248(9)	5402.6(1)

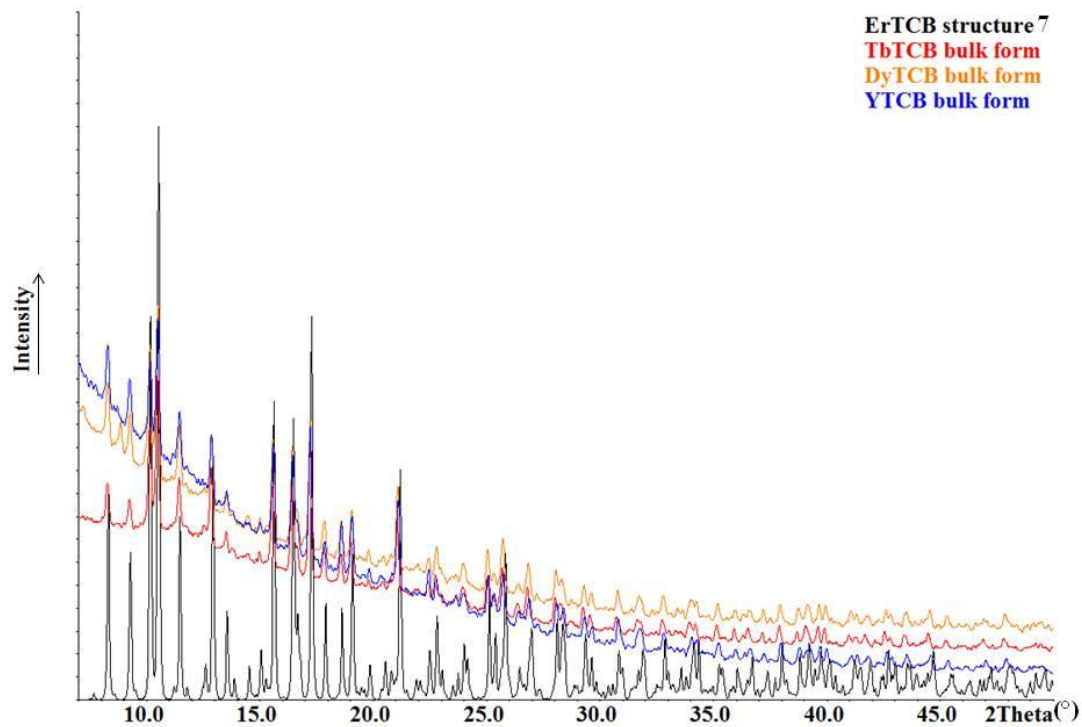


Figure 3.3.3. Powder diffractograms of TbTCB, DyTCB and YTCB in comparison with the powder diffractogram calculated from single-crystal structure data of ErTCB (7).

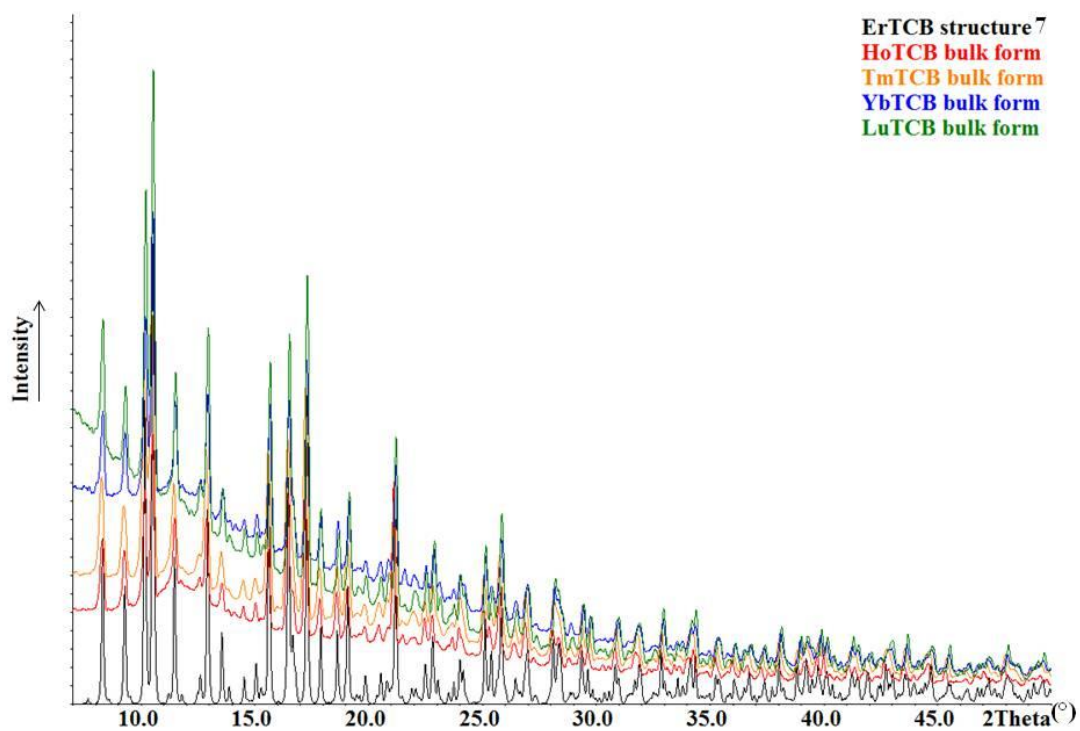


Figure 3.3.4. Powder diffractograms of HoTCB, TmTCB, YbTCB and LuTCB in comparison with the powder diffractogram calculated from single-crystal structure data of ErTCB (7).

Table 3.3.2. The effective ionic radii (ir)⁶¹ of $^{VIII}HRE^{3+}$ together with the lattice parameters in $[HRE(H_2O)_7][[B(CN)_4]_3]$ ($P2_1/n$) refined from the peak files created from the powder diagrams.

Compound	ir (Å)	a (Å)	b (Å)	c (Å)	β (°)	V (Å ³)
TbTCB	1.040	13.769(2)	21.250(3)	19.165(3)	96.505(1)	5571.4(9)
DyTCB	1.027	13.771(1)	21.252(3)	19.168(2)	96.506(7)	5573.9(7)
YTCB	1.019	13.775(3)	21.254(4)	19.168(2)	96.503(2)	5575.7(2)
HoTCB	1.016	13.770(1)	21.254(2)	19.167(2)	96.504(9)	5573.5(7)
ErTCB	1.004	13.774(3)	21.254(2)	19.165(2)	96.493(1)	5574.4(1)
TmTCB	0.994	13.771(2)	21.255(2)	19.162(3)	96.48(1)	5573.3(9)
YbTCB	0.985	13.770(2)	21.254(2)	19.157(3)	96.510(1)	5570.6(1)
LuTCB	0.977	13.770(2)	21.253(2)	19.167(2)	96.512(1)	5573.0(8)

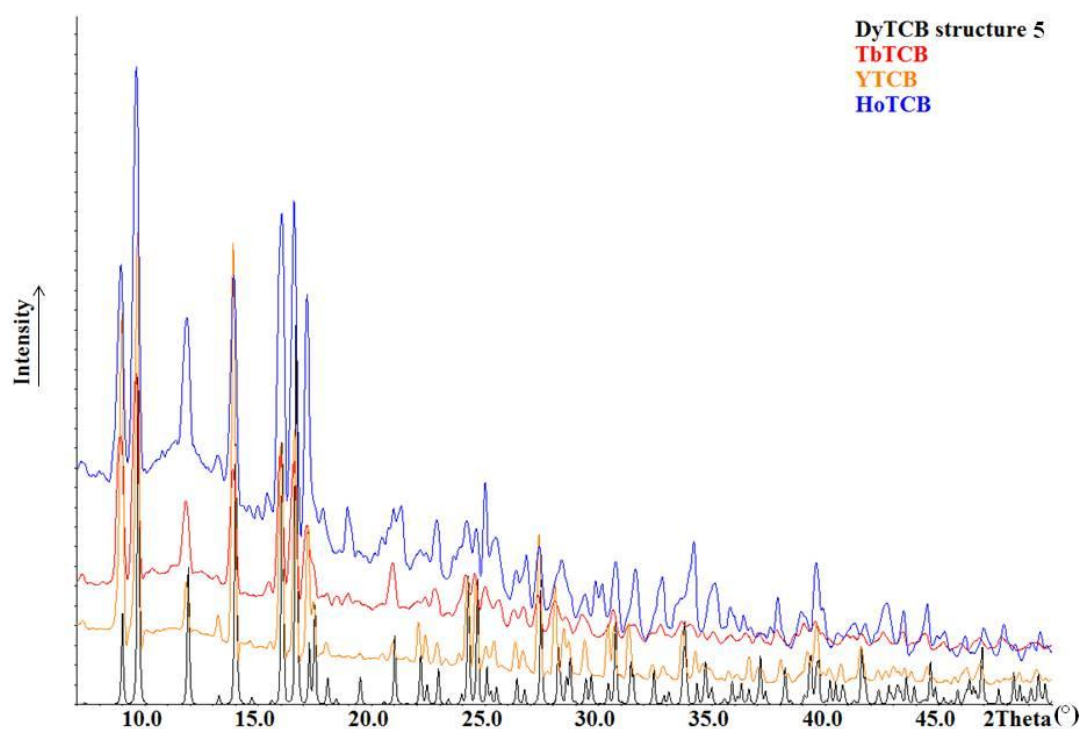


Figure 3.3.5. Powder diffractograms of TbTCB, YTCB and HoTCB in comparison with the powder diffractogram calculated from single-crystal structure of DyTCB (**5**). Some additional peaks are also observed in the diffractograms due to the lack of sample quality at room temperature.

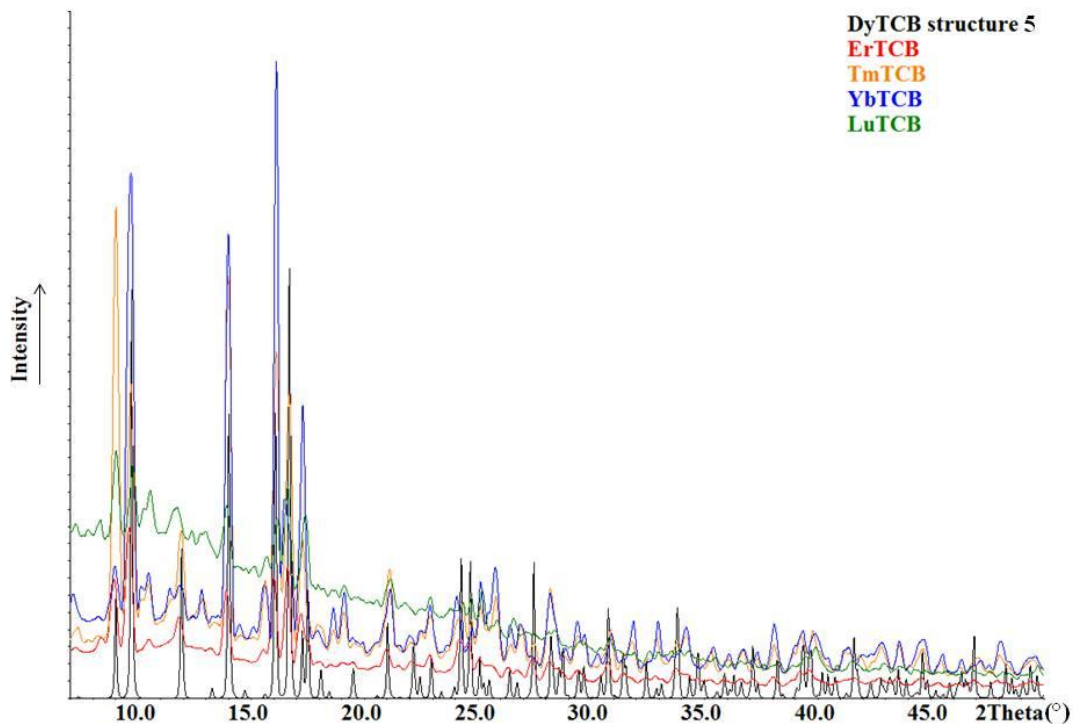


Figure 3.3.6. Powder diffractograms of ErTCB, TmTCB, YbTCB and LuTCB in comparison with the powder diffractogram calculated from single-crystal structure data of DyTCB (**5**). Some additional peaks also observed in the diffractograms due to the lack of sample quality at room temperature.

The lattice parameters for each heavy rare earth tetracyanidoborates were refined from the peak files created from the powder diagrams of the bulk structure (**7**). For the structure **5**, the comparison of the lattice parameters was done with the single-crystal data of compounds 4-6. The lattice parameters are given in table 3.3.2. and 3.3.3., where no regular serial decreasing is observed. A decrease of the lattice parameters in proceeding from the lightest to the heaviest compound would be expected, but was not observed of the heavy rare earth tetracyanidoborate structures.

Table 3.3.3. The effective ionic radii (r_{eff})⁶¹ of VIII HRE^{3+} together with the lattice parameters in $[\text{HRE}(\text{H}_2\text{O})_8][[\text{B}(\text{CN})_4]_3 \cdot 3 \text{H}_2\text{O}]$ ($C2/c$), where HRE = Tb, Dy or Y.

Compound	r_{eff} (Å)	a (Å)	b (Å)	c (Å)	β (°)	V (Å ³)
TbTCB	1.040	15.9786(8)	20.5317(8)	21.1413(8)	112.226(3)	6420.45(5)
DyTCB	1.027	16.0293(3)	20.5472(4)	21.1881(4)	112.234(1)	6459.58(2)
YTCB	1.019	16.0468(7)	20.5478(9)	21.1799(9)	112.259(2)	6463.16(5)

3.4 Vibrational spectroscopy

IR spectra were recorded from isostructural tetracyanidoborates with light rare earth cations (La^{3+} – Gd^{3+} , except Pm^{3+}) (Fig. 3.4.1). A Raman spectrum was recorded for $[\text{Eu}(\text{H}_2\text{O})_5][\text{B}(\text{CN})_4]_3 \cdot 0.5 \text{H}_2\text{O}$. The vibrational spectrum of the tetracyanidoborate anion has already been analyzed completely in an earlier report about its synthesis.⁵ Infrared absorption bands are shown in Table 3.4.1. Three of the nine fundamental vibrations of the $[\text{B}(\text{CN})_4]^-$ anion are observed in the spectra of $[\text{LRE}(\text{H}_2\text{O})_5][\text{B}(\text{CN})_4]_3 \cdot 0.5 \text{H}_2\text{O}$ in the region of 550–3500 cm^{-1} . The weak band around 2260 cm^{-1} corresponds to the CN stretching vibration T_2 (ν_6). The asymmetric BC vibration, ν_7 , in the T_2 mode is observable between 900 and 1000 cm^{-1} . It shows a $^{10}\text{B}/^{11}\text{B}$ - isotope pattern which consists of one strong band (^{11}B , ν_7) with a shoulder (^{10}B , ν_7). The intensity ratio from this isotope pattern should be about 1 to 4, but as the pattern is disturbed by Fermi resonance combination vibrations ($\nu_3 + \nu_5$), the intensity ratio is only about 1 to 1.5. The strong absorption bands above 3200 cm^{-1} and around 1600 cm^{-1} are fundamental bands of water which originate from the stretching (ν_1 , ν_3) and deformation (ν_2) vibrations, respectively.⁷⁰ The broad band at about 600 cm^{-1} originates from water as well, even though it is not due to the fundamental vibrations, but due to the so called librational motions of the water molecules (L_2).⁷¹

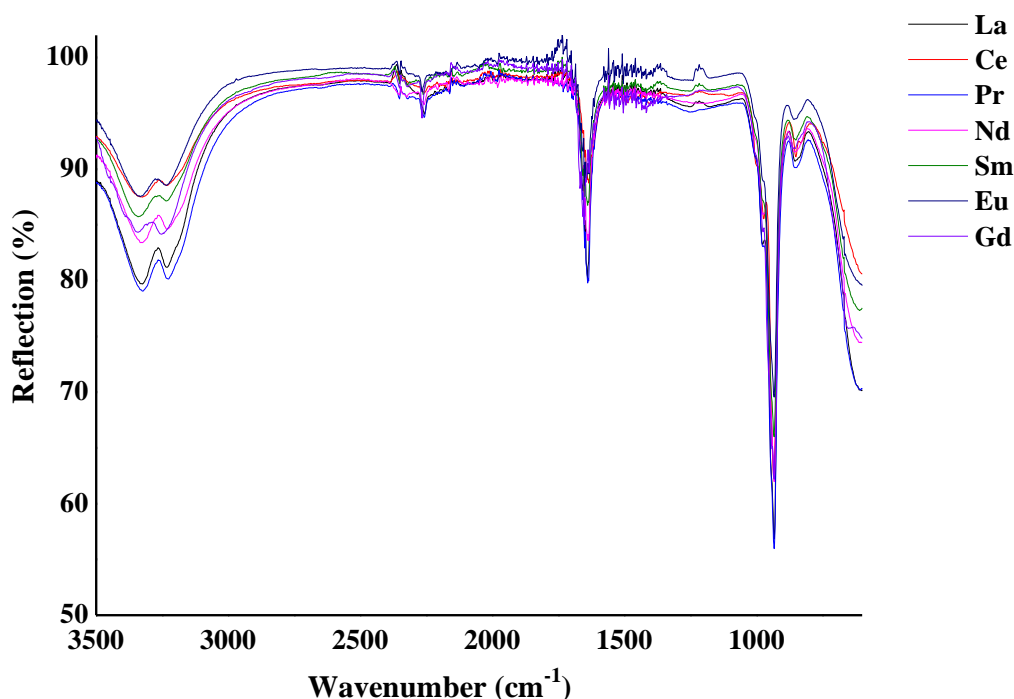


Figure 3.4.1. IR-spectra of $[\text{LRE}(\text{H}_2\text{O})_5][\text{B}(\text{CN})_4]_3 \cdot 0.5 \text{H}_2\text{O}$, (LRE = La^{3+} – Gd^{3+} , except Pm^{3+}).

The CN stretching mode is observed in the IR spectra of all $[\text{LRE}(\text{H}_2\text{O})_5][\text{B}(\text{CN})_4]_3 \cdot 0.5 \text{H}_2\text{O}$ in the region $2256\text{--}2266 \text{ cm}^{-1}$ (Table 3.4.1). The bands in this region originate from the cyanido groups. The wavenumber increases across the rare earth series. This trend can be explained by the lanthanide contraction. Since the radii of cation decreases, there is a strengthening of the coordinated CN bond. The bands from the noncoordinated cyanido groups would be expected to be observable in the lower wavenumbers, but they are not detected in the IR spectra.

Table 3.4.1. Experimental infrared band positions with correspondent attribution of $[\text{LRE}(\text{H}_2\text{O})_5][\text{B}(\text{CN})_4]_3 \cdot 0.5 \text{H}_2\text{O}$.

[LRE(H ₂ O) ₅][B(CN) ₄] ₃	Attribution						
	[B(CN) ₄] ⁻				H ₂ O		
LRE	$\nu_3 + \nu_5$	$\nu_7, {}^{11}\text{B}$	$\nu_7, {}^{10}\text{B}$	ν_6	L ₂	ν_2	$\nu_1 + \nu_3$
La	855	933	977	2256	601	1639	3234;3332
Ce	851	935	974	2258	601	1635	3232;3326
Pr	849	933	976	2258	606	1639	3227;3323
Nd	856	933	975	2258	590	1635	3233;3332
Sm	852	934	976	2262	610	1639	3234;3342
Eu	858	934	976	2266	590	1633	3234;3334
Gd	855	934	976	2266	588	1633	3252;3341

In the Raman spectrum of $[\text{Eu}(\text{H}_2\text{O})_5][\text{B}(\text{CN})_4]_3 \cdot 0.5 \text{H}_2\text{O}$, the CN stretching mode is separated into two bands with shoulders (Fig. 3.4.2 and 3.4.3). The band at 2262 cm^{-1} originates from the coordinated cyanido groups and its shoulder at higher wavenumber from the twofold coordinated ones. Furthermore, the band at 2244 cm^{-1} and its shoulder originate from the noncoordinated cyanido groups. They are at higher wavenumbers than expected and are comparable to the wavenumbers of the CN stretching mode in monovalent tetracyanidoborates.^{9,17}

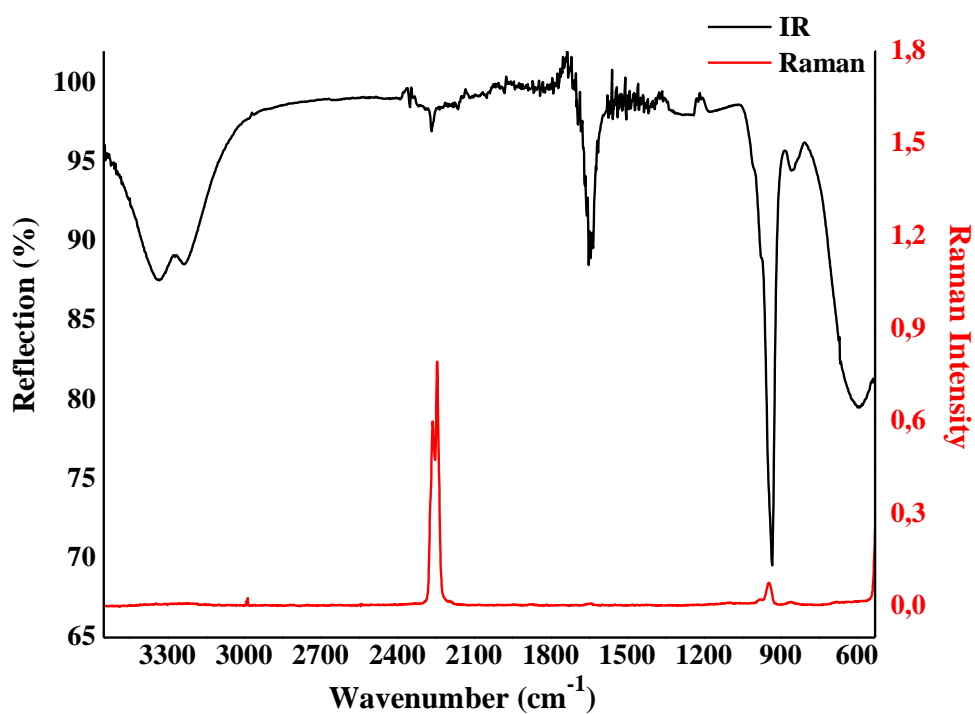


Figure 3.4.2. IR and Raman Spectra of $[\text{Eu}(\text{H}_2\text{O})_5][\text{B}(\text{CN})_4]_3 \cdot 0.5 \text{H}_2\text{O}$.

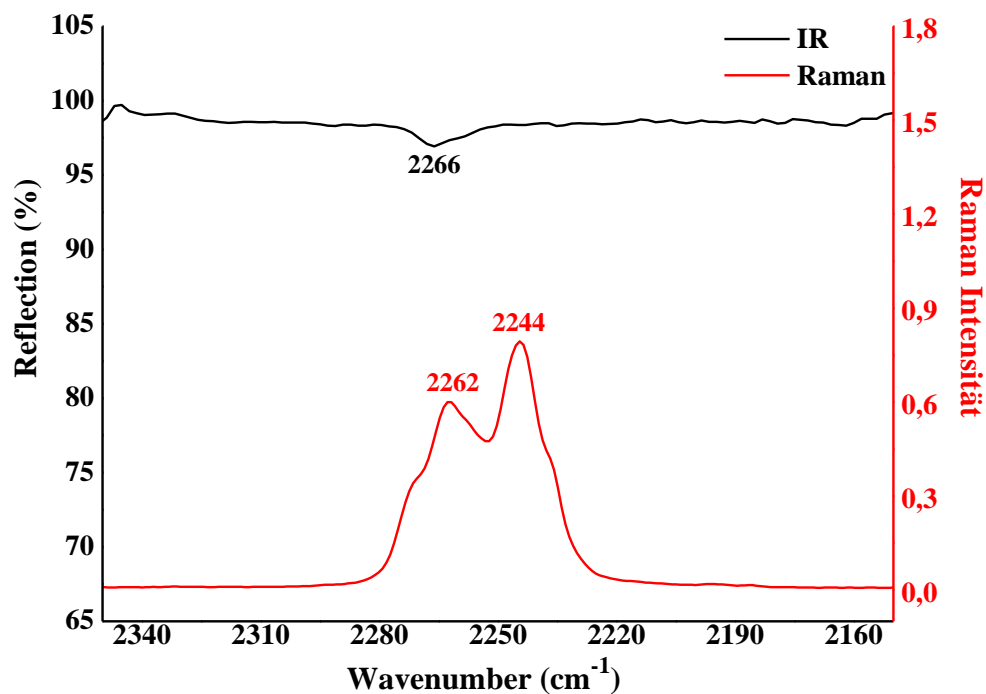


Figure 3.4.3. The CN stretching mode in $[\text{Eu}(\text{H}_2\text{O})_5][\text{B}(\text{CN})_4]_3 \cdot 0.5 \text{H}_2\text{O}$.

IR spectra were also recorded from all tetracyanidoborates with heavy rare earth metal cations (Tb^{3+} – Lu^{3+} and Y^{3+}), but Raman spectrum was recorded only from $[\text{Er}(\text{H}_2\text{O})_7][\text{B}(\text{CN})_4]_3$ (Fig. 3.4.4 and 3.4.5). The IR spectra are identical among each other, which reveals along with the crystal structure analysis the isostructurality of all $[\text{HRE}(\text{H}_2\text{O})_7][\text{B}(\text{CN})_4]_3$.

Infrared absorption bands are shown in Table 3.4.2. Likewise, the spectra of light rare earth tetracyanidoborates (Table 3.4.1), also the corresponding spectra of heavy rare earth compounds exhibit three of the nine fundamental vibrations of the $[\text{B}(\text{CN})_4]^-$ anion in the region of 550–3500 cm^{-1} .

The CN stretching mode is very weak in the IR spectrum of $[\text{HRE}(\text{H}_2\text{O})_7][\text{B}(\text{CN})_4]_3$, but in the Raman spectrum this mode is much stronger, where it is separated into three bands 2242, 2253 (with a shoulder) and 2271 cm^{-1} (Fig. 3.4.6). According to the crystal structure (Fig. 3.2.8., p. 24) one CN group of $[\text{B}(\text{CN})_4]^-$ is coordinated to Er^{3+} and it corresponds to the highest CN stretching frequencies, which are also observable in the IR spectra. Other CN groups are linked with water molecules through hydrogen bonds ($\text{H}\cdots\text{N} = 1.941\text{--}2.132 \text{ \AA}$) and correlates with the bands 2253 and 2242 cm^{-1} and with the shoulder of the first band. This band at 2253 cm^{-1} is slightly lower than that of the coordinated groups in the divalent compounds, but higher than that of the noncoordinated ones.¹³ The band is at higher wavenumber than expected and can be compared with the wavenumbers of the stretching modes in monovalent tetracyanidoborates.⁹ This indicates the interaction between the cyanido groups and the water molecules. A similar phenomenon has already been observed in the Raman spectrum of $[\text{Fe}(\text{H}_2\text{O})_6][\text{B}(\text{CN})_4]_3$.⁸

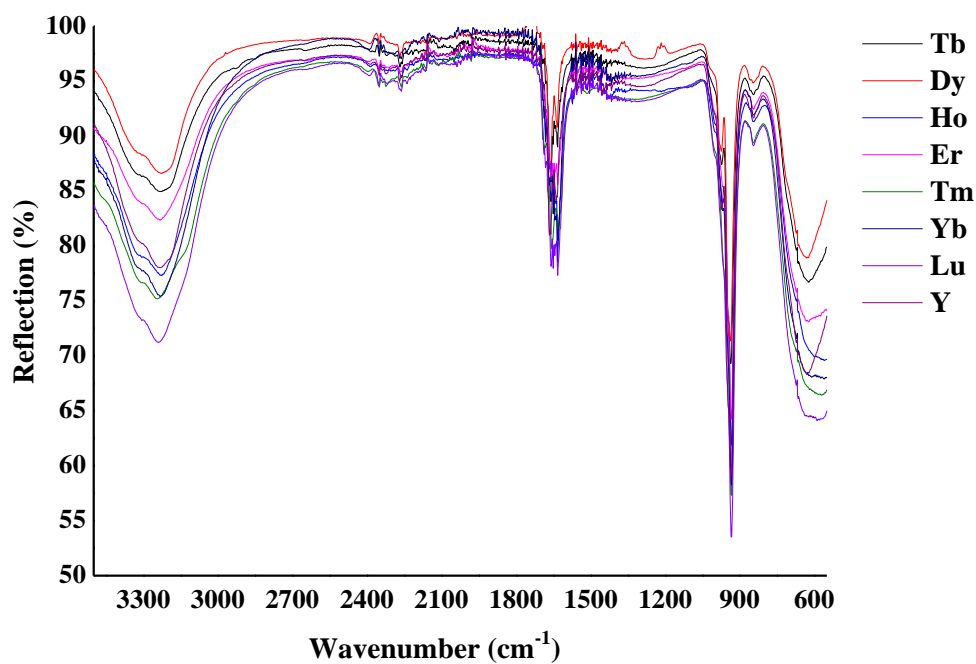


Figure 3.4.4. IR-Spectra of $[\text{HRE}(\text{H}_2\text{O})_7][\text{B}(\text{CN})_4]_3$, (HRE = Tb^{3+} – Lu^{3+} , and Y^{3+}).

Table 3.4.2. Experimental infrared band positions with correspondent attribution of $[\text{HRE}(\text{H}_2\text{O})_7][\text{B}(\text{CN})_4]_3$.

[HRE(H ₂ O) ₇][B(CN) ₄] ₃	Attribution						
	[B(CN) ₄] [−]				H ₂ O		
HRE	$\nu_3 + \nu_5$	$\nu_7, {}^{11}\text{B}$	$\nu_3, {}^{10}\text{B}$	ν_6	L ₂	ν_3	ν_1
Tb	845	937	973	2268	623	1634; 1661	3230
Dy	845	938	974	2268	631	1636; 1666	3226
Ho	846	934	970	2266	633	1633	3226
Er	844	935	968	2268	624	1633; 1660	3234
Tm	844	936	972	2266	628	1634; 1667	3226
Yb	845	934	968	2268	560	1633	3233
Lu	846	934	968	2270	589	1633; 1660	3242
Y	845	936	973	2270	631	1639; 1666	3233

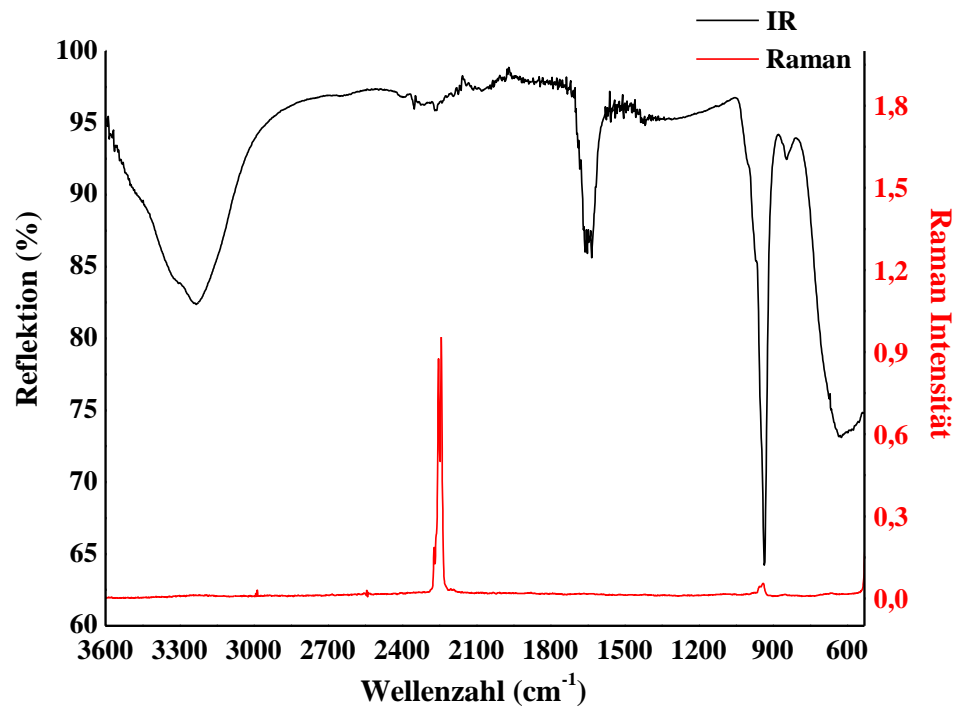


Figure 3.4.5. IR and Raman spectra of $[\text{Er}(\text{H}_2\text{O})_7][\text{B}(\text{CN})_4]_3$.

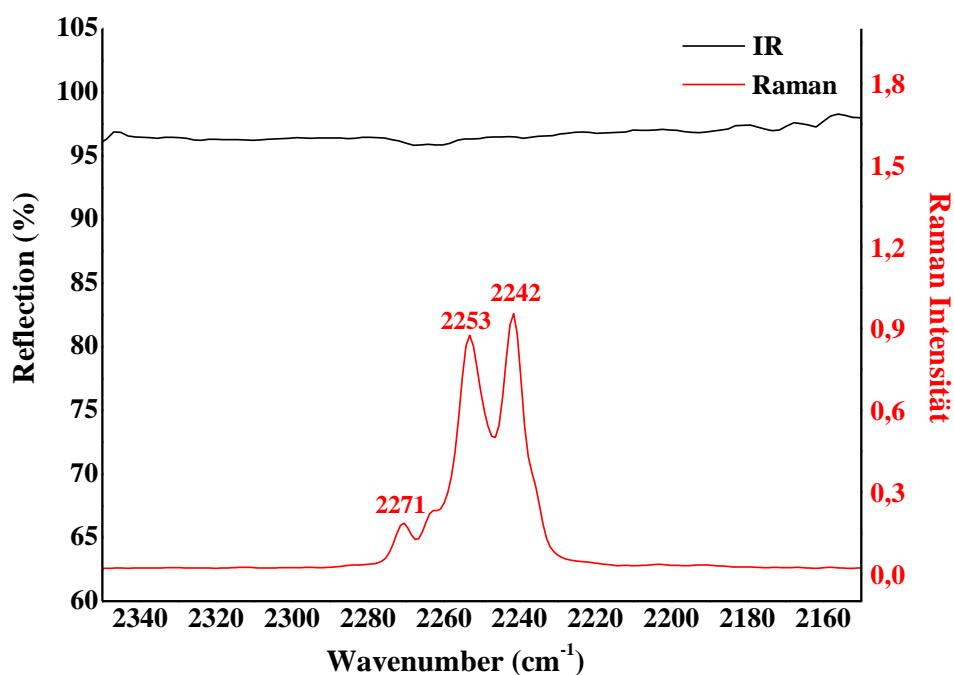


Figure 3.4.6. The CN stretching mode in $[\text{Er}(\text{H}_2\text{O})_7][\text{B}(\text{CN})_4]_3$.

The CN stretching mode is very weak in the IR spectra of $[\text{HRE}(\text{H}_2\text{O})_7][\text{B}(\text{CN})_4]_3$ and even weaker than in the spectra of $[\text{LRE}(\text{H}_2\text{O})_5][\text{B}(\text{CN})_4]_3 \cdot 0.5 \text{ H}_2\text{O}$. This is compatible with the crystal structures (Fig. 3.2.1., p. 15 and 3.2.8., p. 24), where four CN groups coordinate each light rare earth metal cation, whereas only one CN group coordinates each heavy rare earth cation. Therefore, the CN stretching mode originating from the coordinated CN groups is stronger in $[\text{LRE}(\text{H}_2\text{O})_5][\text{B}(\text{CN})_4]_3 \cdot 0.5 \text{ H}_2\text{O}$ than in $[\text{HRE}(\text{H}_2\text{O})_7][\text{B}(\text{CN})_4]_3$ (Fig. 3.4.7). Furthermore, this mode in the spectra of $[\text{LRE}(\text{H}_2\text{O})_5][\text{B}(\text{CN})_4]_3 \cdot 0.5 \text{ H}_2\text{O}$ is located on the average at 2261 cm^{-1} , whereas the same mode in the spectra of $[\text{HRE}(\text{H}_2\text{O})_7][\text{B}(\text{CN})_4]_3$ lies at about 2268 cm^{-1} . This increase in wavenumber of the CN stretching mode goes along with the decreasing ionic radius of the metal cation, because the lone pair (σ -CN orbital) is lowered in energy by the $\text{M} \cdots \text{N}-\text{C}$ interaction causing a strengthening of the C-N bond.¹⁵ In addition to the differences in the CN stretching modes, there are also differences in absorption bands arising from the water molecules. They are slightly stronger in the spectrum of $[\text{HRE}(\text{H}_2\text{O})_7][\text{B}(\text{CN})_4]_3$ than in the one of $[\text{LRE}(\text{H}_2\text{O})_5][\text{B}(\text{CN})_4]_3 \cdot 0.5 \text{ H}_2\text{O}$, which indicates the larger number of water molecules in $[\text{HRE}(\text{H}_2\text{O})_7][\text{B}(\text{CN})_4]_3$.

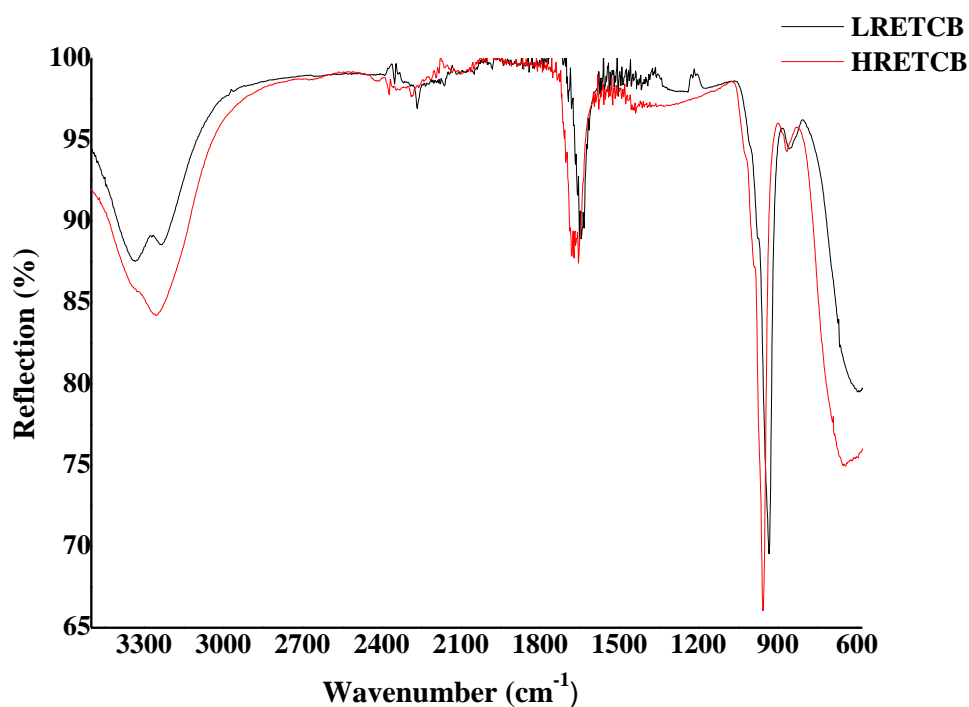


Figure 3.4.7. IR spectrum of a $[\text{LRE}(\text{H}_2\text{O})_5][\text{B}(\text{CN})_4]_3 \cdot 0.5 \text{H}_2\text{O}$ (LRETCB) in comparison to the IR spectrum of a $[\text{HRE}(\text{H}_2\text{O})_7][\text{B}(\text{CN})_4]_3$ (HRETCB).

The ErTCB was thermally dehydrated according to its thermal properties (section 3.1.6). The dehydrated compound was analyzed with the aid of infrared spectroscopy and compared with analysis of hydrous ErTCB (Figure 3.4.8.). The IR spectra indicate that the thermal dehydration occurs in ErTCB. In comparison to the hydrous compound, the dehydrated ErTCB shows only weak absorption bands of water molecules. Therefore, the water can be thermally removed almost completely from the compound. This dehydration method is suitable for all RETCBs. The CN stretching mode gets considerably stronger after dehydration. This is an evidence for the coordination of more than one TCB group with the rare earth cation after dehydration.

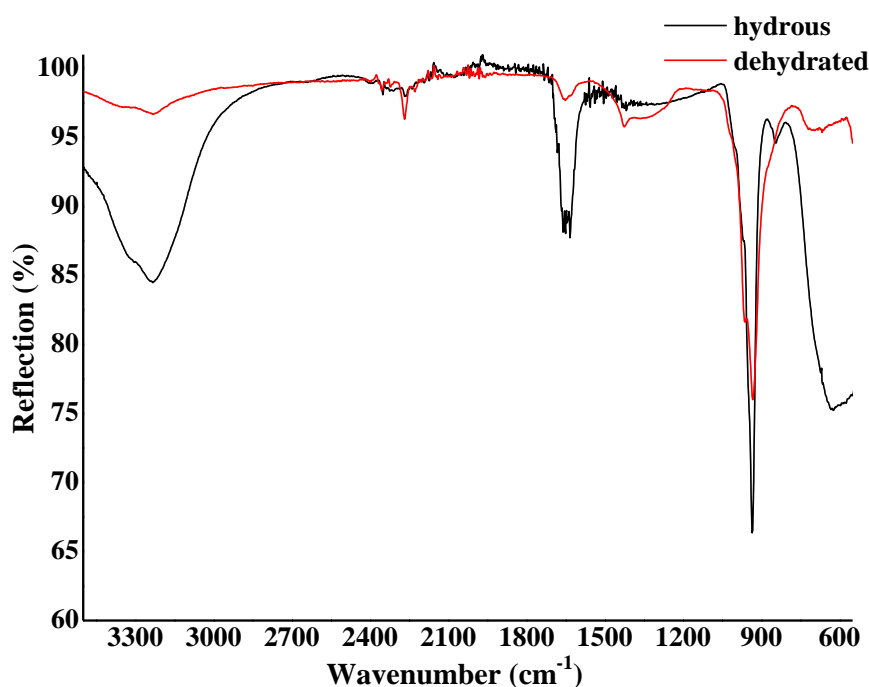


Figure 3.4.8. IR Spectrum of hydrous ErTCB in comparison with the thermal dehydrated ErTCB.

The preparation of anhydrous inorganic compounds by dehydration with aid of thionyl chloride SOCl_2 is a common dehydration method. It was applied for the first time by Hecht in 1947 for the preparation of a number of mono- and bi-valent anhydrous chlorides.⁷² Similarly, hydrated rare earth chlorides and several other compounds can be readily dehydrated by refluxing with SOCl_2 according to equation 3.4.1.



In addition to thermal dehydration, this chemical dehydration method with thionyl chloride was also used for the dehydration of lanthanum tetracyanidoborate, because the rare earth compounds of higher atomic weight are more difficult to dehydrate. For example, whereas the reaction time for the dehydration of lanthanum chloride with SOCl_2 is only about one hour, the same reaction time for the gadolinium chloride is already about 15 hours and the dehydration of erbium chloride even takes up to 110 hours.⁷² Therefore, the thermal dehydration is more adequate for heavy rare earth compounds.

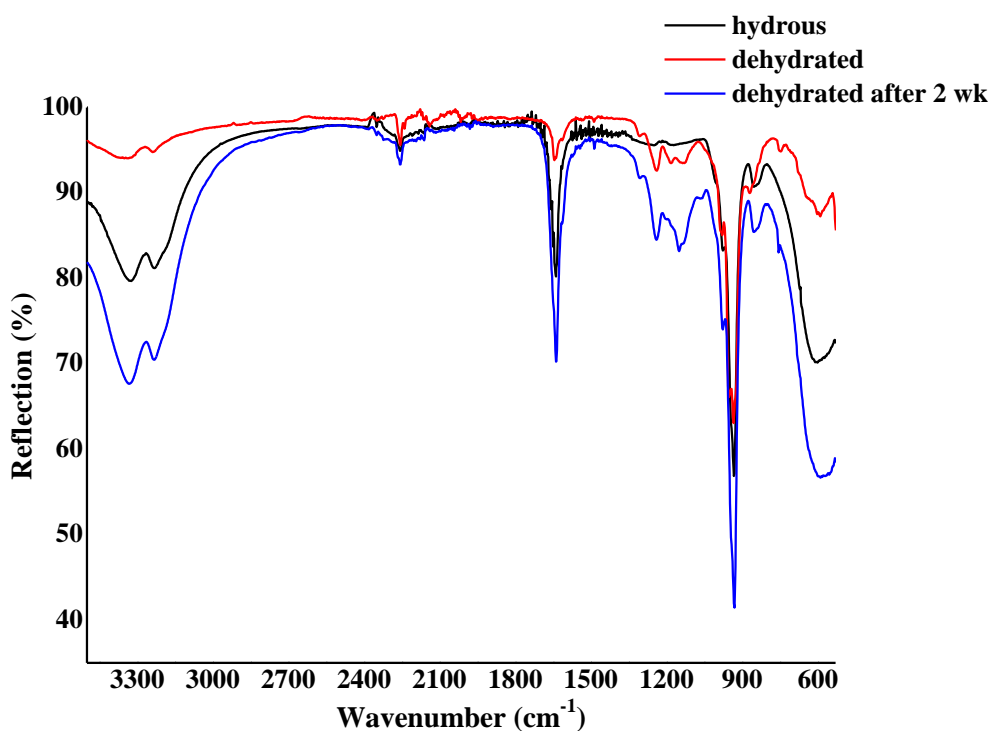


Figure 3.4.9. IR spectra of lanthanum tetracyanidoborates. Hydrous, dehydrated compounds with a dehydrated compound after two weeks exposure to air.

After three hours of reflux with SOCl_2 , the dehydrated lanthanum tetracyanidoborate, LaTCB, was analyzed by infrared spectroscopy. The results were compared with the IR spectrum of hydrous LaTCB (Fig. 3.4.9.). The measurements reveal that the dehydration of LaTCB with SOCl_2 was successful, since the absorption bands originating from water molecules decrease considerably after dehydration. However, the dehydration is incomplete, which is obvious as the absorption bands of water are still observable. Moreover, the spectra of dehydrated compounds show new bands between 1300 and 1000 cm^{-1} . The new bands could originate from sulfoxide groups which absorb in this region.⁷³ This might indicate that the SOCl_2 not only dehydrates LaTCB but also alters or contaminates the compound, which is not desired during the dehydration process. Therefore, the dehydration with SOCl_2 is not adequate for rare earth tetracyanidoborates.

The hygroscopicity of dehydrated LaTCB was determined by exposing the dehydrated compound to ambient air for two weeks and repeating the measurement of the IR spectrum afterwards (Fig. 3.4.9). The measurements illustrate the high hygroscopicity of dehydrated LaTCB. After two weeks of exposure to air, the compound exhibits very strong absorption

bands of water. Thus, the dehydrated LaTCB should be stored under inert atmosphere, ideally in a glove box.

3.5 Nuclear magnetic resonance spectroscopy

The tetracyanidoborat anion contains five NMR active nuclei, ^{11}B ($I = 3/2$, 80.42%), ^{10}B ($I = 3$, 19.58%), ^{13}C ($I = 1/2$, 1.108%), ^{14}N ($I = 1$, 99.635%) and ^{15}N ($I = 1/2$, 0.365%). Of those five, ^{11}B and ^{13}C were recorded from $[\text{Eu}(\text{H}_2\text{O})_5][\text{B}(\text{CN})_4]_3 \cdot 0.5 \text{H}_2\text{O}$ in trideuteroacetonitrile. Because of the tetrahedral symmetry of the TCB anion in the solution, the ^{13}C signal splitting is not caused by the quadrupole moment of boron nuclei, but by the coupling pattern, a quartet at 119.8 ppm with ^{11}B ($I = 3/2$, $^1J_{\text{CB}} = 71.1 \text{ Hz}$) (Fig. 3.5.1). Another possible coupling pattern, a septet with ^{10}B , cannot be observed. The chemical shift, $\delta_{\text{C}} = 119.8 \text{ ppm}$, is typical for cyanidoborate ($[\text{BH}_3\text{CN}]^-$ 144.9, $[\text{BH}_2(\text{CN})_2]^-$ 134.0, $[\text{BH}(\text{CN})_3]^-$ 127.9 ppm)⁷⁴ and confirms that the analyzed compound is indeed cyanidoborate and not isocyanidoborate ($[\text{BH}_2(\text{NC})_2]^-$ 160.9, $[\text{BH}(\text{NC})_3]^-$ 165.0 ppm)⁷⁴. In comparison with the CN^- ions in aqueous solution ($\delta_{\text{C}} = 165.8 \text{ ppm}$)⁷⁵, the ^{13}C resonance is shifted to lower frequencies.⁵ The coupling constant, $^1J_{\text{CB}} = 71.1 \text{ Hz}$, is similar to the coupling constants measured in other tetracyanidoborates.^{5, 76}

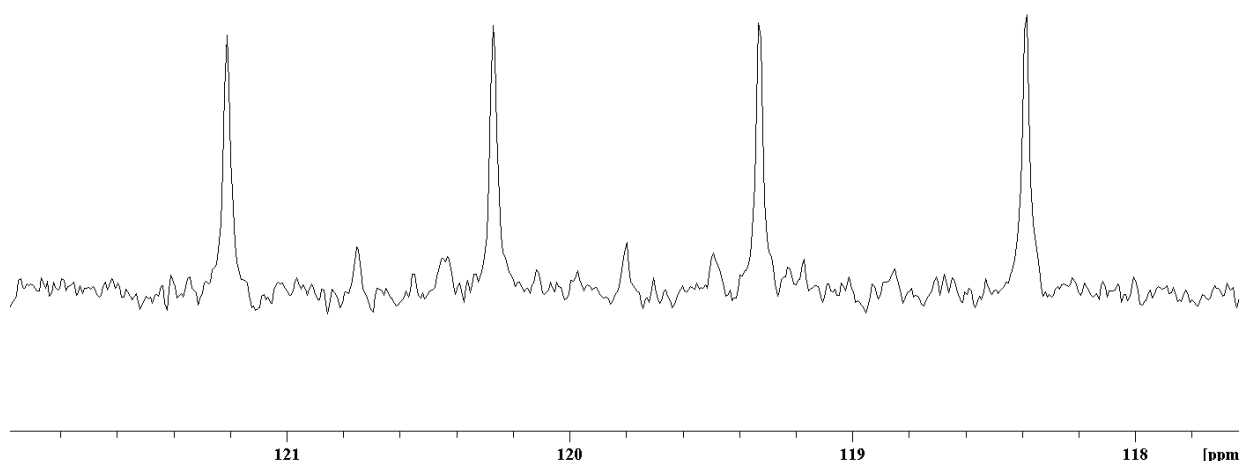


Figure 3.5.1. ^{13}C -NMR spectrum of $[\text{Eu}(\text{H}_2\text{O})_5][\text{B}(\text{CN})_4]_3 \cdot 0.5 \text{H}_2\text{O}$.

The ^{11}B -NMR spectrum shows a sharp singlet at $\delta_{\text{B}} = -39.1$ ppm with ^{13}C satellites ($^1J_{\text{BC}} = 71.1$ Hz) with an expected intensity ratio of 1 to 45 (Fig. 3.5.2). The chemical shift is at low frequency in comparison to other tetraborate anions ($[\text{BF}_4]^-$ -1.4, $[\text{BCl}_4]^-$ 7.1, $[\text{BBr}_4]^-$ -24.1, $[\text{B}(\text{CNS})_4]^-$ -16.7, $[\text{B}(\text{NCO})_4]^-$ -11.5 ppm), which indicates a high electron density at boron atom. However, it is typical for cyanidoborates ($[\text{BH}_3\text{CN}]^-$ -43.5, $[\text{BH}_2(\text{CN})_2]^-$ -39.9, $[\text{BH}(\text{CN})_3]^-$ -37.5 ppm)⁷⁴ and again confirms that the compound is not isocyanidoborate ($[\text{BH}_2(\text{NC})_2]^-$ -21.1, $[\text{BH}(\text{NC})_3]^-$ -17.3 ppm)⁷⁴.

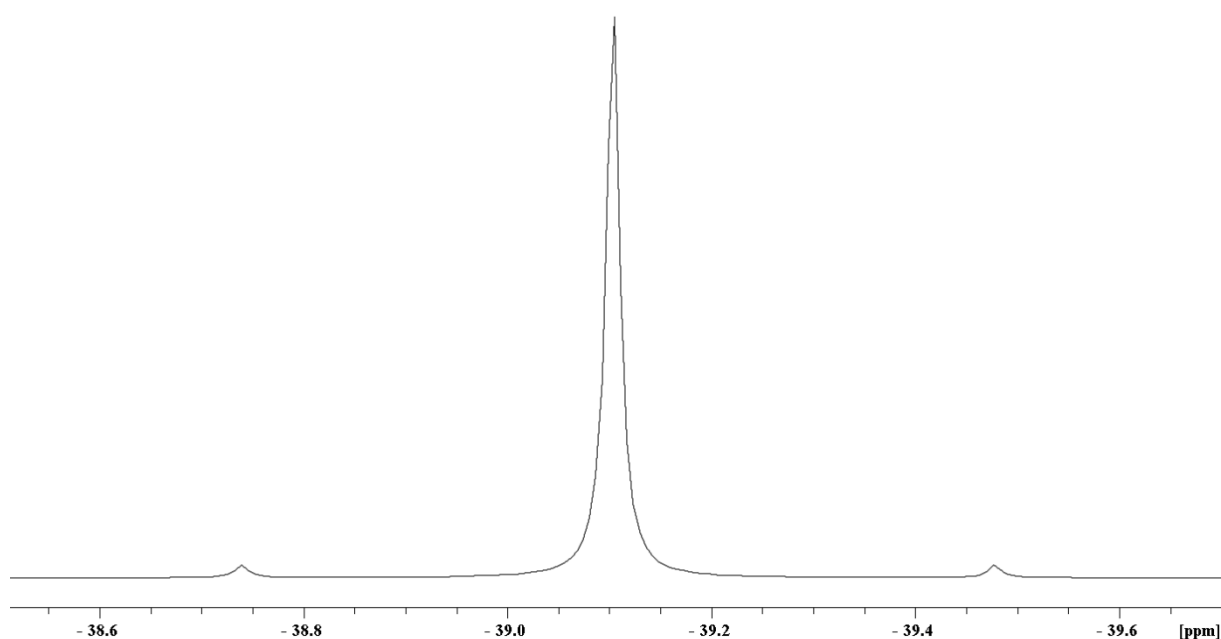


Figure 3.5.2. ^{11}B -NMR spectrum of $[\text{Eu}(\text{H}_2\text{O})_5][\text{B}(\text{CN})_4]_3 \cdot 0.5 \text{H}_2\text{O}$.

Similar, in the case of the light rare earth tetracyanidoborate, $[\text{Eu}(\text{H}_2\text{O})_5][\text{B}(\text{CN})_4]_3 \cdot 0.5 \text{H}_2\text{O}$, only ^{11}B ($I = 3/2$, 80.42%) and ^{13}C ($I = 1/2$, 1.11%) of the five NMR active nuclei of the tetracyanidoborate anion were recorded from the heavy rare earth tetracyanidoborate, $[\text{Er}(\text{H}_2\text{O})_7][\text{B}(\text{CN})_4]_3$, in trideuteroacetonitrile. The ^{13}C signal splitting due to the coupling pattern is a quartet at 123.1 ppm with ^{11}B ($I = 3/2$, $^1J_{\text{CB}} = 71.0$ Hz) (Fig. 3.5.3). Another possible coupling pattern, a septet with ^{10}B is here, like in the spectrum of $[\text{Eu}(\text{H}_2\text{O})_5][\text{B}(\text{CN})_4]_3 \cdot 0.5 \text{H}_2\text{O}$, not observable. The chemical shift, $\delta_{\text{C}} = 123.1$ ppm, is typical for cyanidoborates, and it is identical with the chemical shifts in other tetracyanidoborates.^{5, 76} The coupling constant, $^1J_{\text{CB}} = 71.0$ Hz, equals to the coupling constants measured in $[\text{Eu}(\text{H}_2\text{O})_5][\text{B}(\text{CN})_4]_3 \cdot 0.5 \text{H}_2\text{O}$.

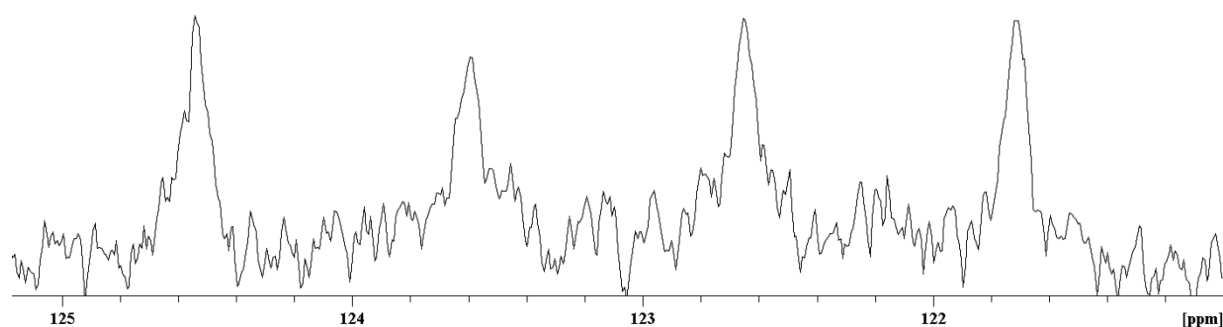


Figure 3.5.3. ^{13}C -NMR spectrum of $[\text{Er}(\text{H}_2\text{O})_7][\text{B}(\text{CN})_4]_3$

The ^{11}B -NMR spectrum shows a sharp singlet at $\delta_{\text{B}} = -36.7$ ppm with ^{13}C satellites ($^1J_{\text{BC}} = 70.8$ Hz) in an expected intensity ratio of 1 to 45 (Fig. 3.5.4.). The chemical shift is at low frequency in comparison with other borate anions ($[\text{BF}_4]^-$ -1.4, $[\text{BCl}_4]^-$ 7.1, $[\text{BBr}_4]^-$ -24.1, $[\text{B}(\text{CNS})_4]^-$ -16.7, $[\text{B}(\text{NCO})_4]^-$ -11.5 ppm], but a little bit higher than the average shifts measured in other tetracyanidoborates.^{5,76}

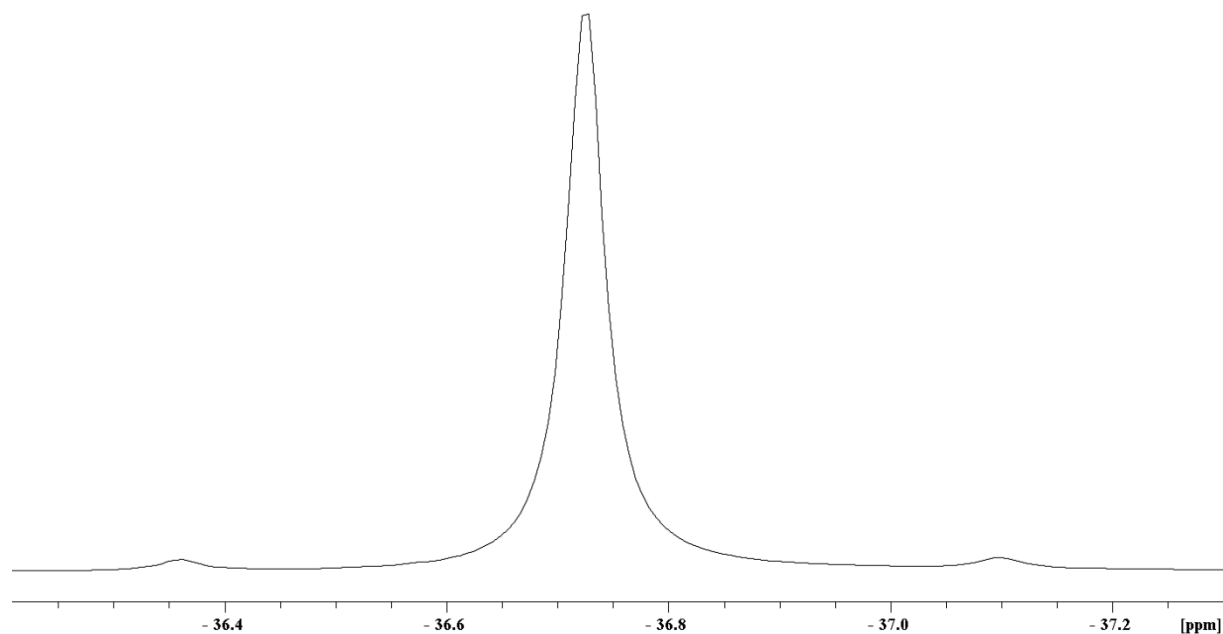


Figure 3.5.4. ^{11}B - NMR spectrum $[\text{Er}(\text{H}_2\text{O})_7][\text{B}(\text{CN})_4]_3$

3.6 Thermochemical properties

The DSC curve of $[\text{Eu}(\text{H}_2\text{O})_5][\text{B}(\text{CN})_4]_3 \cdot 0.5 \text{H}_2\text{O}$ shows three endothermic peaks and two exothermic peaks (Fig. 3.6.1). The loss of coordinated water molecules occurs in several steps. The first step begins at 89°C (onset) and ends at 93°C with a dehydration enthalpy of 22.5 $\text{kJ}\cdot\text{mol}^{-1}$. This corresponds to about 0.5 water molecules per mol, as the enthalpy⁷⁷ of water evaporation at 90°C is 41.1 $\text{kJ}\cdot\text{mol}^{-1}$. The second step shows a broad band between 95°C and 126°C with a dehydration enthalpy of 90.9 $\text{kJ}\cdot\text{mol}^{-1}$. This equals 2.3 water molecules per mol, as the enthalpy of water at 120°C is 38.7 $\text{kJ}\cdot\text{mol}^{-1}$.⁷⁷ The corresponding mass losses determined from the TG curve are -5.2% \sim 1.7 H_2O and -7.8% \sim 2.6 H_2O . The third endothermic peak at 430°C (onset) with an energy of 2.7 $\text{kJ}\cdot\text{mol}^{-1}$ probably corresponds to the transition from crystalline to amorphous state. This third peak could also arise from the loss of the rest water. The decomposition of the compound is indicated by two peaks at 444°C (onset) with an exothermic energy of 2.6 $\text{kJ}\cdot\text{mol}^{-1}$ and at 521°C (onset) with an exothermic energy of 78.7 $\text{kJ}\cdot\text{mol}^{-1}$. In the TG curve the mass loss related to the decomposition already begins at 365°C with a mass loss of -19.2%. The DSC curve shows also two drifts at 400 °C and 565 °C arisen from a device error.

Furthermore, when the other light rare earth tetracyanidoborate, $[\text{La}(\text{H}_2\text{O})_5][\text{B}(\text{CN})_4]_3 \cdot 0.5 \text{H}_2\text{O}$ was heated for three days at 320°C, the color of the salt changed from white to dark brown. The change of color indicates that the compound starts to decompose at 320°C or even below this temperature. It seems advisable to set an upper temperature limit below 300°C. According to the dehydration enthalpies of the endothermic peaks and the corresponding mass losses the thermal dehydration of the compound is not complete. The dehydration of the residual water (1-2.7 H_2O) does not occur before the decomposition of the compound. Thus, the complete dehydration of the compound cannot be achieved thermally.

Because of the chemical and physical similarity of the light rare earth tetracyanidoborates, it can be assumed that these thermal properties of lanthanum and europium compounds are representative for all tetracyanidoborates with rare earth cations, $\text{RE} = \text{La}^{3+}\text{--Gd}^{3+}$ in their bulk form. Therefore, the temperature range for the thermal dehydration of these compounds should be set somewhere between 130°C and 300°C.

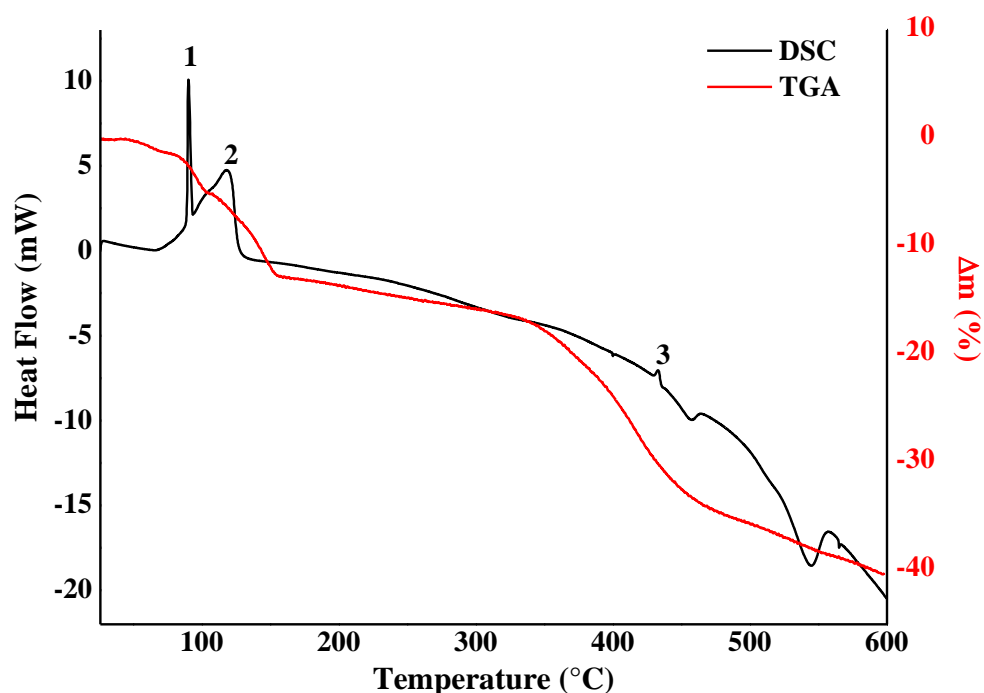


Figure 3.6.1. DSC and TGA curves of $[\text{Eu}(\text{H}_2\text{O})_5][\text{B}(\text{CN})_4]_3 \cdot 0.5 \text{H}_2\text{O}$. Program: 25–600 °C, 5 K/min.

The DSC curve of $[\text{Er}(\text{H}_2\text{O})_7][\text{B}(\text{CN})_4]_3$ shows three endothermic peaks and one exothermic peak (Fig. 3.6.2). The loss of the coordinated water molecules occurs at least in two steps. The first step begins at 63°C (onset) and ends at 85°C with a dehydration enthalpy of $62.6 \text{ kJ}\cdot\text{mol}^{-1}$. This corresponds to about 1.5 water molecules as the enthalpy⁷⁷ of evaporation of water at 70°C is $42.0 \text{ kJ}\cdot\text{mol}^{-1}$. The second step takes place between 120°C and 153°C with dehydration enthalpy of $215.5 \text{ kJ}\cdot\text{mol}^{-1}$. This equals to 5.5 water molecules as enthalpy⁷⁷ of water at 140°C is $38.6 \text{ kJ}\cdot\text{mol}^{-1}$. In the TG curve the corresponding mass losses are -5.6% ~ 2 H₂O and -13.1% ~ 4.6 H₂O. The third endothermic peak at 426°C (onset) with an energy of $3.7 \text{ kJ}\cdot\text{mol}^{-1}$ probably corresponds to the transition from crystalline state to amorphous one. It could also arise from the loss of residual water molecules, since the enthalpy of evaporation is very small above 400°C. The last peak at 542°C (onset) with an exothermic energy of $133.4 \text{ kJ}\cdot\text{mol}^{-1}$ is due to the decomposition of the compound. The drift at 522 °C in the DSC curve arises from a device error.

In the TG curve the mass loss related to the decomposition begins already at 320°C with total mass loss of -22.2%. DSC curves of $[\text{Er}(\text{H}_2\text{O})_7][\text{B}(\text{CN})_4]_3$ and $[\text{Dy}(\text{H}_2\text{O})_7][\text{B}(\text{CN})_4]_3$ were also recorded with a faster heating rate (10 K/min). The results are equal to the DSC curve

with a heating rate of 5 K/min. Because of the differences of the DSC and TG results, $[\text{Dy}(\text{H}_2\text{O})_7][\text{B}(\text{CN})_4]_3$ was heated in a quartz ampoule at 350°C for 3 hours at a pressure of $1 \cdot 10^{-6}$ mbar. The dysprosium salt changed from white to light brown and contained black spots after heating. Obviously, the decomposition of the compound starts already below 350°C . Furthermore, another sample of $[\text{Dy}(\text{H}_2\text{O})_7][\text{B}(\text{CN})_4]_3$ was also heated in a closed quartz ampoule at 400°C for one week. After that, the salt was completely black, which indicates the complete decomposition at 400°C . Therefore, the TG measurement seems to show the decomposition more accurately than the DCS measurement.

Such as the light rare earth tetracyanidoborates with $\text{RE} = \text{La}^{3+}\text{--Gd}^{3+}$, also the heavy rare earth tetracyanidoborates with $\text{RE} = \text{Tb}^{3+}\text{--Lu}^{3+}$, Y^{3+} are physically and chemically similar. Therefore, the thermal properties of dysprosium and erbium tetracyanidoborate are representative for all tetracyanidoborates with heavy rare earth metal cations in their bulk form. Thus, the thermal dehydration of these compounds can be conducted between 153°C and 320°C . At least six water molecules can be removed from the compound by heating.

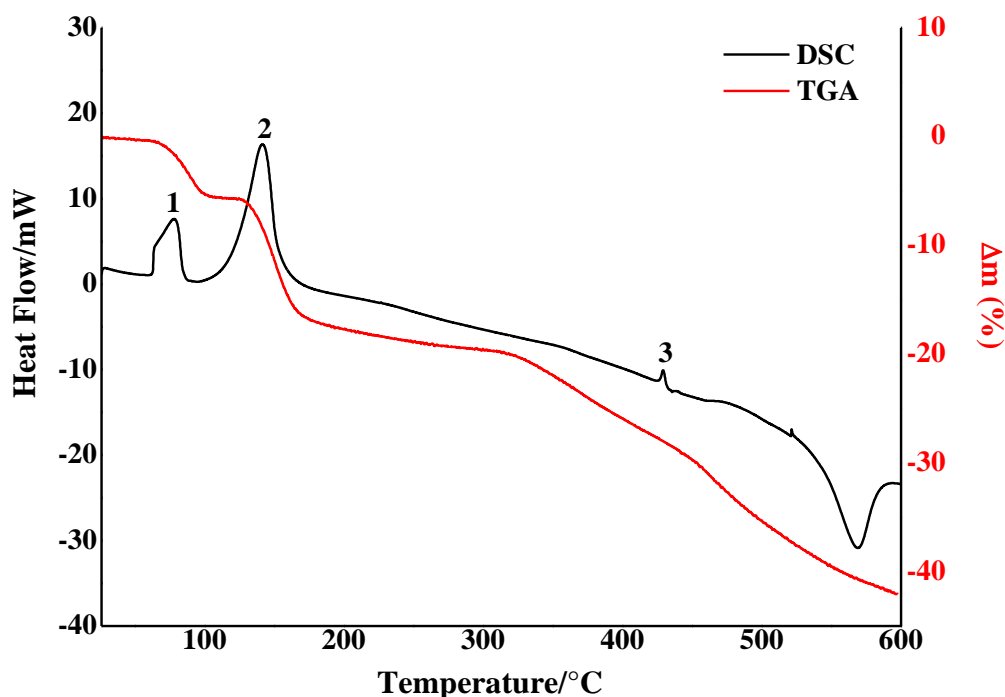


Figure 3.6.2. DSC and TGA curves of $[\text{Er}(\text{H}_2\text{O})_7][\text{B}(\text{CN})_4]_3$. Program: 25–600°C, 5 K/min.

3.7 Solubilities

The solubilities of all light rare earth tetracyanidoborates are very similar to the solubilities of the heavy rare earth tetracyanidoborates in water, acetonitrile and tetrahydrofuran (Table 3.7.1). The solubilities increase along with the polarity of the solvent. These compounds are also soluble in ethanol, acetone and dimethyl sulfoxide, DMSO, but insoluble in dichloromethane and chloroform. In comparison with other rare earth compounds, the solubility in water of rare earth tetracyanidoborates is considerably higher than the solubility of poorly water soluble rare earth phosphates⁷⁸ and carbonates⁷⁹, but much lower than the solubility of the highly soluble rare earth chlorides⁸⁰ and sulfates⁸¹.

Some rare earth compounds exhibit clear differences in solubility between light and heavy rare earth compounds. Generally, the water solubility of heavy rare earth compounds is better than the solubility of light rare earth compounds.^{80,81} Among the tetracyanidoborates exist slight differences in the solubilities between light and heavy rare earth compounds as well. However, this solubility trend is only valid in water and, e.g. in acetonitrile the average solubility of LRETCB is slightly higher than of HRETCB. In THF the solubility is about the same among all RETCB compounds. Compared to previously characterized tetracyanidoborates, the water solubility of the most alkali metal tetracyanidoborates⁹ and the solubility of the divalent $\text{Zn}[\text{B}(\text{CN})_4]_2$ and $\text{Cu}[\text{B}(\text{CN})_4]_2$ ¹³ is higher than the one of the rare earth tetracyanidoborates. Nevertheless, the water solubility of RETCBs is slightly higher than the one of the divalent $\text{Co}[\text{B}(\text{CN})_4]_2$ ¹⁴ and $\text{Fe}[\text{B}(\text{CN})_4]_2$ ⁸ and much higher than the solubility of monovalent $\text{Ag}[\text{B}(\text{CN})_4]$ and $\text{Cu}[\text{B}(\text{CN})_4]$ ⁹.

Table 3.7.1. Average solubilities in gL^{-1} (in mmolL^{-1}) of rare earth tetracyanidoborate in different solvents at 22°C. LRE = La^{3+} – Gd^{3+} , except Pm^{3+} . HRE = Tb^{3+} – Lu^{3+} and Y^{3+} .

compound	water	acetonitrile	tetrahydrofurane
$[\text{LRE}(\text{H}_2\text{O})_5][\text{B}(\text{CN})_4]_3 \cdot 0.5\text{H}_2\text{O}$	27.5 (44.4)	10.2 (17.3)	4.5 (7.7)
$[\text{HRE}(\text{H}_2\text{O})_7][\text{B}(\text{CN})_4]_3$	29.9 (47.3)	9.0 (14.3)	4.6 (7.3)

3.8 Optical absorption and emission properties

3.8.1 Preface

The luminescence properties of rare earth metal ions have been studied broadly in various hosts for years. To enhance the luminescence intensities the trivalent rare earth ions are traditionally doped into ultraviolet-light-absorbing host media, such as yttria which is probably the best host for rare earth ions due to the similarities in the chemical properties and ionic radius of rare earths.⁸² Furthermore, strongly absorbing chromophores are generally used to stimulate luminescence from rare earth ions. Ideally, these often aromatic ligands are directly coordinated to the rare earth center in order to induce a fast and efficient energy transfer. Although the spectral position of the emission lines is almost independent of the host lattice due to the shielding from the environment by the outer core 5s and 5p, the luminescence efficiency is largely dependent on the choice of host. Thus, it is important to study the luminescent properties of rare earth cations with different hosts.⁸³

Improvement of sensitivity and selectivity of luminescence detection methods plays an important role for the development of new REE based phosphors. Therefore, it is also necessary for the trace determination of the rare earth ions. In 1990 a new method, which utilizes counterions as energy absorbing and transferring compounds, was published.⁸⁴ In this method, the rare earth ion forms a complex with crown ether and an aromatic benzoate anions works as energy transferring counterion. The complexation with the synergistic extracting agent, crown ether, enables the extraction from the aqueous phase into the organic phase. The extraction prevents the luminescence quenching which originates from the high-energy vibrations of the OH groups. The luminescence efficiency can be even four times better in organic phase than in the aqueous one. Furthermore, when the rare earth ion is connected with a counterion, the luminescence efficiency gets 17 times better. This means that the elimination of the quenching effect and the improvement of the excitation of the rare earth ion can enhance the efficiency up to 67 times.⁸⁴

The smaller the energy gap between the ground state and emissive state of the rare earth ions is, the more efficient is the nonradiative decay through solvent or ligand vibrations, like OH, NH and CH. Thus, the luminescence of the Eu(III) ion is more sensitive against quenching

than the luminescence of the Tb(III) ion. The use of heavy water instead of ordinary water is one way to reduce the quenching effect of high-energy vibrating HO groups. The O-D vibrations of heavy water are energetic considerably lower ($\nu(\text{O-D}) = 2200 \text{ cm}^{-1}$) than those of the ordinary water ($\nu(\text{O-H}) = 3600 \text{ cm}^{-1}$). Furthermore, the lifetimes of luminescence are longer in heavy water than in the ordinary water.⁸⁵

There are three types of electronic transitions involving rare earth ions: sharp intra-configurational 4f-4f transitions, broader 4f-5d transitions and broad charge-transfer transitions (metal-to-ligand, MLCT or ligand-to-metal, LMCT). Not all transitions are permitted and allowed ones are described by selection rules. The Laporte's parity selection rule necessitates that states with the same parity cannot be connected by electric dipole (ED) transitions; thus, f-f-transitions are forbidden. Nonetheless, when a ligand-field influences on the rare earth ion, non-centrosymmetric interactions permit the mixing of electronic states of opposite parity into the 4f wavefunctions, which somewhat relaxes the selection rules and the transition becomes partially allowed. This process is called an induced (or forced) electric dipole transition.⁸⁵

The promotion of a 4f electron into the 5d sub-shell is parity allowed. Unlike the f-f transitions, these transitions are largely dependent on the environment. This is due to the 5d orbitals which are external and interact directly with the ligand orbitals. The 4f-5d transitions have high energies and are normally found for rare earth ions like Ce^{III}, Pr^{III} and Tb^{III}. The charge-transfer transitions, both LMCT and MLCT, are also allowed and have high energies as well. These transitions are common only for rare earth ions with high affinity of reduction, so that just the LMCT of Eu^{III} and Yb^{III} (possibly Sm^{III} and Tm^{III}) are commonly observed. Instead, this kind of transition is widespread for the d-transition metal ions. This is occasionally not well understood, and the literature features many wrong assignments to MLCT transitions made by analogy to d-metal complexes.^{85, 86}

Due to the adequate UV absorption properties of cyanido group, the tetracyanidoborate anion could work as a suitable counterion for RE ions. In the energy transfer process the band gap of the guest (RE³⁺) should fall within the band gap of the host (counterion) to favor transport of electrons from the host to the guest.⁸⁷ According to the UV-Vis measurements of tetracyanidoborates the energy gaps for $n_{\text{N}}^0 \rightarrow \pi_{\text{CN}}^*$ transitions of the anion are up to 6.1 eV.⁵ The energy gaps of the approximate energy levels related to the optical transitions in RE ions

are smaller than 4.3 eV.^{85, 88} Furthermore, it is well established that the energy gap between the triplet state of the counterion and the emissive level of RE ion plays an important role in effective charge transfer process. By extensive study on the energy gap it is experimentally proved that energy transfer process is much more effective in case if the energy gap between the triplet state and emissive level of RE ion is more than 0.25 eV.⁸⁹ The lowest triplet state energy of the tetracyanidoborat anion is 3.96 eV, whereas the commonly observed emissive levels of the RE ions (except Gd^{3+}) lie below 3.59 eV. This means that the energy gap between the triplet states of tetracyanidoborate anion and the emissive states of RE ions is larger than 0.25 eV.^{5,88} Therefore, an effective energy transfer can occur between the tetracyanidoborate anion and the most rare earth ions.

Excitation of trivalent RE ion is two-step process (Fig. 3.8.1.1); firstly the counterion is excited from the ground state to the first excited state (S_1) under ultraviolet wavelength irradiation which further relaxes to lower vibrational level of excited state rapidly. From here it can relax either by non-radiatively (NR) or radiatively by releasing energy as photons through fluorescence (F) or can undergo non-radiative inter system crossing (ISC) to triplet state (T_1), which can also be deactivated radiatively by spin forbidden transition called as phosphorescence (P). Secondly, the energy can be transferred from triplet state of counterion non-radiatively through an intramolecular energy-transfer (ET) process to the excited states of RE^{3+} (f^* , f^{**} ,...). Both the singlet and triplet state of a counterion can transfer energy to the excited state of rare earth ion, but due to short lifetime of singlet state the direct energy transfer from this state is not so significant.⁸⁹

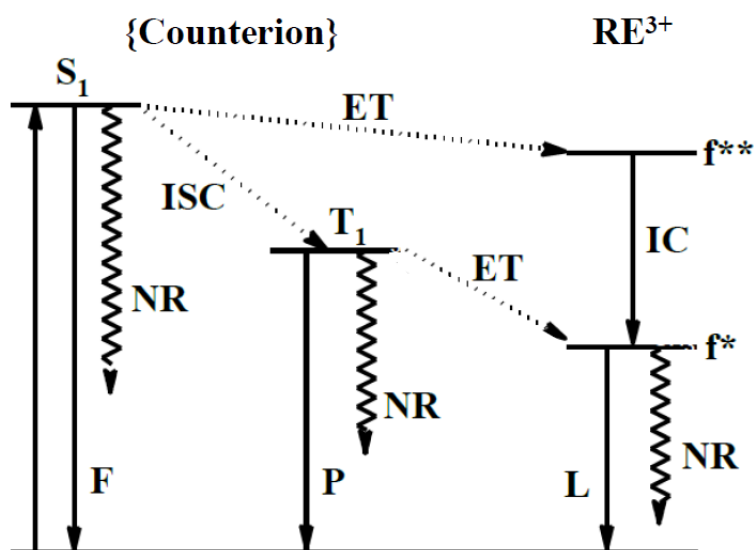


Figure 3.8.1.1. Energy transfer diagram of the excitation process of rare earth ion.

The tetracyanidoborate anion coordinates with the rare earth cations which also increase the possibility for an efficient energy transfer between the anion and cation. Furthermore, the anion does not contain high energy vibrational groups and the dehydration of the rare earth tetracyanidoborates eliminates the nonradiative effect of the OH oscillators of the water molecules. Another possible quenching mechanism might be expected due to energy transfer between two adjacent RE^{3+} ions. However, this strong concentration quenching is only possible if the RE^{3+} - RE^{3+} distance is 5 Å or shorter. After dehydration of the heavy rare earth tetracyanidoborates, the cations have to be coordinated by more tetracyanidoborate anions to maintain the high coordination number of the cation. Thus, presumably there is going to be at least one tetracyanidoborate between two RE^{3+} ions. The length of the tetracyanidoborate anion is 4.5 Å on the average. Moreover, the N- RE^{3+} bond lengths are about 2.5 Å. This means that the distance between two rare earth ions in $\text{RE-C}\equiv\text{N-B-C}\equiv\text{N-RE}$ plane has to be at least $(4.5+2\cdot 2.5)\text{Å} = 9.5\text{ Å} > 5\text{ Å}$. However, there is no evidence that the RE^{3+} - RE^{3+} distance is always more than 5 Å. Therefore, the energy migration through exchange interaction cannot be ruled out.

3.8.2 Preparation of the samples: Dehydration

All compounds were dried under vacuum stepwise at first at ca. 100°C for a couple of hours and afterwards at ca. 160 °C over a period of 12 hours. In case of dysprosium and samarium compounds, the samples were prepared by dissolving a dried RETCB ($\text{RE} = \text{Dy}^{3+}$ or Sm^{3+}) about 140 mg into 20 mL dry acetonitrile and heating the solution under reflux for 30 minutes. Both the dissolution and reflux occurred under argon atmosphere. The europium and terbium liquid samples were prepared by placing about 180 mg dried RETCB ($\text{RE} = \text{Eu}^{3+}$ or Tb^{3+}) into a 100 mL flask which was added to a dry Soxhlet apparatus in glovebox and the Soxhlet chamber were filled with 3 Å molecular sieves. Consequently, the Soxhlet apparatus with the flask containing a rare earth compound was connected to a Schlenk line and flushed with argon. 80 mL dry acetonitrile was added subsequently into the 100 ml flask under argon atmosphere. The acetonitrile was heated and mixed with a magnetic stir bar to improve the solubility of the RETCB. The heated solvent vapour traveled up to a distillation arm and flooded into the chamber housing the molecular sieves. The sieves adsorbed the residual water originated from the RETCB. When the chamber was almost full, it automatically emptied with the solvent running back down to the distillation flask. This cycle was repeated

many times over 14 hours, so that the solution got as dry as possible. After that the solution was concentrated with aid of pressure to receive a saturated solution. The solution was also stored into a glovebox, where the cuvettes were also filled with the luminescence solutions for the measurements. Additionally to the measurements from the liquid samples, the luminescence properties were also studied from the thermally dried solid samples of europium and terbium tetracyanidoborates.

3.8.3 Properties of the dehydrated samples

The solubility of tetracyanidoborates with rare earth cations was found to decrease after dehydration. The solubility in acetonitrile of samarium, europium, terbium and dysprosium tetracyanidoborates was determined before and after dehydration (table 3.8.3.1). In all cases, the solubility decreases considerably after dehydration. The decreased solubility of dehydrated rare earth compounds is a commonly known fact among the rare earth compounds. Therefore, it is also expected in the rare earth tetracyanidoborates. Furthermore, the dehydrated compounds are very hygroscopic and should be stored under shielding gas in a glove box. This hygroscopicity comes from the strong oxophilicity of rare earth cations, which further originates from the high Lewis acidity of these cations.⁹⁰ Moreover, the dehydrated compounds exhibit presumable stronger luminescence, because the luminescence quenching through the high-energy vibrations of the OH groups is reduced.⁸⁴ Therefore, the dehydration of the rare earth tetracyanidoborates is an important procedure for preparing samples for the luminescence measurements.

Table 3.8.3.1. Solubilities in acetonitrile in gL^{-1} (in mmolL^{-1}) of some rare earth tetracyanidoborates at 22°C under atmospheric pressure before and after dehydration.

Compound	Before dehydration	After dehydration
SmTCB	14 (23)	6 (11)
EuTCB	20 (34)	12 (22)
TbTCB	13 (21)	6 (12)
DyTCB	19 (30)	7 (14)

3.8.4 UV–Vis absorbance measurements

The absorption spectra of samarium, europium, terbium und dysprosium tetracyanidoborates were recorded in acetonitrile in the UV–Vis range. The tetracyanidoborate anion absorbs in the UV-C range (Fig. 3.8.4.1) due to the $n_N^0 \rightarrow \pi_{CN}^*$ transitions of the anion. The absorption band around 198 nm, which is observable in spectra of all four rare earth compounds, is characteristic for $n_N^0 \rightarrow \pi_{CN}^*$ ($S = 0$) transition of tetracyanidoborate anion.⁵ The band at 219 nm is observable only in the spectrum of the terbium compound. It presumably corresponds to the 4f-5d transition of the Tb^{3+} , because this transition at 219 nm ($\nu = 45\,662\text{ cm}^{-1}$) is commonly observed.⁸⁵ The spectra of samarium and dysprosium tetracyanidoborates show another absorption band at 255 nm. This band cannot arise from the 4f-5d transition within the Sm^{3+} and Dy^{3+} ions, because these transitions are found at higher energies around 170 nm.⁸⁵ The band is also not typical for $[B(CN)_4]^-$ absorption.⁵ Therefore, it probably originates from the charge-transfer transition, N-RE³⁺. The absorption spectrum of europium tetracyanidoborate is featureless in the region of 200–350 nm. Therefore, possible transitions, which induce the absorption, could not be determined. Such a featureless absorption spectrum of a Eu^{3+} ion is also recorded for example from its Pybox complex.⁹¹

The absorption spectra of rare earth compounds is not dependent on the crystal structure, but on the 4f electronic structure of the rare earth elements.⁹² The absorption bands arising from the optical f-f-transitions from the ground state to the excited states appear most often between 300 and 500 nm. They are considerably weaker than the bands originating from the absorption of the tetracyanidoborate anion (Fig. 3.8.4.2). The characteristic absorption bands for Sm^{3+} are located at 345, 363, 375, 391, 402, 417, 464 and 478 nm and are associated to the transitions from $^6H_{5/2}$ to $^4K_{17/2}$, $^4D_{3/2}$, $^6P_{7/2}$, $^4L_{15/2}$, $^4G_{7/2}$, $^4P_{5/2}$, $^4I_{13/2}$ and $^4I_{11/2}$ respectively.^{93, 94} In the spectrum of europium tetracyanidoborate one sharp absorption band for Eu^{3+} is observable at 395 nm, which corresponds to the transition from the ground level 7F_0 to the excited level 5L_6 . Four other bands at 374, 380, 384 and 465 nm could be associated to the transitions from 7F_0 to 5G_4 , 5G_2 , 5G_1 , and 5D_2 levels.⁹⁵ In the absorption spectrum of terbium compound, there are weak bands between 350-380 nm which correspond to the intra-4f transitions of Tb^{3+} ion (7F_j - 5D_3).⁸⁶ The spectrum of $[Dy(H_2O)_n][B(CN)_4]_3$ shows sharp absorption bands at 326, 352, 365, 388 and 451 nm, which can be associated with the transitions from the ground state $^6H_{15/2}$ to the excited levels of $^6M_{17/2}$, $^6P_{7/2}$, $^4P_{3/2}$, $^4K_{17/2}$ and $^4I_{15/2}$.^{82,96}

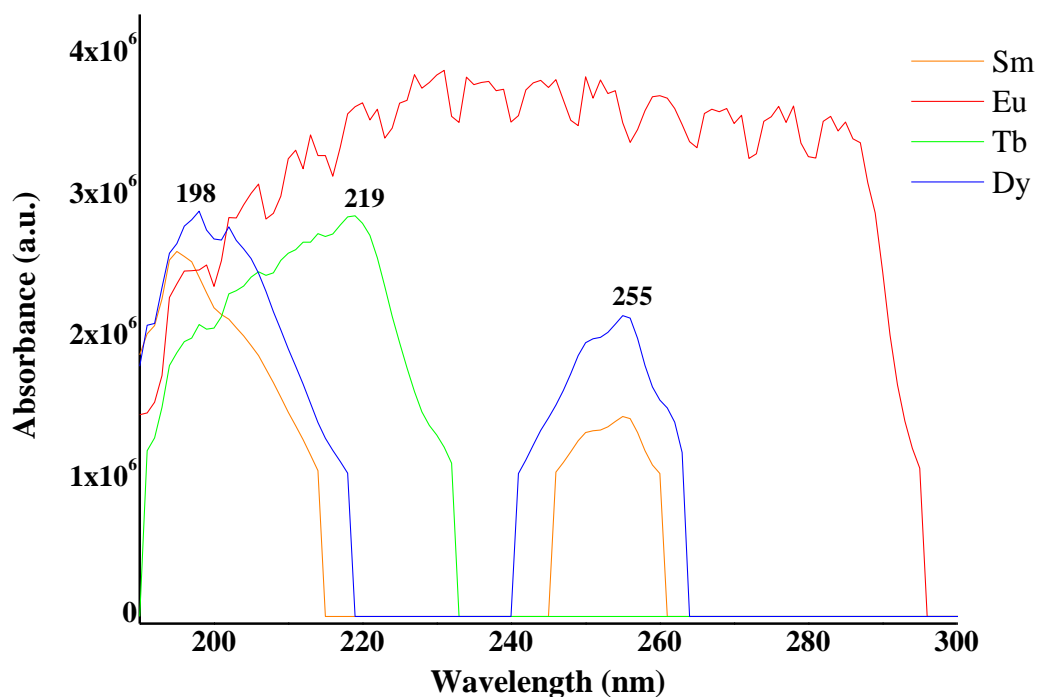


Figure 3.8.4.1. Absorption spectra of $[\text{LRE}(\text{H}_2\text{O})_n][\text{B}(\text{CN})_4]_3$, (LRE = Sm^{3+} , Eu^{3+} , $n = 1-1.5$) and $[\text{HRE}(\text{H}_2\text{O})_n][\text{B}(\text{CN})_4]_3$, (HRE = Tb, Dy, $n = 0.5-1$) in the range of 190–300 nm.

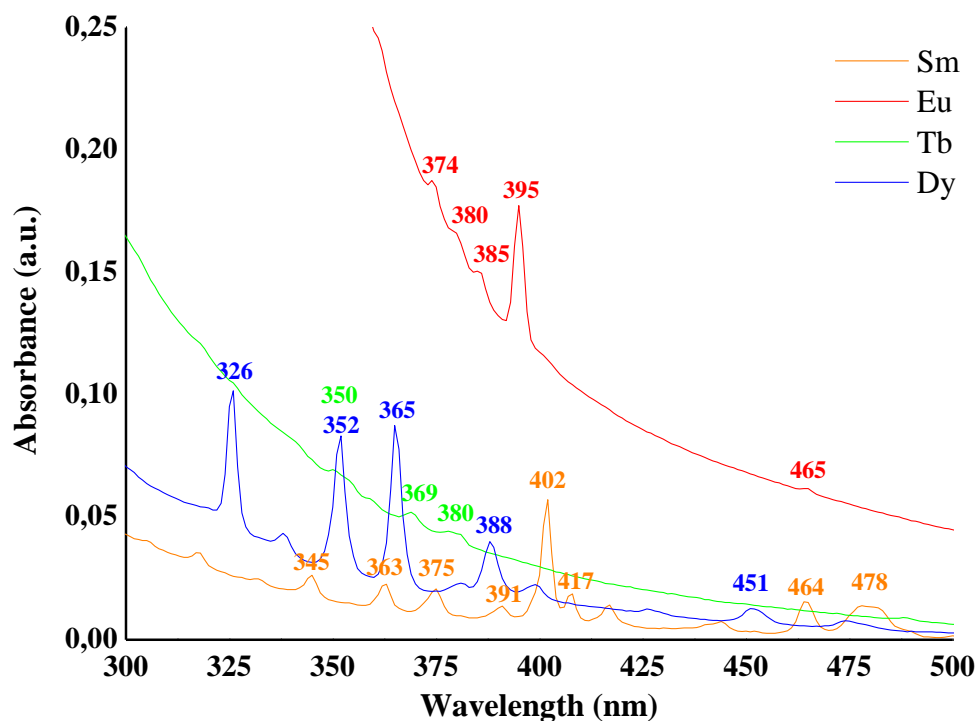


Figure 3.8.4.2. Absorption spectra of $[\text{LRE}(\text{H}_2\text{O})_n][\text{B}(\text{CN})_4]_3$, (LRE = Sm^{3+} , Eu^{3+} , $n = 1-1.5$) and $[\text{HRE}(\text{H}_2\text{O})_n][\text{B}(\text{CN})_4]_3$, (HRE = Tb, Dy, $n = 0.5-1$) in the range of 300–500 nm.

3.8.5 Excitation with ultraviolet lamp

$[\text{Eu}(\text{H}_2\text{O})_n][\text{B}(\text{CN})_4]_3 \cdot m\text{H}_2\text{O}$ was excited with an UV lamp before ($n = 5$, $m = 0.5$) and after ($n = 1-1.5$, $m = 0$) dehydration to examine the quenching effect from the high-energy vibrations of the OH groups (Figure 3.8.5.1).

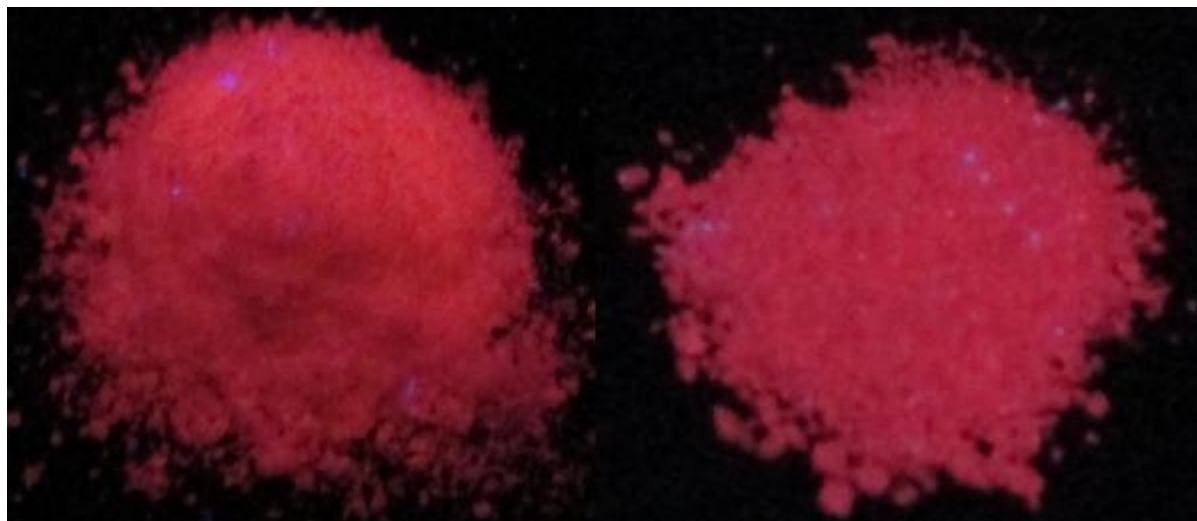


Figure 3.8.5.1. $[\text{Eu}(\text{H}_2\text{O})_5][\text{B}(\text{CN})_4]_3 \cdot 0.5 \text{H}_2\text{O}$ (left) and dried $[\text{Eu}(\text{H}_2\text{O})_n][\text{B}(\text{CN})_4]_3$ ($n = 1-1.5$) (right) under ultraviolet light, with excitation wavelength, $\lambda = 254 \text{ nm}$.

According to the thermal analysis, dehydration by heating removes at least 4 water molecules per each europium ion. The luminescence efficiency of Eu^{3+} should get considerably better after dehydration. However, there is no noticeable difference in the luminescence intensities before and after dehydration. One possible explanation for that could be the strong concentration quenching in the dehydrated compound. When the water molecules are removed from the compound it is presumable that the $\text{RE}^{3+}-\text{RE}^{3+}$ distances decrease, which activates the concentration quenching. This quenching depends strongly on the temperature being the most effective in high temperatures. Therefore, the dehydrated $[\text{Eu}(\text{H}_2\text{O})_n][\text{B}(\text{CN})_4]_3$ was cooled down with liquid nitrogen and compared with dehydrated $[\text{Eu}(\text{H}_2\text{O})_n][\text{B}(\text{CN})_4]_3$ at room temperature (Figure 3.8.5.2). Nevertheless, the temperature seems not to have much influence to the intensity of $[\text{Eu}(\text{H}_2\text{O})_n][\text{B}(\text{CN})_4]_3$ luminescence since the europium compounds, both the cooled one and the one at room temperature, exhibit equal intensities. However, this method is very inexact and, therefore, the concentration quenching should be determined more accurately from low-temperature luminescence measurements.

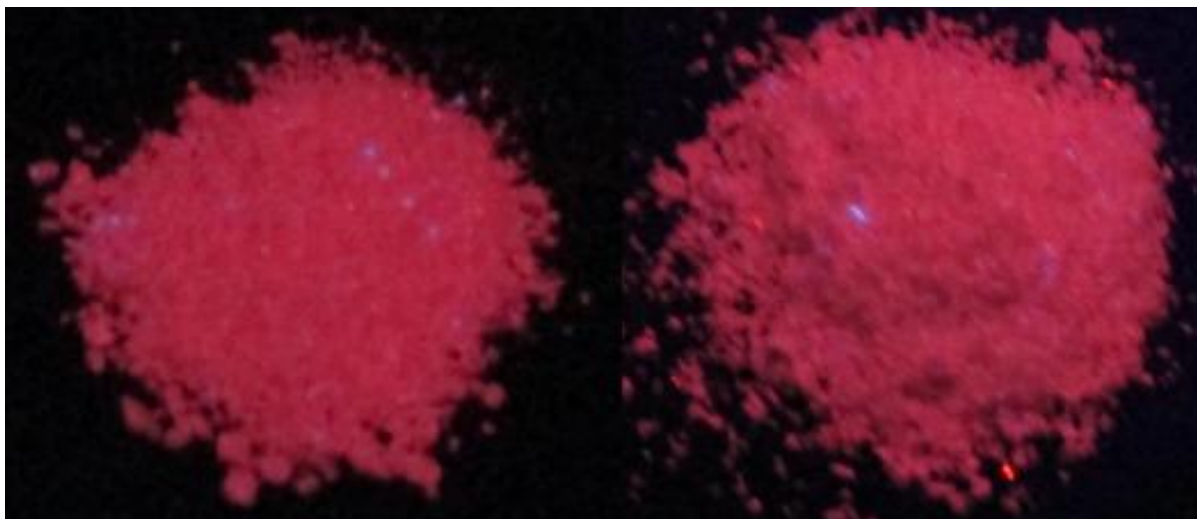


Figure 3.8.5.2. Dried $[\text{Eu}(\text{H}_2\text{O})_n][\text{B}(\text{CN})_4]_3$ ($n = 1-1.5$) in at 23°C (left) and cooled with liquid nitrogen (right) under ultraviolet light, with excitation wavelength, $\lambda = 254$ nm.

With the aid of the UV lamp, the samples were excited with two different wavelengths, 254 nm and 366 nm. Furthermore, the dehydrated sample was compared with a known $\text{Y}_2\text{O}_3:\text{Eu}^{3+}$ phosphor, which was synthesized and characterized according to reference 97. For both $[\text{Eu}(\text{H}_2\text{O})_n][\text{B}(\text{CN})_4]_3$ and $\text{Y}_2\text{O}_3:\text{Eu}^{3+}$ the more suitable excitation was with the short-wave UV, 254 nm (Figure 4.5.3.). This excitation makes the $\text{Y}_2\text{O}_3:\text{Eu}^{3+}$ phosphor glow very intensively, whereas the $[\text{Eu}(\text{H}_2\text{O})_n][\text{B}(\text{CN})_4]_3$ exhibits just a pink color but does not glow. Moreover, the color tone of these two europium compounds differs clearly from each other, which indicates that the characteristics f-f transitions of Eu^{3+} are differently activated. Therefore, these compounds induce emissions with dissimilar intensities.

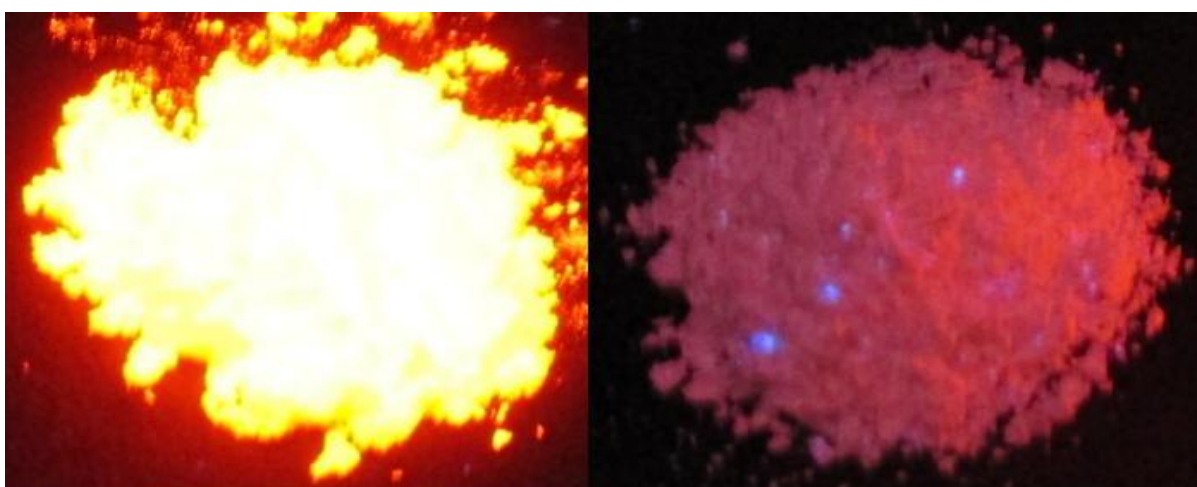


Figure 3.8.5.3. Standard phosphor $\text{Y}_2\text{O}_3:\text{Eu}^{3+}$ (left) and dried $[\text{Eu}(\text{H}_2\text{O})_n][\text{B}(\text{CN})_4]_3$ ($n = 1-1.5$) (right) under ultraviolet light, with excitation wavelength, $\lambda = 254$ nm.

Both $\text{Y}_2\text{O}_3:\text{Eu}^{3+}$ and $[\text{Eu}(\text{H}_2\text{O})_n][\text{B}(\text{CN})_4]_3$ were also excited with the UV light of 366 nm (Figure 3.8.5.4.). This excitation wavelength seems not to be as suitable as the excitation wavelength of 254 nm and for this reason the samples do not exhibit intensive luminescence. For $\text{Y}_2\text{O}_3:\text{Eu}^{3+}$ this result is expected, because the light of 366 nm is not able to induce the charge transfer $\text{Eu}^{3+}-\text{O}^{2-}$ which is responsible for Eu^{3+} excitation. Due to the excitation of 366 nm only the intraconfigurational 4f-4f transitions are possible. By reason of the small dipole strengths of f-f transitions, this kind of absorption rarely yields proper emissions.⁸⁵

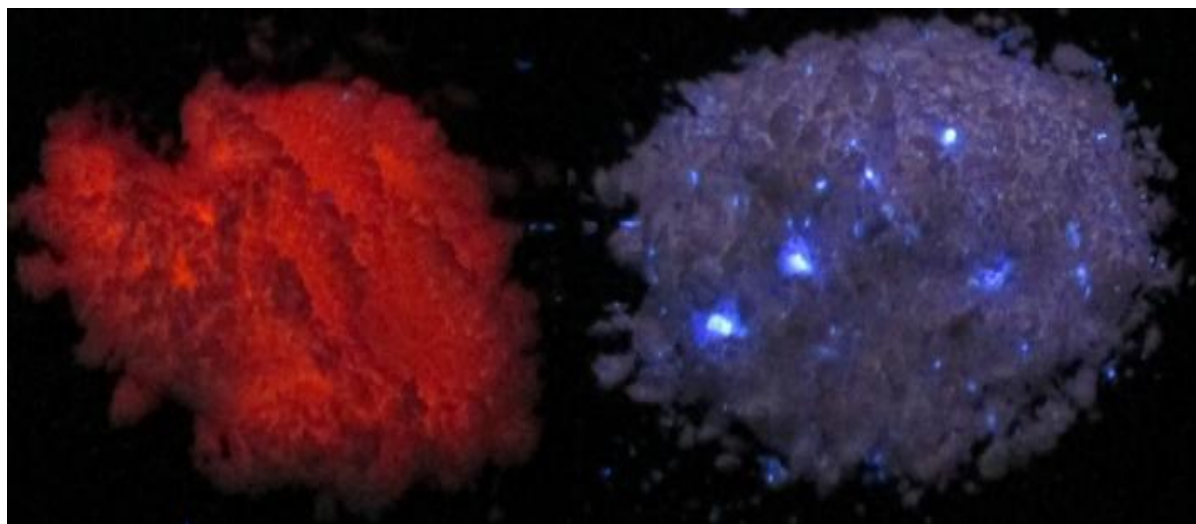


Figure 3.8.5.4. Standard phosphor $\text{Y}_2\text{O}_3:\text{Eu}^{3+}$ (left) and dried $[\text{Tb}(\text{H}_2\text{O})_n][\text{B}(\text{CN})_4]_3$ ($n = 1-0$) (right) under ultraviolet light, with excitation wavelength, $\lambda = 366$ nm.

$[\text{Tb}(\text{H}_2\text{O})_n][\text{B}(\text{CN})_4]_3$ was also excited with the UV lamp before ($n = 7$) and after ($n = 1-0$) dehydration to examine the quenching effect from the high-energy vibrations of the OH groups in the terbium compound (Figure 3.8.5.5). According to the thermal analysis, the dehydration removes six or more water molecules per each terbium ion. Unlike in the case of $[\text{Eu}(\text{H}_2\text{O})_n][\text{B}(\text{CN})_4]_3$, the dehydration increases considerably the luminescence efficiency this time. Whereas the hydrous powder exhibits just very weak green color, glows the dehydrated one intensively green under UV light. Thus, the concentration quenching activated by dehydration takes improbably place in the terbium compound.



Figure 3.8.5.5. $[\text{Tb}(\text{H}_2\text{O})_7][\text{B}(\text{CN})_4]_3$ (left) and dried $[\text{Tb}(\text{H}_2\text{O})_n][\text{B}(\text{CN})_4]_3$ ($n = 1-0$) (right) under ultraviolet light, with excitation wavelength, $\lambda = 254$ nm.

Similar to $[\text{Eu}(\text{H}_2\text{O})_n][\text{B}(\text{CN})_4]_3$, the dehydrated terbium compound was excited with two different wavelengths, 254 nm and 366 nm, and were compared with the known $\text{Y}_2\text{O}_3:\text{Eu}^{3+}$ phosphor. Since the luminescence intensity was compared and not the color tone of the luminescence, the europium phosphor was qualified as reference for terbium compound, too. The short-wave UV excitation of 254 nm was also more suitable for the $[\text{Tb}(\text{H}_2\text{O})_n][\text{B}(\text{CN})_4]_3$ (Figure. 3.8.5.6). This excitation makes both the $\text{Y}_2\text{O}_3:\text{Eu}^{3+}$ and the terbium compound glow equal intensively, which indicates that the $[\text{Tb}(\text{H}_2\text{O})_n][\text{B}(\text{CN})_4]_3$ could work as an adequate green phosphor.

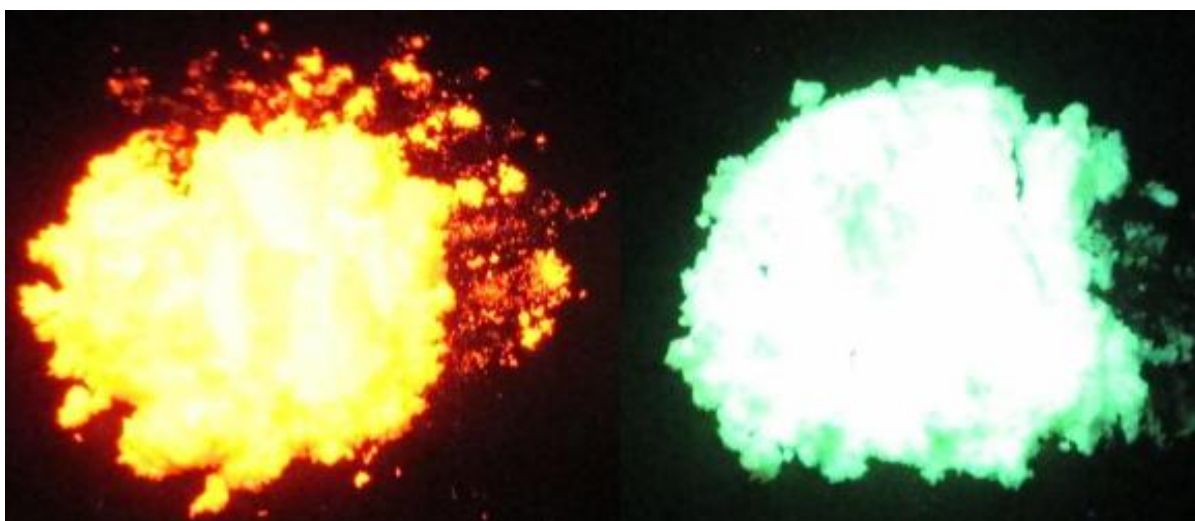


Figure 3.8.5.6. Standard phosphor $\text{Y}_2\text{O}_3:\text{Eu}^{3+}$ (left) and dried $[\text{Tb}(\text{H}_2\text{O})_n][\text{B}(\text{CN})_4]_3$ ($n = 1-0$) (right) under ultraviolet light, with excitation wavelength, $\lambda = 254$ nm.

Under long-wave UV light of 366 nm, neither the $[\text{Tb}(\text{H}_2\text{O})_n][\text{B}(\text{CN})_4]_3$ nor $\text{Y}_2\text{O}_3:\text{Eu}^{3+}$ were activated properly (Figure 3.8.5.7.). They do not glow, but emit only weak light of characteristic colors. The charge-transfers or 4f-5d transitions, which are responsible for the absorption of these compounds, occur normally below the long-wave UV range.

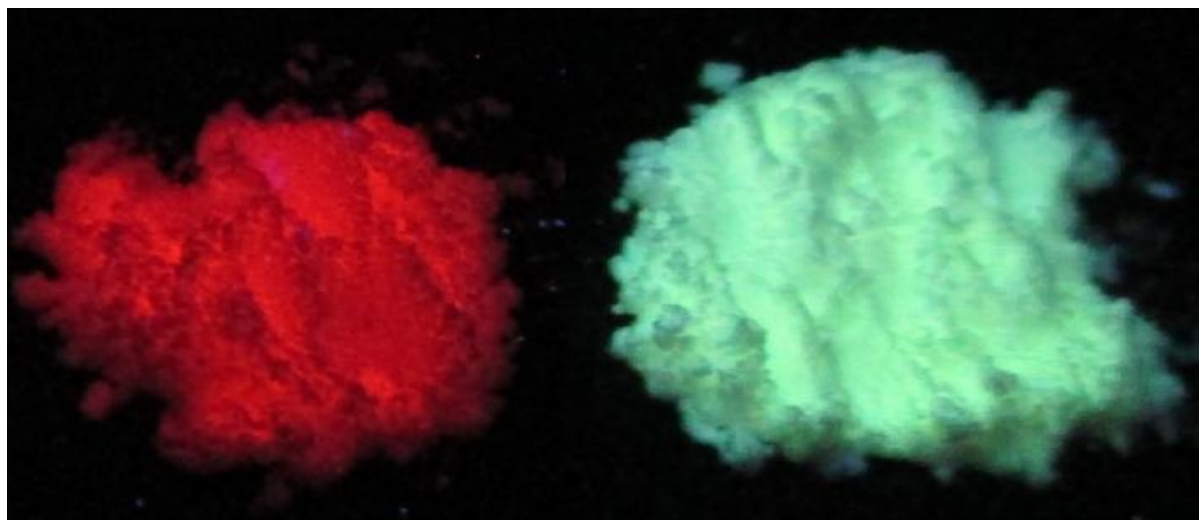


Figure 3.8.5.7. Standard phosphor $\text{Y}_2\text{O}_3:\text{Eu}^{3+}$ (left) and dried $[\text{Tb}(\text{H}_2\text{O})_n][\text{B}(\text{CN})_4]_3$ ($n = 1-0$) (right) under ultraviolet light, with excitation wavelength, $\lambda = 366$ nm.

3.8.6 Luminescence measurements

Since Sm^{III} , Eu^{III} , Tb^{III} and Dy^{III} ions exhibit typically emissions in the range of visible light, luminescence of tetracyanidoborates with these cations were measured. The measurements were done from saturated anhydrous acetonitrile solutions. Additionally, the luminescence measurements of europium and terbium tetracyanidoborates were performed of dried solid samples.

The excitation and emission spectra of $[\text{Eu}(\text{H}_2\text{O})_n][\text{B}(\text{CN})_4]_3$ powder are shown in Figure 3.8.6.1. Both spectra consist of sharp bands which are characteristic for the intraconfigurational 4f-4f transitions. Thus, an induced or forced ED transition occurs in $[\text{Eu}(\text{H}_2\text{O})_n][\text{B}(\text{CN})_4]_3$ (see page 54). Sharp excitation bands at 297, 316, 360, 373, 378, 384, 393 and 464 nm correspond to transitions of Eu^{3+} from the ground level $^5\text{F}_0$ to excited levels $^5\text{H}_1$ (297), $^5\text{H}_6$ (316), $^5\text{D}_4$ (360), $^5\text{G}_4$ (373), $^5\text{G}_2$ (378), $^5\text{G}_1$ (384), $^5\text{L}_6$ (393) and $^5\text{D}_2$ (464).⁹⁵ The transition $^5\text{F}_0 \rightarrow ^5\text{L}_6$ at 393 nm was found to be responsible for the excitation of Eu^{3+} and best emission intensities were achieved with this excitation wavelength.

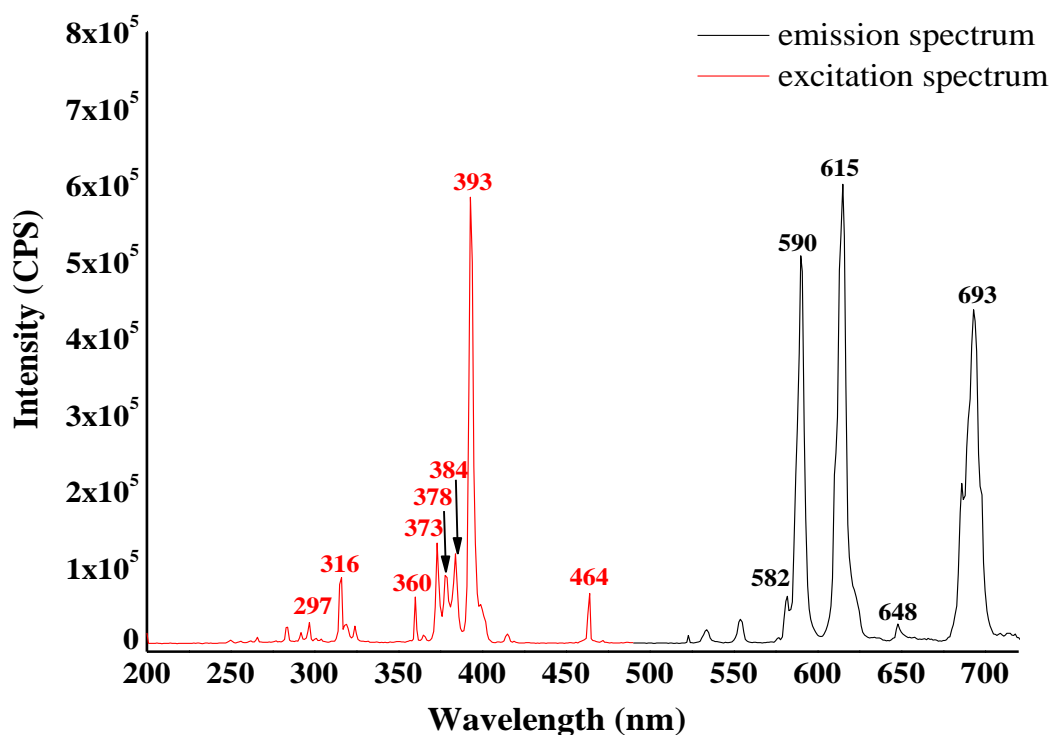


Figure 3.8.6.1. Excitation ($\lambda_{em}=615$ nm) and emission ($\lambda_{exc}=393$ nm) spectra of $[\text{Eu}(\text{H}_2\text{O})_n][\text{B}(\text{CN})_4]_3$ powder.

The emission spectrum (Fig. 4.6.1) of $[\text{Eu}(\text{H}_2\text{O})_n][\text{B}(\text{CN})_4]_3$ shows five typical emission bands for Eu^{3+} ion, which can be attributed to the electronic transitions of ${}^5\text{D}_0 \rightarrow {}^7\text{F}_0$ (582), ${}^5\text{D}_0 \rightarrow {}^7\text{F}_1$ (590), ${}^5\text{D}_0 \rightarrow {}^7\text{F}_2$ (615), ${}^5\text{D}_0 \rightarrow {}^7\text{F}_3$ (648) and ${}^5\text{D}_0 \rightarrow {}^7\text{F}_4$ (693). The transition ${}^5\text{D}_0 \rightarrow {}^7\text{F}_2$ has the strongest intensity. This is also the case for example in $\text{Y}_2\text{O}_3:\text{Eu}^{3+}$ phosphor⁹⁷ and in europium-containing copolymer, poly[MMA-MA-co-Eu(TTA)₂phen]⁹⁸. However, in these two europium compounds the other transitions are very weak, whereas in $[\text{Eu}(\text{H}_2\text{O})_n][\text{B}(\text{CN})_4]_3$ also the ${}^5\text{D}_0 \rightarrow {}^7\text{F}_1$ and ${}^5\text{D}_0 \rightarrow {}^7\text{F}_4$ are quite strong. It is acknowledged that the ${}^5\text{D}_0 \rightarrow {}^7\text{F}_2$ electric-dipole transition is very sensitive to relative small changes in the chemical surroundings of Eu^{3+} ions. The intensity of this transition is extremely affected by the degree in the center of symmetry in the environments around Eu^{3+} ions.

Inversely, the ${}^5\text{D}_0 \rightarrow {}^7\text{F}_1$ transition is allowed by magnetic-dipole considerations and therefore, it is rather insensitive to the local symmetry. Thus, the symmetry of the crystal sites, in which the Eu^{3+} ions are located, can be determined by the ratio of the ${}^5\text{D}_0 \rightarrow {}^7\text{F}_1$ and ${}^5\text{D}_0 \rightarrow {}^7\text{F}_2$ transitions.⁹⁹ Due to the fact that the electric dipole transition ${}^5\text{D}_0 \rightarrow {}^7\text{F}_2$ at 615 nm is dominant over the magnetic dipole transition ${}^5\text{D}_0 \rightarrow {}^7\text{F}_1$ at 590 nm, it can be assumed that the Eu^{3+} ions are located in a site without inversion symmetry in $[\text{Eu}(\text{H}_2\text{O})_n][\text{B}(\text{CN})_4]_3$, $\text{Y}_2\text{O}_3:\text{Eu}^{3+}$ and

poly[MMA-MA-co-Eu(TTA)₂phen]. However, in Eu³⁺-doped CaF₂ the ratio of the transitions is reverse indicating that the locations of Eu³⁺ ions are in a site with inversion symmetry.¹⁰⁰ Therefore, by using certain host materials for europium(III) ion, the color tone of Eu³⁺ emission can be changed to the desired direction.

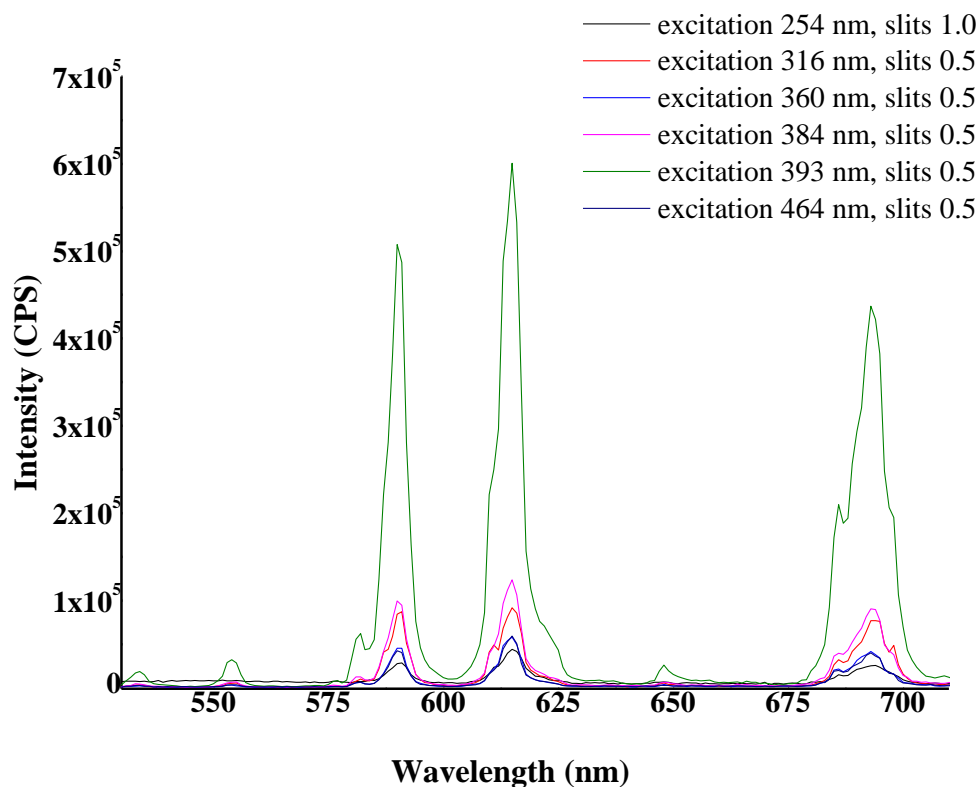


Figure 3.8.6.2. Emission spectra of [Eu(H₂O)_n][B(CN)₄]₃ powder with different excitation wavelengths and excitation and emission slits.

Considering the excitation with aid of an ultraviolet lamp, the excitation wavelength of 254 nm seems to be more adequate than the long wave excitation of 366 nm (Fig. 3.8.5.3 and 3.8.5.4). According to the excitation spectrum (Fig 3.8.6.1) neither 254 nm nor 366 nm is an advantageous excitation wavelength for [Eu(H₂O)_n][B(CN)₄]₃. However, the emission spectrum of the europium compound was recorded using all the potential excitations wavelengths to make sure that the optimal excitation occurs through the ⁵F₀→⁵L₆ transition. The emission spectra (Fig. 3.8.6.2.) show the superiority of 393 nm excitation. Only with this excitation also the weaker emission bands at 582 nm and 648 nm are observable. Furthermore, the excitation of 254 nm induces the weakest emission bands even though the emission and excitations slit widths are wider than in the measurements with other excitation

wavelengths. Therefore, the excitation wavelength of 393 nm is really the ideal one and the transition ${}^5F_0 \rightarrow {}^5L_6$ is responsible for the optimal excitation of Eu^{3+} in $[\text{Eu}(\text{H}_2\text{O})_n][\text{B}(\text{CN})_4]_3$.

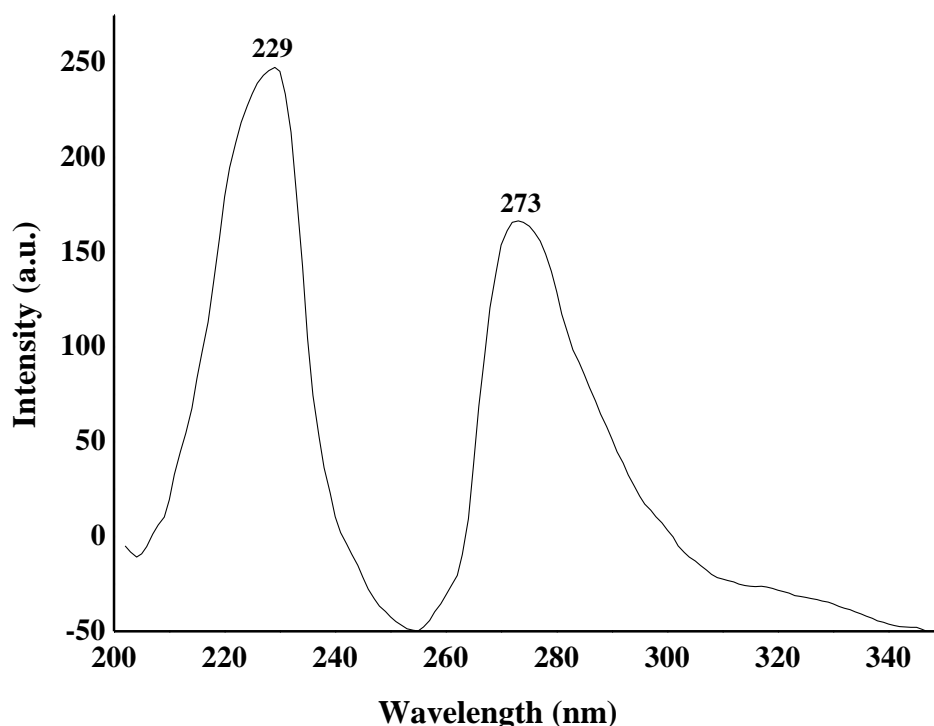


Figure 3.8.6.3. Excitation ($\lambda_{\text{em}} = 596 \text{ nm}$) spectrum of $[\text{Sm}(\text{H}_2\text{O})_n][\text{B}(\text{CN})_4]_3$ in acetonitrile $c \sim 6 \text{ g/l}$.

Photoluminescence properties of $[\text{Sm}(\text{H}_2\text{O})_n][\text{B}(\text{CN})_4]_3$ were measured in saturated acetonitrile solution. The excitation spectrum (Fig. 3.8.6.3) reveals two wide excitation bands which are typical for the N-Sm³⁺ charge-transfer transitions. Due to the higher intensity at 229 nm, this excitation wavelength was chosen for recording the emission spectrum (Fig. 3.8.6.4). In the spectrum appear four characteristic emission bands for the luminescence of Sm³⁺ ion at the wavelengths of 563, 596, 644 and 702 nm. These bands originate from the f-f-transitions from the excited state ${}^4G_{5/2}$ to the lower energetic states ${}^6H_{5/2}$ (560), ${}^6H_{7/2}$ (595), ${}^6H_{9/2}$ (640) and ${}^6H_{11/2}$ (700).⁸⁵

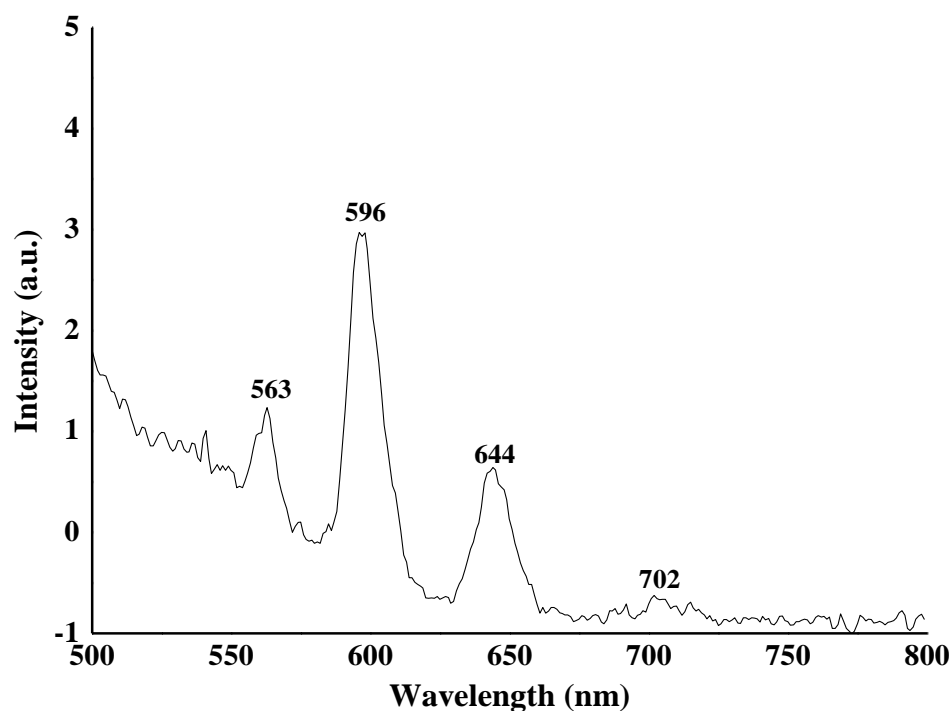


Figure 3.8.6.4. Emission spectrum ($\lambda_{\text{exc}} = 229 \text{ nm}$) of $[\text{Sm}(\text{H}_2\text{O})_n][\text{B}(\text{CN})_4]_3$ in acetonitrile $c \sim 6 \text{ g/l}$.

For the $[\text{Tb}(\text{H}_2\text{O})_n][\text{B}(\text{CN})_4]_3$ powder, the excitation wavelength of 254 nm was found optimal to receive a proper emission spectrum. The excitation spectrum monitored at 540 nm, consists of a broad band from 245 to 275 nm and a couple of sharp lines between 340–380 nm (Figure 3.8.6.5.). These sharp bands originate from intra-4f transitions of Tb^{3+} ion (${}^7\text{F}_j - {}^5\text{D}_3$). The broad band could correspond to the N- Tb^{3+} charge-transfer transition which forms unstable divalent Tb^{2+} in the excited state. Therefore, this transition is expected to be located in the high energy range (245-275 nm).⁸⁶ The narrow and sharp emission bands from 480 to 620 nm correspond to the transitions from the emissive state ${}^5\text{D}_4$ to the ${}^7\text{F}_6$ (486 nm), ${}^7\text{F}_5$ (542 nm), ${}^7\text{F}_4$ (580 nm), ${}^7\text{F}_3$ (618 nm), ${}^7\text{F}_2$ (643 nm), ${}^7\text{F}_1$ (663 nm) and ${}^7\text{F}_0$ (674 nm) levels.⁸⁵

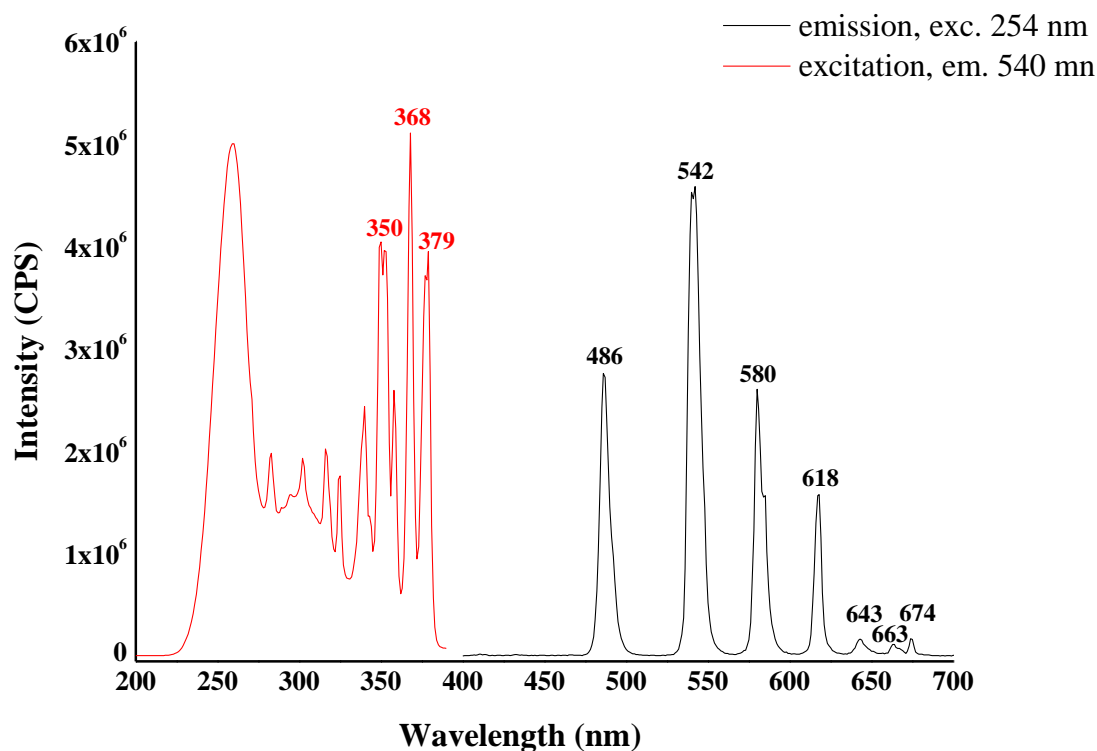


Figure 3.8.6.5. Emission and excitation spectra of [Tb(H₂O)_n][B(CN)₄]₃ powder.

The emission spectrum of [Tb(H₂O)_n][B(CN)₄]₃ was also recorded from the anhydrous acetonitrile solution and compared with the result of [Tb(H₂O)_n][B(CN)₄]₃ powder (Figure 3.8.6.6). The emission bands originating from the transitions $^5D_4 \rightarrow ^7F_J$ ($J = 3-6$) exist precisely on the same wavelengths. The weak bands from the $^5D_4 \rightarrow ^7F_J$ ($J = 1, 2$) can only be perceived in the emission spectrum measured from the powder. Furthermore, the emissions of Tb³⁺ from the acetonitrile solution are very weak in comparison to the ones from the powder. This is due to the lower concentration of Tb³⁺ in [Tb(H₂O)_n][B(CN)₄]₃ acetonitrile solution ($c([\text{Tb}(\text{H}_2\text{O})_n][\text{B}(\text{CN})_4]_3) \sim 6 \text{ g/l} \rightarrow c(\text{Tb}^{3+}) \sim 1.9 \text{ g/l} \rightarrow 0.19\%$). The mass fraction is about 32% in the powder, and therefore 160 times greater than in the solution. Moreover, the high-energy vibrations of C-H in the acetonitrile quench luminescence. Besides, the scattering of light in solids differs from the scattering in liquids. Therefore, the luminescence efficiency from powder is not comparative to the efficiency from solution. Due to the fact that the fluorescence quantum yield was possible to determinate only from the solution, the comparison between the powder and solution was done to demonstrate the superior fluorescence properties of the powdery sample.

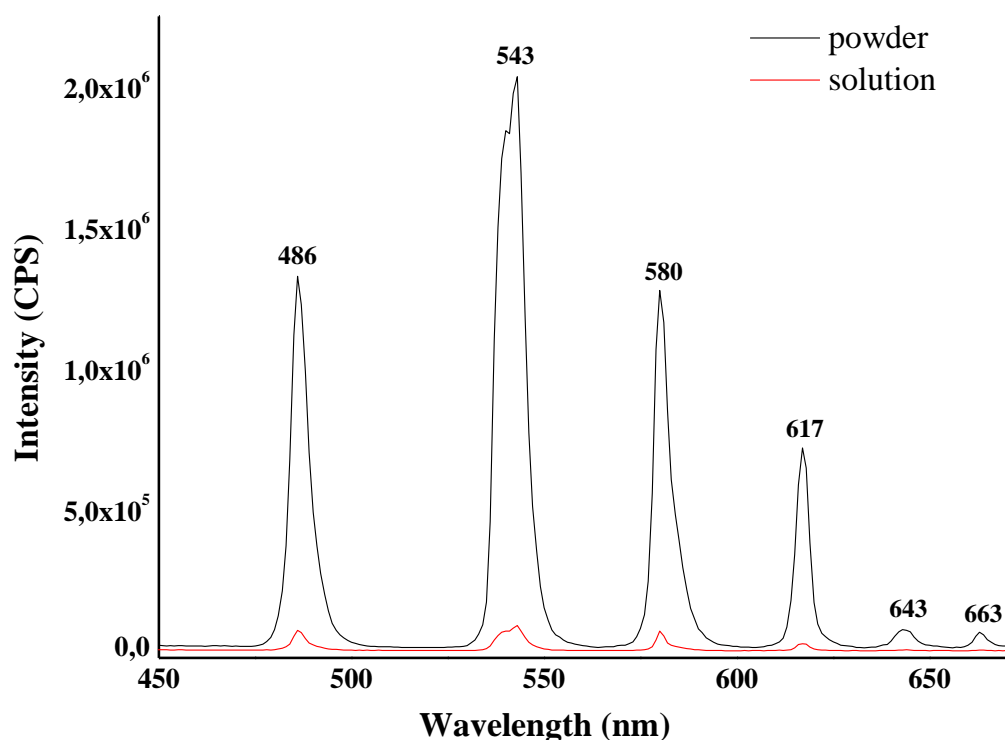


Figure 3.8.6.6. Emissionspectra of $[\text{Tb}(\text{H}_2\text{O})_n][\text{B}(\text{CN})_4]_3$ powder and acetonitrile solution, $c \sim 6$ g/l. Excited at 350 nm.

The fluorescence quantum yield of the $[\text{Tb}(\text{H}_2\text{O})_n][\text{B}(\text{CN})_4]_3$ in anhydrous acetonitrile was determined from the equation 3.8.6.1, where QY is the quantum yield of $[\text{Tb}(\text{H}_2\text{O})_n][\text{B}(\text{CN})_4]_3$, QY_{ref} is the quantum yield of quinine bisulphate (QBS) in H_2SO_4 ($\text{QY}_{\text{ref}} = 0.52^{100}$), n is the refractive index of CH_3CN ($n = 1.344$), n_{ref} is the refractive index of 0.05 M H_2SO_4 ($n_{\text{ref}} = 1.333$), I is the integrated intensity of $[\text{Tb}(\text{H}_2\text{O})_n][\text{B}(\text{CN})_4]_3$ emission peak at 543 nm, I_{ref} is the integrated intensity of QBS, A is the absorbance of $[\text{Tb}(\text{H}_2\text{O})_n][\text{B}(\text{CN})_4]_3$ in CH_3CN at the exciting wavelength, $\lambda = 350$ nm and A_{ref} is the absorbance of QBS in H_2SO_4 at the exciting wavelength, $\lambda = 350$ nm.

$$\text{QY} = \text{QY}_{\text{ref}} \frac{n^2}{n_{\text{ref}}^2} \frac{I}{A} \frac{A_{\text{ref}}}{I_{\text{ref}}} \quad (3.8.6.1)$$

The absorbance of both $[\text{Tb}(\text{H}_2\text{O})_n][\text{B}(\text{CN})_4]_3$ in CH_3CN and QBS in H_2SO_4 was measured to be 0.09 at 350 nm. The intensities from the emission maxima (Figure 3.8.6.7) were integrated and added to the equation. With this determination manner, the quantum yield of

$[\text{Tb}(\text{H}_2\text{O})_n][\text{B}(\text{CN})_4]_3$ in anhydrous acetonitrile is only 1.3%, which is pretty low for a rare earth phosphor. The high-energy vibrations of C-H in the acetonitrile certainly quench luminescence and partly weaken the quantum yield. Furthermore, the comparison with the $\text{Y}_2\text{O}_3:\text{Eu}^{3+}$ phosphor (Figure 3.8.5.6.) expresses better efficiency which with the quantum yield of 1.3% to assume is. Therefore, the quantum yield of $[\text{Tb}(\text{H}_2\text{O})_n][\text{B}(\text{CN})_4]_3$ should be measured from the anhydrous powder to obtain an absolute result. Unfortunately, a quantum yield measurement directly from the powdery sample was not possible to execute, because of the lack of measuring devices. Thus, it can just be speculated that the real quantum yield of $[\text{Tb}(\text{H}_2\text{O})_n][\text{B}(\text{CN})_4]_3$ is a lot of better than 1.3%.

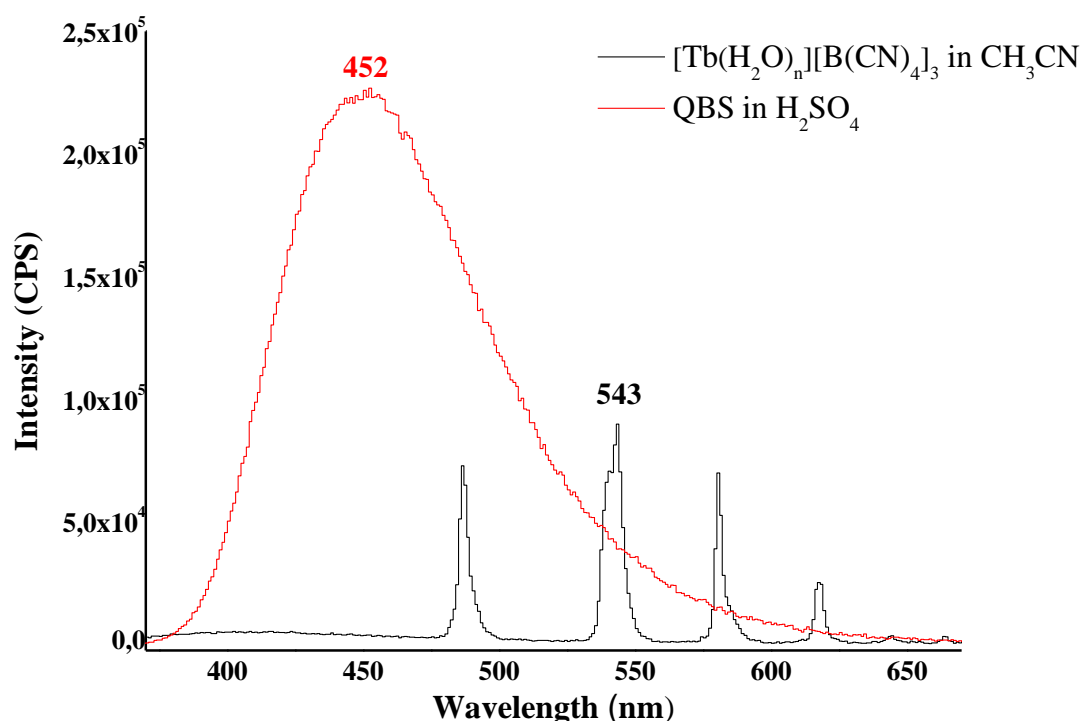


Figure 3.8.6.7. Emissionspectra of $[\text{Tb}(\text{H}_2\text{O})_n][\text{B}(\text{CN})_4]_3$ acetonitrile solution, $c \sim 6$ g/l and QBS in 0.05 M H_2SO_4 with excitation wavelength of 350 nm.

The lifetime of Tb^{3+} luminescence in $[\text{Tb}(\text{H}_2\text{O})_n][\text{B}(\text{CN})_4]_3$ was determined to be in the millisecond range by means of time-resolved streak camera measurements. Because of the repetitions rate of the used laser, a time range long enough was not able to cover for the determination of an accurate response time. Thus, the accurate lifetime could not be measured, but it probably lies in the milliseconds time range. The rare-earth based luminescent materials have usually long luminescence lifetimes due to f-f-electron inner shell

transitions. These transitions are parity forbidden for electric dipole emission and, therefore, they induce long lifetimes.¹⁰¹ Thus, the measured lifetime is reasonable and the $[\text{Tb}(\text{H}_2\text{O})_n][\text{B}(\text{CN})_4]_3$ exhibits predictably phosphorescence.

The excitation spectrum of $[\text{Dy}(\text{H}_2\text{O})_n][\text{B}(\text{CN})_4]_3$ in acetonitrile ($c \sim 7 \text{ g/l}$) measured in the range 200–450 nm is shown in Fig. 3.8.6.8. It contains two intensive and broader excitation bands at 228 nm and 272 nm and four narrow bands between 320 and 410 nm. The broader bands originate probably from the N-Dy³⁺ charge-transfer transitions. The excitation wavelengths of these transitions were chosen for the emission spectra. The weaker and narrower excitation bands are characteristic for hypersensitive 4f-4f transitions from the ground level $^6\text{H}_{15/2}$ to the higher energetic $^4\text{M}_{17/2}$ (327 nm), $^6\text{P}_{7/2}$ (352 nm), $^4\text{I}_{11/2}$ (367 nm) and $^4\text{I}_{13/2}$ (389 nm) levels.⁸²

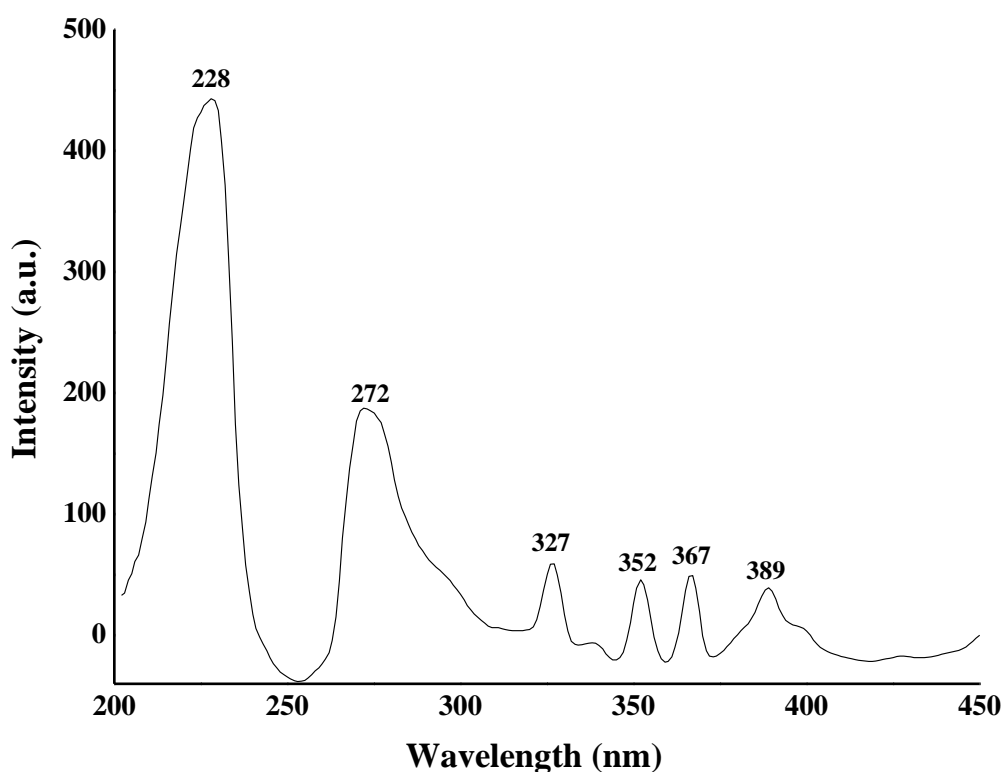


Figure 3.8.6.8. Excitation spectrum of $[\text{Dy}(\text{H}_2\text{O})_n][\text{B}(\text{CN})_4]_3$ in acetonitrile, $c \sim 7 \text{ g/l}$, monitored at 480 nm.

The excitation wavelength of 228 nm is more suitable for the Dy³⁺ emission of the $[\text{Dy}(\text{H}_2\text{O})_n][\text{B}(\text{CN})_4]_3$ in acetonitrile (Figure 3.8.6.9.). The excitation with 272 nm gives only very weak emission bands, whereas with 228 nm excitation also the weak red emissions at

656 and 749 nm are observable. The four emission bands correspond to the intraconfigurational transitions of Dy^{3+} ion from the emissive level ${}^4\text{F}_{9/2}$ to ${}^6\text{H}_J$ ($J = 15/2, 13/2, 11/2$ and $9/2$). The most intensive blue emission at 480 nm originates from ${}^4\text{F}_{9/2} \rightarrow {}^6\text{H}_{15/2}$. It is not that sensitive to the host like the yellow emission at 572 nm (${}^4\text{F}_{9/2} \rightarrow {}^6\text{H}_{13/2}$). The blue emission is slightly stronger than the yellow one. This indicates that the Dy^{3+} ion is located at a high symmetry with an inversion center. If the Dy^{3+} ion is located at a low symmetry without an inversion center the yellow emission is dominant.⁸² Thereby, in the $[\text{Dy}(\text{H}_2\text{O})_n][\text{B}(\text{CN})_4]_3$ the Dy^{3+} ion seems to be located at high symmetry with an inversion center and the tetracyanidoborate anion might not be the ideal host for dysprosium, if the yellow emission is desired. However, due to the fact that the mixing of blue and yellow light leads to white light and the intensities of blue and yellow emissions differ not that much from each other, the $[\text{Dy}(\text{H}_2\text{O})_n][\text{B}(\text{CN})_4]_3$ could possibly be applied in white phosphors.

The weaker red emission bands originate from the ${}^4\text{F}_{9/2} \rightarrow {}^6\text{H}_{11/2}$ (656 nm) and ${}^4\text{F}_{9/2} \rightarrow {}^6\text{H}_{9/2}$ (749 nm) transitions. In comparison with the approximate corresponding wavelengths for the intraconfigurational f-f transitions of Dy^{3+} ion given in ref. 85, the blue and yellow emissions are slightly red shifted. However, these emissions are found to be at even longer wavelengths in other dysprosium phosphors.^{82, 102}

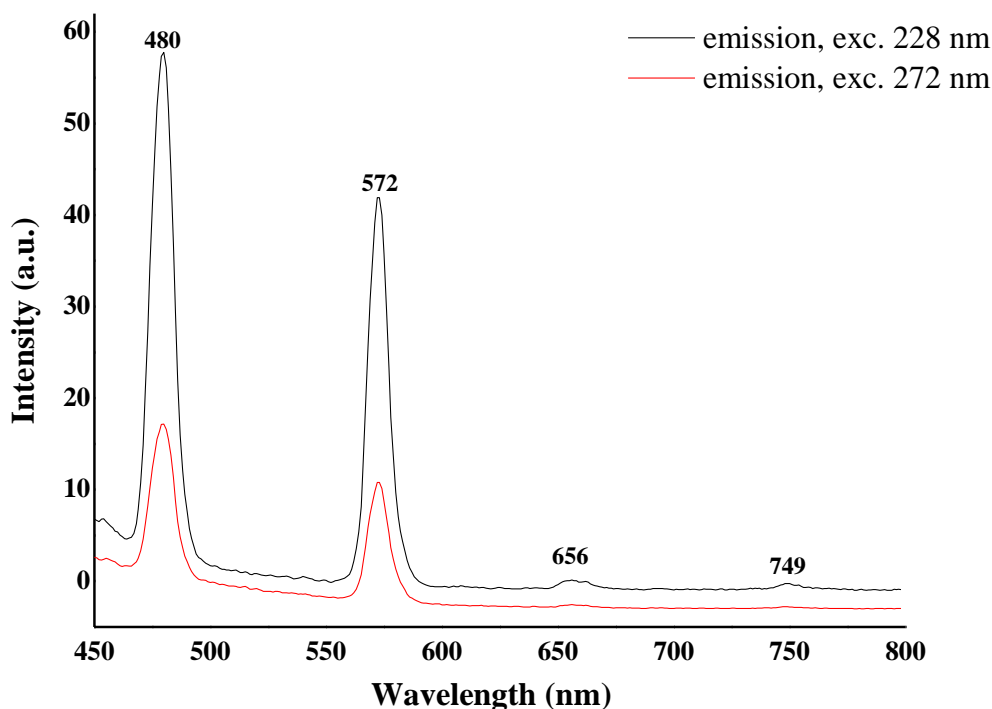


Figure 3.8.6.9. Emission spectra of Figure 3.5.4. Excitation spectrum of $[\text{Dy}(\text{H}_2\text{O})_n][\text{B}(\text{CN})_4]_3$ in acetonitrile, $c \sim 7$ g/l.

3.9 Experimental section

Syntheses of $[\text{LRE}(\text{H}_2\text{O})_5][\text{B}(\text{CN})_4]_3 \cdot 0.5 \text{H}_2\text{O}$. 5–10 mL 0.21–0.32 M $\text{H}[\text{B}(\text{CN})_4]$ (1.5– 3.2 mmol) were added to a 50 mL round-bottomed flask and an adequate amount of light rare earth oxide/hydroxide (molar ratio for acid to oxide was 6 to 1 and for acid to hydroxide 3 to 1) was added into the acid in small portions. The mixture was stirred with a magnet bar and heated in a water bath. The value of pH was controlled constantly with Unitest pH paper until the reaction was complete at pH 7.0. To receive a clear aqueous solution of rare earth tetracyanidoborate, the solution was filtered and the water was slowly evaporated at room temperature to obtain clear single crystals for X-ray structure determination. Besides Pr and Nd, the light rare earth metals form colorless crystals. $[\text{Pr}(\text{H}_2\text{O})_5][\text{B}(\text{CN})_4]_3 \cdot 0.5 \text{H}_2\text{O}$ is light green because of its Pr^{3+} . Furthermore, $[\text{Nd}(\text{H}_2\text{O})_5][\text{B}(\text{CN})_4]_3 \cdot 0.5 \text{H}_2\text{O}$ exhibits the same color-changing behavior seen in some other neodymium salts, being light magenta in normal daylight and colorless in artificial light.

The yield of $[\text{La}(\text{H}_2\text{O})_5][\text{B}(\text{CN})_4]_3 \cdot 0.5 \text{H}_2\text{O}$ was 4.874 g (80.91%). $\text{LaO}_{5.5}\text{H}_{11}\text{B}_3\text{C}_{12}\text{N}_{12}$ ($M = 582.662 \text{ g/mol}$): calcd. C 24.74, N 28.85, H 1.90; found C 24.50, N 27.65, H 1.89. IR (ATR, $\text{cm}^{-1} \nu_{\text{max}}$): 3332, 3234, 2256, 1639, 1133, 977, 933, 855, 601. The yield of $[\text{Ce}(\text{H}_2\text{O})_5][\text{B}(\text{CN})_4]_3 \cdot 0.5 \text{H}_2\text{O}$ was 109 mg (48.97%). $\text{CeO}_{5.5}\text{H}_{11}\text{B}_3\text{C}_{12}\text{N}_{12}$ ($M = 583.874 \text{ g/mol}$): calcd. C 24.68, N 28.79, H 1.90; found C 23.15, N 27.51, H 2.63. IR (ATR, $\text{cm}^{-1} \nu_{\text{max}}$): 3326, 3232, 2258, 1635, 974, 935, 851, 601. The yield of $[\text{Pr}(\text{H}_2\text{O})_5][\text{B}(\text{CN})_4]_3 \cdot 0.5\text{H}_2\text{O}$ was 142 mg (70.01%). $\text{PrO}_{5.5}\text{H}_{11}\text{B}_3\text{C}_{12}\text{N}_{12}$ ($M = 584.666 \text{ g/mol}$): calcd. C 24.65, N 28.76, H 1.90; found C 24.38, N 27.41, H 2.16. IR (ATR, $\text{cm}^{-1} \nu_{\text{max}}$): 3323, 3227, 2258, 1651, 1639, 976, 933, 849, 606. The yield of $[\text{Nd}(\text{H}_2\text{O})_5][\text{B}(\text{CN})_4]_3 \cdot 0.5 \text{H}_2\text{O}$ was 163 mg (48.09%). $\text{NdO}_{5.5}\text{H}_{11}\text{B}_3\text{C}_{12}\text{N}_{12}$ ($M = 588.000 \text{ g/mol}$): calcd. C 24.51, N 28.59, H 1.89; found C 23.67, N 27.57, H 2.20. IR (ATR, $\text{cm}^{-1} \nu_{\text{max}}$): 3332, 3233, 2258, 1635, 975, 933, 856, 590. The yield of $[\text{Sm}(\text{H}_2\text{O})_5][\text{B}(\text{CN})_4]_3 \cdot 0.5 \text{H}_2\text{O}$ was 339 mg (90.84%). $\text{SmO}_{5.5}\text{H}_{11}\text{B}_3\text{C}_{12}\text{N}_{12}$ ($M = 594.120 \text{ g/mol}$): calcd. C 24.26, N 28.30, H 1.87; found C 24.87, N 26.77, H 2.04. IR (ATR, $\text{cm}^{-1} \nu_{\text{max}}$): 3342, 3234, 2262, 1651, 1651, 1639, 976, 934, 852, 610. The yield of $[\text{Eu}(\text{H}_2\text{O})_5][\text{B}(\text{CN})_4]_3 \cdot 0.5 \text{H}_2\text{O}$ was 320 mg (64.49%). $\text{EuO}_{5.5}\text{H}_{11}\text{B}_3\text{C}_{12}\text{N}_{12}$ ($M = 595.704 \text{ g/mol}$): calcd. C 24.19, N 28.22, H 1.86; found C 23.77, N 26.91, H 2.22. IR (ATR, $\text{cm}^{-1} \nu_{\text{max}}$): 3334, 3234, 2266, 1633, 976, 934, 858, 590. The yield of $[\text{Gd}(\text{H}_2\text{O})_5][\text{B}(\text{CN})_4]_3 \cdot 0.5 \text{H}_2\text{O}$ was 438 mg (87.52%). $\text{GdO}_{5.5}\text{H}_{11}\text{B}_3\text{C}_{12}\text{N}_{12}$ ($M = 601.011 \text{ g/mol}$): calcd C 23.98 N

27.97, H 1.85; found C 23.20, N 26.68, H 1.91. IR (ATR, cm^{-1} ν_{max}): 3341, 3252, 2266, 1651, 976, 934, 855, 588.

Synthesis of $[\text{HRE}(\text{H}_2\text{O})_7][\text{B}(\text{CN})_4]_3$. 5–10 mL 0.21–0.32 M $\text{H}[\text{B}(\text{CN})_4]$ (1.5–3.2 mmol) were added in a 50 mL round-bottomed flask and an adequate amount of heavy rare earth oxide/hydroxide (molar ratio for acid to oxide was 6 to 1 and for acid to hydroxide 3 to 1) was added into the acid in small portions. The mixture was stirred with a magnet bar and heated in a water bath. The value of pH was controlled constantly with Unitest pH paper until the reaction was complete at pH 7.0. To receive a clear aqueous solution of rare earth tetracyanidoborate, the solution was filtered and the water was slowly evaporated to obtain clear single crystals for X-ray structure determination. Besides Ho and Er, the heavy rare earth metals form colorless crystals. $[\text{Ho}(\text{H}_2\text{O})_7][\text{B}(\text{CN})_4]_3$ exhibits the same color-changing behavior seen in another holmium salts, being yellow in natural lighting and bright pink in fluorescent lighting. $[\text{Er}(\text{H}_2\text{O})_7][\text{B}(\text{CN})_4]_3$ is pink because of its pink-colored Er^{3+} .

The yield of $[\text{Tb}(\text{H}_2\text{O})_7][\text{B}(\text{CN})_4]_3$ was 289 mg (81.6%). $\text{TbO}_7\text{H}_{14}\text{B}_3\text{C}_{12}\text{N}_{12}$ ($M = 629.712$ g/mol): calcd. C 22.89, N 26.70, H 2.24; found C 23.63, N 26.19, H 2.09. IR (ATR, cm^{-1} ν_{max}): 3230, 2268, 1661, 1634, 973, 937, 845, 623. The yield of $[\text{Dy}(\text{H}_2\text{O})_7][\text{B}(\text{CN})_4]_3$ was 777 mg (87.73%). $\text{DyO}_7\text{H}_{14}\text{B}_3\text{C}_{12}\text{N}_{12}$ ($M = 633.278$ g/mol): calcd. C 22.76, N 26.55, H 2.23; found C 23.25, N 24.98, H 1.86. IR (ATR, cm^{-1} ν_{max}): 3226, 2268, 1666, 1636, 974, 938, 846, 631. The yield of $[\text{Ho}(\text{H}_2\text{O})_7][\text{B}(\text{CN})_4]_3$ was 384 mg (98.8%). $\text{HoO}_7\text{H}_{14}\text{B}_3\text{C}_{12}\text{N}_{12}$ ($M = 635.712$ g/mol): calcd. C 22.67, N 26.45, H 2.22; found C 20.57, N 25.44, H 3.11. IR (ATR, cm^{-1} ν_{max}): 3226, 2266, 1633, 970, 934, 846, 633. The yield of $[\text{Er}(\text{H}_2\text{O})_7][\text{B}(\text{CN})_4]_3$ was 1.59 g (82.3%). $\text{ErO}_7\text{H}_{14}\text{B}_3\text{C}_{12}\text{N}_{12}$ ($M = 638.042$ g/mol): calcd. C 22.59, N 26.35 H 2.21; found C 22.70, N 24.69, H 2.51. IR (ATR, cm^{-1} ν_{max}): 3234, 2268, 1660, 1633, 968, 935, 844, 624. The yield of $[\text{Tm}(\text{H}_2\text{O})_7][\text{B}(\text{CN})_4]_3$ was 447 mg (81.2%). $\text{TmO}_7\text{H}_{14}\text{B}_3\text{C}_{12}\text{N}_{12}$ ($M = 639.712$ g/mol): calcd. C 22.53, N 26.28, H 2.21; found C 23.00, N 25.78, H 2.65. IR (ATR, cm^{-1} ν_{max}): 3226, 1667, 1634, 972, 936, 844, 628. The yield of $[\text{Yb}(\text{H}_2\text{O})_7][\text{B}(\text{CN})_4]_3$ was 182 mg (56.5%). $\text{YbO}_7\text{H}_{14}\text{B}_3\text{C}_{12}\text{N}_{12}$ ($M = 643.822$ g/mol): calcd. C 22.39, N 26.11, H 2.19; found C 21.76, N 24.14, H 2.38. IR (ATR, cm^{-1} ν_{max}): 3233, 1633, 968, 934, 845, 560. The yield of $[\text{Lu}(\text{H}_2\text{O})_7][\text{B}(\text{CN})_4]_3$ was 283.4 mg (62.7%). $\text{LuO}_7\text{H}_{14}\text{B}_3\text{C}_{12}\text{N}_{12}$ ($M = 645.752$ g/mol): calcd C 22.32, N 26.04 H 2.19; found C 22.43, N 25.11, H 2.53. IR (ATR, cm^{-1} ν_{max}): 3242, 2270, 1660, 1633, 968, 934, 846, 589. The yield of $[\text{Y}(\text{H}_2\text{O})_7][\text{B}(\text{CN})_4]_3$ was 178 mg (45.4%). $\text{YO}_7\text{H}_{14}\text{B}_3\text{C}_{12}\text{N}_{12}$ ($M = 559.692$ g/mol): calcd. C 25.75, N 30.04, H 2.52; found C 27.52, N 30.25, H 2.24. IR (ATR, cm^{-1} ν_{max}): 3233, 2270, 1666, 1639, 973, 936, 845, 631.

4 Conclusions

The lack of solubility of the rare earth starting materials is a noticeable limitation on synthesis of new rare earth compounds. Therefore, the reaction with the strong acid, $\text{H}[\text{B}(\text{CN})_4]$, has been found to be the most suitable method for obtaining rare earth tetracyanidoborate hydrates with high yields and high purities.

X-ray single crystal and powder diffraction analysis have shown that like the rare earth compounds in general, also the rare earth tetracyanidoborates form isostructural groups, like $[\text{LRE}(\text{H}_2\text{O})_5][\text{B}(\text{CN})_4]_3 \cdot 0.5 \text{ H}_2\text{O}$, where LRE^{3+} is La, Ce, Pr, Nd, Sm, Eu and Gd; $[\text{HRE}(\text{H}_2\text{O})_7][\text{B}(\text{CN})_4]_3$ and $[\text{HRE}(\text{H}_2\text{O})_8][\text{B}(\text{CN})_4]_3 \cdot 3 \text{ H}_2\text{O}$ where HRE^{3+} is Tb, Dy, Ho, Er, Tm, Yb, Lu and Y. The division into isostructural groups is due to the ionic radii of the cations which decrease in the lanthanide series. This so called lanthanide contraction is also a reason for the trivalent yttrium being chemically and physically similar to the heavy rare earth cations. Furthermore, the coordination number nine is common among the light rare earth cations in tetracyanidoborates, whereas the coordination number 8 is prevalent for the heavy rare earth cations. This is also due to the decreasing ionic radii in the series. The heavier cations have smaller ionic radii. Therefore, the space for the coordination is sufficient only for eight ligands. This different construction of the coordination spheres between light and heavy rare earth cations leads to different structures depending on the energetic efficiency of the structural arrangement.

Along with the coordination number, the lanthanide contraction causes other typical phenomena for the rare earth compounds which are observable in their tetracyanidoborates, too. With decreasing ionic radii, the $\text{RE}^{3+}\text{-O}$ distances get shorter in the rare earth tetracyanidoborate hydrates. Moreover, the decrement in the ionic radii enlarges the forces between cation and coordination ligands. Thus, the wavenumber of the CN stretching mode originating from the coordinated cyanido groups increases across the rare earth series which is observable in the IR spectra of RETCBs. However, along with other phenomena caused by the lanthanide contraction, a decrease of the lattice parameters in proceeding from the lightest to the heaviest rare earth compound does not occur in the RETCBs.

The characterization measurements exhibit, besides the typical features of rare earth compounds, also characteristic properties for the tetracyanidoborate anion. Three of the nine

fundamental vibrations of $[\text{B}(\text{CN})_4]^-$ anion are observable in the IR spectra of rare earth tetracyanidoborate hydrates. Furthermore, the NMR spectra of rare earth tetracyanidoborates show characteristic chemical shifts, coupling constants and coupling patterns for the tetracyanidoborates. The NMR spectroscopic results confirm also that the rare earth tetracyanidoborates indeed are tetracyanidoborates and not their constitutional isomers, isotetracyanidoborates, which have chemical shifts expected at higher frequencies.

According to the thermal analysis, the thermal dehydration is not complete. From the total amount of water, about 78% can be thermally removed from the LRETCBs and about 86% from the HRETCBs. However, in comparison to the chemical dehydration method with thionyl chloride, the thermal dehydration is still more adequate at least for the heavy rare earth compounds, because of the presumable long reaction time for dehydration with SOCl_2 . Furthermore, it has also been observed that the SOCl_2 not only dehydrates but also alters lanthanum tetracyanidoborate. Therefore, the method is not very adequate for the LRETCBs. The dehydration temperature of the light rare earth tetracyanidoborates has been observed to be a little bit lower than the one of the heavy rare earth compounds. This is due to the RE-O distance which is shorter in the heavy rare earth compounds. Therefore, the interaction between the RE cation and the water molecule is greater than in the light rare earth compounds. Thus, the heavier the RE cation is, the greater the energy required to break the RE-O bond.

The impact of the dehydration has been studied on europium and terbium tetracyanidoborates with the aid of ultraviolet lamp excitation. Whereas the dehydration considerably increases the luminescence efficiency of the terbium compound, there is no remarkable difference of the luminescence efficiencies of the europium compound before and after dehydration. Therefore, the quenching effect from the high-energy vibrations of water molecules occurs obviously only in the terbium compound. The comparison with the known $\text{Y}_2\text{O}_3:\text{Eu}^{3+}$ indicates further that the terbium compound has proper luminescence efficiency, while the luminescence of the europium compound seems to be rather weak. However, the possible excitation wavelengths of the ultraviolet lamp were not optimal for europium tetracyanidoborate. Therefore, UV-Vis absorbance and luminescence measurements give more definite results about the optical properties of EuTCB.

The absorption spectra of samarium, europium, terbium and dysprosium tetracyanidoborates show characteristic absorption bands both for tetracyanidoborates and rare earth cations. The broader and stronger bands at shorter wavelengths originate from the absorption of the

tetracyanidoborate anion, from the 4f-5d transition of RE^{3+} or from the N- RE^{3+} charge-transfer transitions. The absorption bands arising from the optical f-f-transition from the ground state to the excited states appear between 300 and 500 nm and are remarkably weaker and sharper than the bands originating from the 4f-5d and N- RE^{3+} transitions or from the absorption of the tetracyanidoborate anion. The stronger absorptions are usually responsible for the excitation of the RE cations. This is also mostly the case in the examined rare earth tetracyanidoborates. The excitation spectra indicate that N- RE^{3+} charge-transfer transitions excite Sm^{3+} , Dy^{3+} and possibly Tb^{3+} in their tetracyanidoborates, while there is no doubt that the excitation of the Eu^{3+} arises from a 4f-4f transition. Nonetheless, the emission spectra of all four compounds show characteristic sharp bands for their rare earth cations. Therefore, the luminescence measurements indicate that the rare earth tetracyanidoborates exhibit rare earth cation specific luminescence properties.

The fluorescence quantum yield of the terbium compound in anhydrous acetonitrile is also determined by comparison of the fluorescence properties with quinine bisulphate as a quantum yield standard. The received quantum yield of the terbium compound in anhydrous acetonitrile is only 1.3%, which is pretty low for a rare earth phosphor. However, the high-energy vibrations of C-H in the acetonitrile certainly quench the luminescence weakening the quantum yield. Moreover, the comparison with the $\text{Y}_2\text{O}_3:\text{Eu}^{3+}$ phosphor expresses better efficiency than the quantum yield implies. Therefore, in order to receive more accurate results, the fluorescence quantum yield determination should be carried out of dehydrated, solvent free RETCB powders.

Due to the lack of solubility of the anhydrous rare earth compounds, it was not possible to grow anhydrous crystals for the single-crystal X-ray diffraction. Under the circumstances the crystal structures were determined from the thermal dehydrated europium and terbium powders with the aid of powder diffraction. However, the dehydration of these compounds causes crystalline-amorphous transformation. Thus, the determination of the anhydrous crystal structure was not possible. Furthermore, to get more accurate information of the luminescence properties of the rare earth compounds, the effect of concentration quenching should be determined properly. Moreover, more specific luminescence lifetime measurements should be performed.

5 Outlook

RETCB based luminescent materials could be developed further to improve their luminescence properties. Traditional phosphors are solid organic materials consisting of a host lattice usually intentionally doped with impurities which normally cause emission.⁴⁹ The absorption and emission properties of rare earth metal cations are due to the optical transitions within the f-manifold. Therefore, isostructural rare earth tetracyanidoborates, like lanthanum or yttrium tetracyanidoborates without f-electrons, could be used as a host lattice for luminescent europium or terbium tetracyanidoborates. This is also a simple method for the elimination of strong concentration quenching, which might be expected if the distance for example between two adjacent Tb^{3+} or Eu^{3+} ions is 5 Å or shorter.⁸⁶

The synthesis of so-called doped phosphors would occur just like the synthesis of pure rare earth tetracyanidoborates, except that the $\text{H}[\text{B}(\text{CN})_4]$ would be made to react with two different rare earth oxides, so that the amount of the host lattice starting material (La_2O_3 or Y_2O_3) should be about 90% and the amount of the rare earth impurity starting material (Eu_2O_3 or Tb_4O_7) about 10%. Because of the physical similarity, the light rare earth cations (La^{3+} and Eu^{3+}) and the heavy rare earth cations (Y^{3+} and Tb^{3+}) can replace each other in the tetracyanidoborates flawlessly and compounds like $[\text{La}_{0.9}\text{Eu}_{0.1}(\text{H}_2\text{O})_5][\text{B}(\text{CN})_4]_3$ and $[\text{Y}_{0.9}\text{Tb}_{0.1}(\text{H}_2\text{O})_7][\text{B}(\text{CN})_4]_3$ could be easily received. Furthermore, for the determination of the ideal $\text{La}^{3+}/\text{Eu}^{3+}$ and $\text{Y}^{3+}/\text{Tb}^{3+}$ ratio, further synthesis with different starting material ratios should be performed and the quantum yield measurements of these compounds should be executed.

Given that the host material cannot transfer the energy to the luminescent impurity, the luminescence efficiency is not strengthened by the host and stays weak. This is also the case in EuTCB which excitation spectrum reveals that the excitation of Eu^{3+} ion occurs due to the intraconfigurational 4f-4f transitions of the cation. Therefore, this luminescence could be sensitized by using a suitable sample (sensitizer) which has a strong emission in the UV/blue region. It should also be able to transfer the energy to Eu^{3+} ion without quenching the luminescence or reducing the Eu^{3+} due to the charge transfer state $\text{RE}^{4+}-\text{RE}^{2+}$.¹⁰³ From the rare earth cations, the Gd^{3+} could be a suitable candidate as sensitizer in EuTCB, because it emits quite conveniently and is not able to reduce the Eu^{3+} .⁸⁵ Thus, by codoping the LaTCB

both with EuTCB and GdTCB or using GdTCB directly as host material, the sensitization could be induced and the luminescence of Eu^{3+} ion increased. The codoped rare earth tetracyanidoborates could be prepared by reaction of HTCB with one host lattice starting material (La_2O_3), with one suitable rare earth impurity starting material (Eu_2O_3) and with a suitable rare earth sensitizer starting material (Gd_2O_3) as described in the previous paragraph.

Due to the emission properties of the rare earth ions, EuTCB could be applied in red phosphors and TbTCB in green phosphors. Furthermore, different approaches are developed for generation of desired white light emission.¹⁰⁴ By combining different phosphors, like red, green and blue or codoping one host material with two or more different ions, a white light emission is possible to generate. Because of the fact that the photoluminescence intensity depends on the excitation wavelengths and the concentration of the rare earth compounds, the development of rare earth containing white phosphors requires further investigation.

Besides the possible strong concentration quenching, the quenching effect from the high-energy vibrations of the OH groups is a remarkable reason for the decrease of the luminescence quantum yields of the rare earth tetracyanidoborate hydrates. However, this kind of quenching can be easily eliminated by using deuterium oxide (D_2O) instead of ordinary water in the preparation of the start material, tetracyanidoborate acid and otherwise using only anhydrous starting materials. The whole synthesis procedure should be kept free from the ordinary water. Consequently, the dehydration of the rare earth tetracyanidoborate deuterates would not be necessary for the improvement of the luminescence quantum yield. Nonetheless, the preparation of tetracyanidoborate acid in deuterium oxide is significantly more expensive than the preparation in ordinary water. Therefore, the rare earth tetracyanidoborates are until now prepared as hydrates and dehydrated afterwards.

6 Analytical Methods

Structure analysis and refinement

Transparent crystals of the rare earth tetracyanidoborate hydrates for X-ray diffraction investigations were grown by slowly evaporation of the solvent from saturated solutions of the salts in aqueous solutions at room temperature under atmospheric pressure. For the single crystal X-ray diffraction suitable crystals were chosen with the aid of a microscope. The crystals were coated with Canada balsam and fixed on top of a thin glass capillary. Data were collected at -100°C with a Bruker-Nonius Apex X8 diffractometer equipped with a CCD detector. Measurements were done using monochromatic Mo-K α radiation ($\lambda = 0.71073 \text{ \AA}$). Preliminary data of the unit cells were obtained from the reflex positions of 12 frames, measured in three different directions of the reciprocal space. After completion of the measurements, the intensities were corrected for Lorentz, polarization and absorption effects using the Bruker-Nonius software.¹⁰⁵ The structures were solved and refined with the aid of the SHELX-97 program package.¹⁰⁶ The non-hydrogen atoms were refined anisotropically. The H atoms were added on idealized positions and refined using riding models.

The bulk form samples for the powder X-ray diffraction were solvent free powders. Other samples were fine powdered crystals from aqueous solutions. The crystals were powdered with the aid of a mortar. Each sample was placed between pieces of Al-layered thin plastic foil. Data were collected with a STOE Transmission Diffractometer System STADI P incl. STOE Bragg-Brentano mode. Measurements were done using monochromatic Cu-K α radiation ($\lambda = 1.54056 \text{ \AA}$) and evaluated with the WinX^{POW} software. The powder diffraction data was compared to the line distribution on the film with the pattern calculated on the basis of single crystal data.

Vibrational spectroscopy

The IR spectra of $[\text{LRE}(\text{H}_2\text{O})_5][\text{B}(\text{CN})_4]_3 \cdot 0.5 \text{ H}_2\text{O}$ ($\text{LRE}^{3+} = \text{La-Gd}$, except Pm), $[\text{HRE}(\text{H}_2\text{O})_7][\text{B}(\text{CN})_4]_3$ ($\text{HRE}^{3+} = \text{Tb-Lu}$, Y) and dehydrated lanthanum und erbium tetracyanidoborates in the range of $4000\text{--}500 \text{ cm}^{-1}$ were recorded with Nicolet 380 FT-IR spectrometer with a Smart Endurance ATR device. Raman spectrum of $[\text{Eu}(\text{H}_2\text{O})_5][\text{B}(\text{CN})_4]_3 \cdot 0.5 \text{ H}_2\text{O}$ and $[\text{Er}(\text{H}_2\text{O})_7][\text{B}(\text{CN})_4]_3$ was obtained in room temperature with a Bruker Vertex 70 Raman spectrometer (Bruker, Karlsruhe, Germany) by using the

1064 nm exciting line of a Nd/YAG Laser. The crystalline sample was measured in an open melting point capillary.

Nuclear magnetic resonance spectroscopy

The nuclear magnetic spectroscopic studies were conducted of $[\text{Eu}(\text{H}_2\text{O})_5][\text{B}(\text{CN})_4]_3 \cdot 0.5 \text{H}_2\text{O}$ and $[\text{Er}(\text{H}_2\text{O})_7][\text{B}(\text{CN})_4]_3$ with a Bruker Avance (300 MHz) spectrometer. Chemical shifts of ^{13}C NMR are expressed downfield from TMS as an external standard ($\delta = 0.00$ ppm) in CD_3CN . ^{11}B NMR shifts are referenced against $\text{BF}_3 \cdot \text{OEt}_2$ ($\delta = 0.00$ ppm) in CD_3CN .

Thermal analysis

The differential scanning calorimetry measurements of $[\text{Eu}(\text{H}_2\text{O})_5][\text{B}(\text{CN})_4]_3 \cdot 0.5 \text{H}_2\text{O}$ and $[\text{Er}(\text{H}_2\text{O})_7][\text{B}(\text{CN})_4]_3$ were performed with a DSC 823e Mettler Toledo apparatus. Thermogravimetry (TG) measurements of $[\text{Eu}(\text{H}_2\text{O})_5][\text{B}(\text{CN})_4]_3 \cdot 0.5 \text{H}_2\text{O}$ and $[\text{Er}(\text{H}_2\text{O})_7][\text{B}(\text{CN})_4]_3$ were carried out with a Setaram Labsys TG instrument. The DSC and TG measurements were conducted with heating rates of 5 K/min and 10 K/min.

Elemental analysis

The carbon, hydrogen and nitrogen percentages of $[\text{LRE}(\text{H}_2\text{O})_5][\text{B}(\text{CN})_4]_3 \cdot 0.5 \text{H}_2\text{O}$ ($\text{LRE}^{3+} = \text{La-Gd}$, except Pm) and $[\text{HRE}(\text{H}_2\text{O})_7][\text{B}(\text{CN})_4]_3$ ($\text{HRE}^{3+} = \text{Tb-Lu, Y}$) were analyzed by a flash EA 112 series elemental analyzer.

Solubilities

The solubilities of $[\text{LRE}(\text{H}_2\text{O})_5][\text{B}(\text{CN})_4]_3 \cdot 0.5 \text{H}_2\text{O}$ ($\text{LRE}^{3+} = \text{La-Gd}$, except Pm) and $[\text{HRE}(\text{H}_2\text{O})_7][\text{B}(\text{CN})_4]_3$ ($\text{HRE}^{3+} = \text{Tb-Lu, Y}$) in water, acetonitrile and tetrahydrofuran were determined quantitatively at 22°C under atmospheric pressure. Saturated solutions of rare earth metal compounds were prepared in small glass vials. Exactly 1.0 ml of the solvent was placed into empty weighed vials. After that, powdery title compounds were added to their vials till a deposit was noticed. The solvent was evaporated until the material was dry and the vials were weight again. The masses were measured afterwards again and the solubilities calculated. Qualitative solubilities in aceton, pyridine, dichloromethane and chloroform were also determined.

Measurements of the optical properties

The luminescence measurements of acetonitrile solutions of $[\text{Eu}(\text{H}_2\text{O})_n][\text{B}(\text{CN})_4]_3$, $[\text{Sm}(\text{H}_2\text{O})_n][\text{B}(\text{CN})_4]_3$ ($n \sim 1-1.5$), $[\text{Tb}(\text{H}_2\text{O})_n][\text{B}(\text{CN})_4]_3$ and $[\text{Dy}(\text{H}_2\text{O})_n][\text{B}(\text{CN})_4]_3$ ($n \sim 0-1$) in 10 mm cuvettes (Quartz SUPRASIL, Hellma) were carried out with a spectrophotometer (Cary Eclipse, Agilent Technologies). The luminescence was also measured of thermally dried $[\text{Eu}(\text{H}_2\text{O})_n][\text{B}(\text{CN})_4]_3$ and $[\text{Tb}(\text{H}_2\text{O})_n][\text{B}(\text{CN})_4]_3$ powders in a 1 mm cuvette (Quartz SUPRASIL, Hellma) with a spectrofluorometer (FluoroMax-4, Horiba Scientific) and the luminescence lifetime was determined with aid of a streak camera system (Streakscope C10627, Hamatsu). For determination of the fluorescence quantum yield the absorption and fluorescence spectra of $[\text{Tb}(\text{H}_2\text{O})_7][\text{B}(\text{CN})_4]_3$ in acetonitrile solution and a fluorescence standard, quinine bisulphate in 0.05 M aqueous H_2SO_4 were also measured with an UV-Vis spectrometer (Specord 50, Analytic Jena) and a spectrofluorometer (FluoroMax-4, Horiba Scientific).

7 Bibliography

- [1] G. Wittig, P. Raff, *Z. Naturforsch.* **1951**, 6 b, 225–226.
- [2] E. Bessler, J. Goubeau, *Z. anorg. allg. Chem.* **1967**, 352, 67–76.
- [3] H. Landesman, R.E. Williams, *J. Am. Chem. Soc.* **1961**, 83, 2663–2666.
- [4] E. Bessler, *Z. Anorg. Allg. Chem.*, **1977**, 430, 38–42.
- [5] E. Bernhardt, G. Henkel, H. Willner, *Z. Anorg. Allg. Chem.*, **2000**, 626, 560–568.
- [6] B. Györi, J. Emri, I. Fehér, *J. Organomet. Chem.*, **1983**, 255, 17–28.
- [7] E. Bernhardt, M. Finze, H. Willner, *Z. Anorg. Allg. Chem.*, **2003**, 629, 1229–1234.
- [8] C. Nitschke, M. Köckerling, *Inorg. Chem.*, **2011**, 50, 4313–4321.
- [9] T. Küppers, E. Bernhardt, H. Willner, H. Rohm, M. Köckerling, *Inorg. Chem.*, **2005**, 44, 1015–1022.
- [10] M. Berkei, E. Bernhardt, M. Schürmann, M. Mehring, H. Willner, *Z. Anorg. Allg. Chem.*, **2002**, 628, 1734–1740.
- [11] M. Neukirch, Dissertation, University of Tübingen, **2007**.
- [12] T. Küppers, E. Bernhardt, C.W. Lehmann, H. Willner, *Z. Anorg. Allg. Chem.*, **2007**, 633, 1666–1672.
- [13] M. Neukirch, S. Tragl, H.-J. Meyer, T. Küppers, H. Willner, *Z. Anorg. Allg. Chem.*, **2006**, 632, 939–944.
- [14] C. Nitschke, M. Köckerling, *Z. Anorg. Allg. Chem.*, **2009**, 635, 503–507.
- [15] C. Nitschke, M. Köckerling, E. Bernhardt, T. Küppers, H. Willner, *Dalton Trans.*, **2014**, 43, 7128–7138.
- [16] T. Küppers, Dissertation, University of Wuppertal, **2007**.
- [17] A. Flemming, M. Hoffmann, M. Köckerling, *Z. Anorg. Allg. Chem.*, **2010**, 636, 562–568.
- [18] P. Izák, M. Köckerling, U. Kragl, *Green Chem.*, **2006**, 8, 947–948.; P. Izák, M. Köckerling, U. Kragl, *Desalination*, **2006**, 199, 96–98.
- [19] T. M. Koller, M. H. Rausch, J. Ramos, P. S. Schulz, P. Wasserscheid, I. G. Economou, A. P. Fröba, *J. Phys. Chem.*, **2013**, B117, 8512–8523.
- [20] J. Scheers, Dissertation, Chalmers University of Technology, **2011**.
- [21] D. Kuang, P. Wang, S. Ito, S. M. Zakeeruddin, M. Grätzel, *J. Am. Chem. Soc.*, **2006**, 128, 7732–7733.
- [22] Y. Bai, Y. Cao, J. Zhang, M. Wang, R. Li, P. Wang, S. M. Zakeeruddin, M. Grätzel, *Nat. Mater.*, **2008**, 7, 626–629.

- [23] P. Izák, K. Friess, V. Hynek, W. Ruth, Z. Fei, J.P. Dyson, U. Kragl, *Desalination*, **2009**, 241, 182–187.
- [24] P. Izák, W. Ruth, Z. Fei, J.P. Dyson, U. Kragl, *Chem. Eng. J.*, **2008**, 139, 318–321.
- [25] S. B. Castor, J. B. Hedrick, *Industrial Minerals and Rocks*, **2006**, 769–792.
- [26] N. Sui, K. Huang, C. Zang, N. Wang, F. Wang, H. Liu, *Ind. Eng. Chem. Res.*, **2013**, 52, 5997–6008.
- [27] A.T. Savichev, Y.N. Vodyanitskii, *Eurasian Soil Sci.*, **2011**, 44, 386–393.
- [28] S. J. Goldstein, S.B. Jacobsen, *Earth. Planet. Sci. Lett.* **1988**, 89, 35–47.
- [29] H. Elderfield, M.J. Greaves, *Nature*, **1982**, 296, 214–219.
- [30] Y. Kato, K. Fujinaga, K. Nakamura, Y. Takaya, K. Kitamura, J. Ohta, R. Toda, T. Nakashima, H. Iwamori, *Nat. Geosci.*, **2011**, 4, 535–539.
- [31] K. F. Khan, S. A. Dar, S.A. Khan, *J. Rare Earth*, **2012**, 30, 507–513.
- [32] R. L. Cullers, L. G. Medaris, *Geochim. Cosmochim. Acta*, **1973**, 37, 1499–1512.
- [33] G. Adachi, N. Imaka, *Chem. Rev.* **1998**, 98, 1479–1514.
- [34] G.A. Bukatova, S. A. Kuznetsov, M. Gaune-Escard, *Russ. J. Electrochem.*, **2007**, 43, 929–935.
- [35] H. Mattausch, M. C. Schaloske, C. Hoch, C. Cheng, A. Simon, *Z. Anorg. Allg. Chem.*, **2008**, 634, 491–497.
- [36] J.H. Lee, R. H. Byrne, *Geochim. Cosmochim. Acta*, **1993**, 57, 295–302.
- [37] B. Yotnoi, A. Rujiwatra, M. L. P Reddy, D. Sarma, S. Natarajan, *Cryst. Growth. Des.* **2011**, 11, 1347–1356.
- [38] B. Kong et al., *J. Phys. Chem. Solids*, **2013**, 74, 1322–1328.
- [39] V. P. Vassiliev, A. Benaissa, A. F. Taldrik, *J. Alloys Compd.*, **2013**, 572, 118–123.
- [40] T. Moeller, D.F. Martin, L. C. Thompson, R. Ferrús, G. R. Feistel, W. J. Randall, *Chem. Rev.*, **1965**, 65, 1–50.
- [41] J. W. Jensen, *J. Chem. Educ.*, **1982**, 59, 634–636.
- [42] G. Aromí et al., *Chem. Eur. J.* **2013**, 19, 5881–5891.
- [43] P. D'Angelo et al., *Inorg. Chem.*, **2011**, 50, 4572–4579.
- [44] I. D. G. Hughes, *Nature*, **2007**, 446, 650–653.
- [45] R. Skomski, D.J. Sellmyer, *J. Rare Earth*, **2009**, 27, 675–679.
- [46] J. Tian et al., *Mater. Lett.*, **2013**, 105, 87–89.
- [47] H. Zhao et al., *Angew. Chem. Int. Ed.*, **2003**, 42, 1015–1018.
- [48] V.E. Campbell et al., *Inorg. Chem.*, **2013**, 52, 5194–5200.
- [49] C.R. Ronda, T. Jüstel, H. Nikol, *J. Alloys Compd.* **1998**, 2752–77, 669–676.

- [50] J.-C. G. Bünzli et al., *Coord. Chem. Rev.*, **2010**, 254, 2623–2633.
- [51] M. Latva et al., *J. Lumin.* **1997**, 75, 149–169.
- [52] E. Bernhardt, Habilitation thesis, University of Wuppertal, **2007**.
- [53] E. Bernhardt, M. Brekei, H. Willner, M. Schürmann, *Z. Anorg. Allg. Chem.* **2003**, 629, 677–685.
- [54] D. Williams, B. Pleune, J. Kouvetakis, M. D. Williams, R.A. Andersen, *J. Am. Chem. Soc.* **2000**, 122, 7735–7741.
- [55] E. Bernhardt, G. Henkel, H. Willner, G. Pawelke, H. Bürger, *J. Chem. Eur.*, **2001**, 7, 4696–4705.
- [56] E. Bernhardt, M. Finze, H. Willner, *Inorg. Chem.*, **2011**, 50, 10268–10273.
- [57] E. Bernhardt, D. J. Brauer, M. Finze, H. Willner, *Angew. Chem. Int. Ed.*, **2006**, 45, 6383–6386.
- [58] B.H. Hamilton, C.J. Ziegler, *Chem. Commun.*, **2002**, 842–843.
- [59] M. Schmidt, A. Kühner, H. Willner, E. Bernhardt, Merck Patent GmbH EP 1205480(A2), **2002**.
- [60] E. Bernhardt, V. Bernhardt-Pitchougina, H. Willner, N. Ignatiev, *Angew. Chem. Int. Ed.*, **2011**, 50, 12085–12088.
- [61] R.D. Shannon, *Acta Cryst.*, **1976**, A 32, 751–767.
- [62] R.A. Zehnder et al., *Inorg. Chem.*, **2011**, 50, 836–846.
- [63] A. Bernsdorf, Dissertation, University of Rostock, **2012**.
- [64] J.C. Taylor, P.W. Wilson, *Acta Cryst.*, **1974**, B30, 2803–2805.
- [65] A. Habenschuss, F.H. Spedding, *J. Chem. Phys.*, **1979**, 70, 2797–2806.
- [66] C. Heinrichs. Dissertation, University of Cologne, **2013**.
- [67] R.A. Zehnder et al. *Inorg. Chem.*, **2010**, 49, 4781–4790.
- [68] A. Habenschuss, F.H. Spedding, *J. Chem. Phys.*, **1979**, 70, 3758.
- [69] A. Habenschuss, F.H. Spedding, *J. Chem. Phys.*, **1980**, 73, 442–449.
- [70] S.Y. Venyaminov, F.G. Prendergast, *Anal. Biochem.* **1997**, 248, 234–245.
- [71] H.R. Zelsmann, *J. Mol. Struct.* **1995**, 350, 95–114.
- [72] J.H. Freeman, M. L. Smith, *J. Inorg. Nucl. Chem.*, **1958**, 7, 224–227.
- [73] F. A. Cotton, R. Francis, W.D. Horrocks, Jr. *J. Phys. Chem.*, **1960**, 64, 1534–1536.
- [74] J. Emri, B. Györi, *Polyhedron*, **1994**, 13, 2353–2357.
- [75] C. Kappenstein, J. Bouquant, R.P. Hugel, *Inorg. Chem.*, **1979**, 18, 2615–2617.
- [76] U. Welz-Biermann, N. Ignatjev, E. Bernhardt, M. Finze, H. Willner. Merck Patent GmbH, Darmstadt, WO 2004/ 072089, A1, **2004**.

- [77] K.N. Marsh, Ed., Recommended Reference Materials for the Realization of Physicochemical Properties, *Blackwell, Oxford*, **1987**.
- [78] R. H. Byrne, X. Liu, J. Schijf, *Geochim. Cosmochim. Ac.*, **1996**, 60, 3341–3346.
- [79] F. H. Firsching, J. Mohammadzadel, *J. Chem. Eng. Data*, **1986**, 31, 40–42.
- [80] T. Mioduski, C. Gumiński, D. Zeng, *J. Phys. Chem. Ref. Data*, **2008**, 37, 1778.
- [81] F. H. Spedding, S. Jaffe, *J. Am. Chem. Soc.*, **1954**, 76, 882.
- [82] M. Jayasimhadri et al., *J. Am. Ceram. Soc.*, **2010**, 93, 494–499.
- [83] M. A. Zaitoun et al., *Spectrochim. Acta, Part A: Mol. Biomol. Spectros.*, **2013**, 115, 810–814.
- [84] C. D. Tran, W. Zhang, *Anal. Chem.*, **1990**, 62, 835–840.
- [85] J.-C. G. Bünzli and S. V. Eliseeva, “Basics of Lanthanide Photophysics”, Lanthanide Luminescence: Photophysical, Analytical and Biological Aspects, *Springer Ser Fluoresc.*, **2010**, 1–45.
- [86] A. Nag, P.J. Schmidt, W. Schnick, *Chem. Mater.*, **2006**, 18, 5738–5745.
- [87] Z. Li and H. Meng, “Organic Light-Emitting Materials and Devices”, *CRC Press*, **2006**, 333.
- [88] J. Vuojola, T. Soukka, *Methods Appl. Fluoresc.*, **2014**, 2, 4.
- [89] S. Mal, Dissertation, Polish academy of sciences, **2012**.
- [90] R. Anwender, “Lanthanides: Chemistry and Use in Organic Synthesis”, Principles in Organolanthanide Chemistry, *Springer-Verlag Berlin Heidelberg*, **1999**, 6.
- [91] A. de Bettencourt-Dias, P.S. Barber, S. Bauer, *J. Am. Chem. Soc.*, **2012**, 134, 6987–6994.
- [92] H.B. Yuan et al., *J. Rare Earth*, **2009**, 27, 3093–11.
- [93] Ch. Srinivasa Rao, C.K. Jayasankar, *Opt. Commun.* **2013**, 286, 204–210.
- [94] E. De la Rosa et al. *Opt. Mater.* **2005**, 27, 1320–1325.
- [95] Y. Fan et al. *Physica B*, **2014**, 450, 99–105.
- [96] R. Praveena et al. *Spectrochim. Acta, Part A*, **2008**, 70, 577–586.
- [97] D.B. Bolstad, A.L. Diaz, *J. Chem.Educ.*, **2002**, 79, 1101–1104.
- [98] H. Yan et al. *Synth. Met.* **2011**, 161, 748–752.
- [99] F. Wang et al. *Solid State Commun.* **2005**, 133, 775–779.
- [100] S.R. Meech, D. Phillips, *J. Photochem.*, **1983**, 23, 193–217.
- [101] A. Penzkofer, *Chem. Phys.*, **2013**, 415, 173–178.
- [102] A. Babu et al., *Opt. Express*, **2011**, 19, 18361–841.
- [103] J-L. Yuan et al., *J. Phys. D: Appl. Phys.* **2008**, 41, 105406.
- [104] K. Suresh et al., *Int. J. Nanomater. Bios.* **2014**, 4, 41–45.

[105] *Bruker-Nonius Inc., Apex-2, V.1.6-8, Saint, V. 6.25a, SADABS-Software for the CCD Detector System*, Madison, WI, USA, **2003**.

[106] G.M. Sheldrick, *SHELX97-Programs for crystal structure analysis (Release 97-2)*; University of Göttingen: Göttingen, Germany, **1997**.

8 Appendix

8.1 Hydrogen bonds in tetracyanidoborates with rare earth metal cations

Table 8.1.1. Hydrogen bond lengths/ \AA and angles/ $^\circ$ in $[\text{La}(\text{H}_2\text{O})_8][\text{B}(\text{CN})_4]_3 \cdot 2 \text{H}_2\text{O}$ (**2**).

D - H...A	d(D - H)	d(H...A)	d(D...A)	\angle (DHA)
$\text{O}_6 - \text{H}_{6\text{A}} \dots \text{N}_7$	0.805	2.257	3.002	154.00
$\text{O}_8 - \text{H}_{8\text{B}} \dots \text{N}_9$	0.820	1.988	2.794	167.11

Table 8.1.2. Hydrogen bond lengths/ \AA and angles/ $^\circ$ in $[\text{Gd}(\text{H}_2\text{O})_8][\text{B}(\text{CN})_4]_3 \cdot 3 \text{H}_2\text{O}$ (**3**).

D - H...A	d(D - H)	d(H...A)	d(D...A)	\angle (DHA)
$\text{O}_2 - \text{H}_{2\text{A}} - \text{N}_6$	0.789	2.016	2.801	172.88
$\text{O}_2 - \text{H}_{2\text{B}} - \text{N}_3$	0.793	1.990	2.780	174.79
$\text{O}_4 - \text{H}_{4\text{A}} - \text{N}_{10}$	0.850	1.972	2.773	156.78

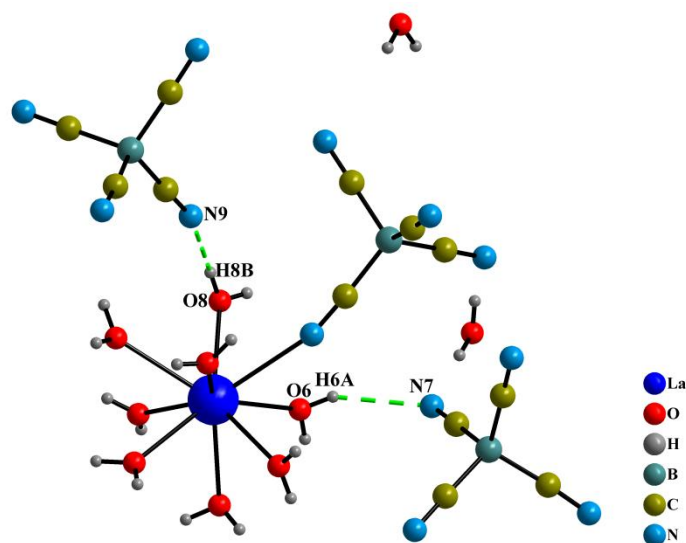


Figure 8.1.1. View of hydrogen bonds in $[\text{La}(\text{H}_2\text{O})_8][\text{B}(\text{CN})_4]_3 \cdot 2 \text{H}_2\text{O}$ (**2**).

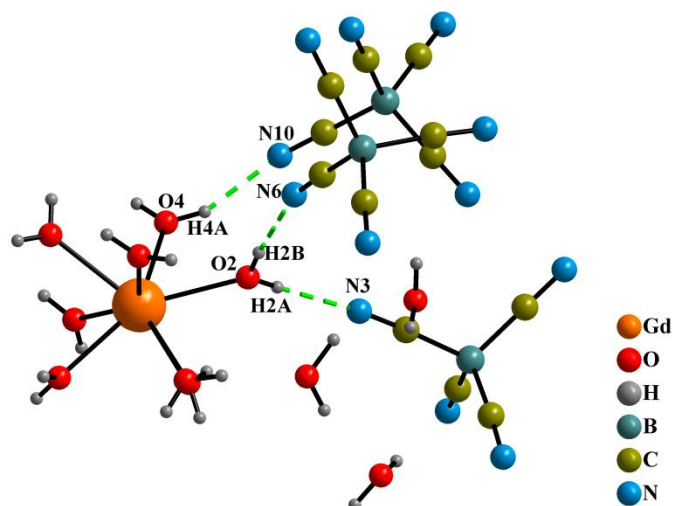


Figure 8.1.2. View of hydrogen bonds in $[\text{Gd}(\text{H}_2\text{O})_8][\text{B}(\text{CN})_4]_3 \cdot 3 \text{H}_2\text{O}$ (**3**).

Table 8.1.3. Hydrogen bond lengths/ \AA and angles/ $^\circ$ in $[\text{Er}(\text{H}_2\text{O})_7][\text{B}(\text{CN})_4]_3$ (**7**).

D - H...A	d(D - H)	d(H...A)	d(D...A)	\angle (DHA)
$\text{O}_{14} - \text{H}_{14} \dots \text{N}_3$	0.823	2.031	2.849	172.14
$\text{O}_{29} - \text{H}_{16} \dots \text{N}_{19}$	0.817	1.941	2.753	171.90
$\text{O}_{30} - \text{H}_4 \dots \text{N}_{13}$	0.782	2.023	2.784	164.32
$\text{O}_9 - \text{H}_1 \dots \text{N}_{22}$	0.709	2.092	2.790	168.48
$\text{O}_6 - \text{H}_{20} \dots \text{N}_{21}$	0.801	2.132	2.924	169.86

Table 8.1.4. Hydrogen bond lengths/ \AA and angles/ $^\circ$ in $[\text{Tb}(\text{H}_2\text{O})_8][\text{B}(\text{CN})_4]_3 \cdot 3\text{H}_2\text{O}$ (**4**).

D - H...A	d(D - H)	d(H...A)	d(D...A)	\angle (DHA)
$\text{O}_2 - \text{H}_{2\text{A}} - \text{N}_5$	0.825	1.989	2.804	170.81
$\text{O}_4 - \text{H}_{4\text{A}} - \text{N}_1$	0.741	2.170	2.904	170.99
$\text{O}_{10} - \text{H}_{10\text{A}} - \text{N}_{12}$	0.850	2.543	3.278	145.40
$\text{O}_{11} - \text{H}_{11\text{A}} - \text{N}_2$	0.850	2.447	3.287	169.91

Table 8.1.5. Hydrogen bond lengths/ \AA and angles/ $^\circ$ in $[\text{Dy}(\text{H}_2\text{O})_8][\text{B}(\text{CN})_4]_3 \cdot 3\text{H}_2\text{O}$ (**5**).

D - H...A	d(D - H)	d(H...A)	d(D...A)	\angle (DHA)
$\text{O}_1 - \text{H}_{1\text{A}} - \text{N}_1$	0.775	2.132	2.905	175.54
$\text{O}_2 - \text{H}_{2\text{B}} - \text{N}_5$	0.756	2.048	2.804	179.67

Table 8.1.6. Hydrogen bond lengths/Å and angles/° in $[\text{Y}(\text{H}_2\text{O})_8][\text{B}(\text{CN})_4]_3 \cdot 3\text{H}_2\text{O}$ (**6**).

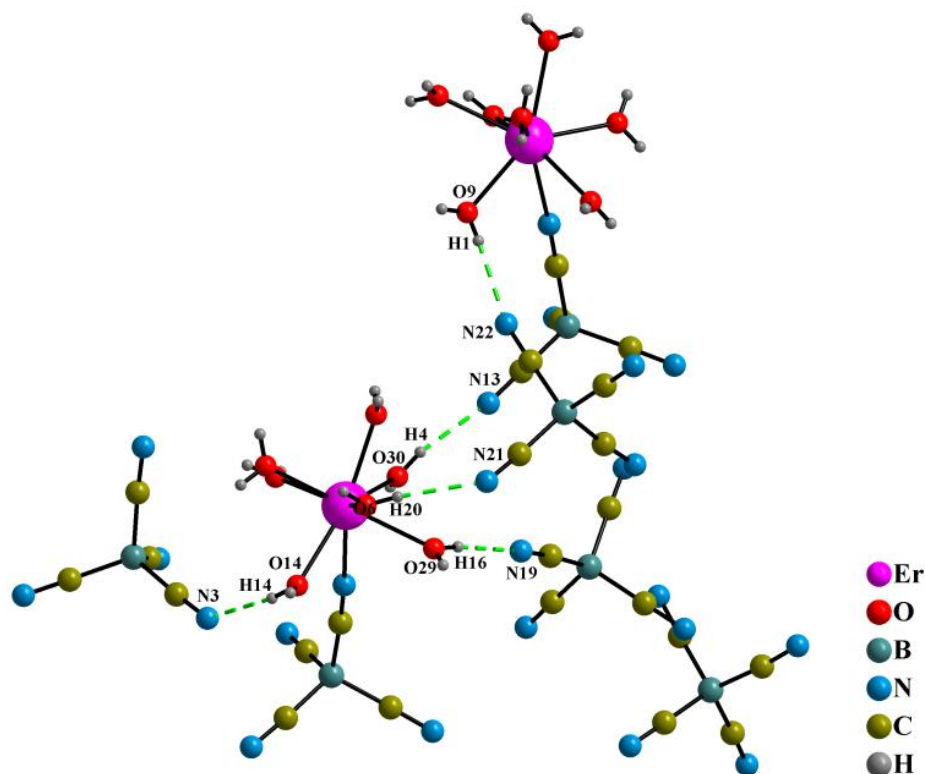
D - H...A	d(D - H)	d(H...A)	d(D...A)	< (DHA)
$\text{O}_2 - \text{H}_{2\text{A}} - \text{N}_5$	0.776	2.040	2.810	172.16
$\text{O}_4 - \text{H}_{4\text{A}} - \text{N}_1$	0.816	2.092	2.905	174.41
$\text{O}_{11} - \text{H}_{11\text{A}} - \text{N}_2$	0.852	2.500	3.338	168.31

Table 8.1.7. Hydrogen bond lengths/Å and angles/° in $[\text{Er}(\text{H}_2\text{O})_8][\text{B}(\text{CN})_4]_3 \cdot \text{CH}_3\text{COCH}_3$ (**8**).

D - H...A	d(D - H)	d(H...A)	d(D...A)	< (DHA)
$\text{O}_5 - \text{H}_{5\text{B}} - \text{N}_{10}$	0.850	2.004	2.810	157.98
$\text{O}_7 - \text{H}_{5\text{B}} - \text{N}_{10}$	0.840	2.280	2.826	122.93

Table 8.1.8. Hydrogen bond lengths/Å and angles/° in $[\text{Lu}(\text{CH}_3\text{CH}_2\text{OH})(\text{H}_2\text{O})_7][\text{B}(\text{CN})_4]_3 \cdot \text{CH}_3\text{CH}_2\text{OH}, 0.5 \text{H}_2\text{O}$ (**9**).

D - H...A	d(D - H)	d(H...A)	d(D...A)	< (DHA)
$\text{O}_4 - \text{H}_{4\text{B}} - \text{N}_{12}$	0.850	2.014	2.8138	156.42
$\text{O}_{17} - \text{H}_{17\text{A}} - \text{N}_6$	0.580	1.940	2.773	166.14

**Figure 8.1.3.** View of hydrogen bonds in $[\text{Er}(\text{H}_2\text{O})_7][\text{B}(\text{CN})_4]_3$ (**7**).

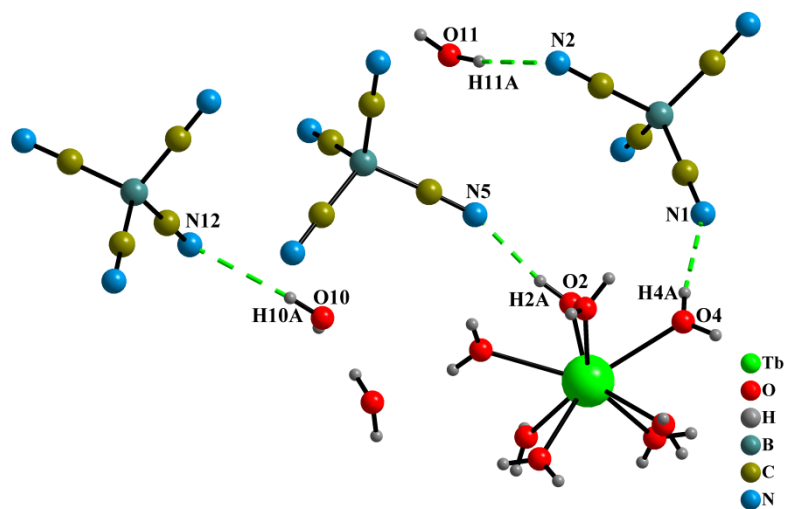


Figure 8.1.4. View of hydrogen bonds in $[\text{Tb}(\text{H}_2\text{O})_8][\text{B}(\text{CN})_4]_3 \cdot 3\text{H}_2\text{O}$ (4).

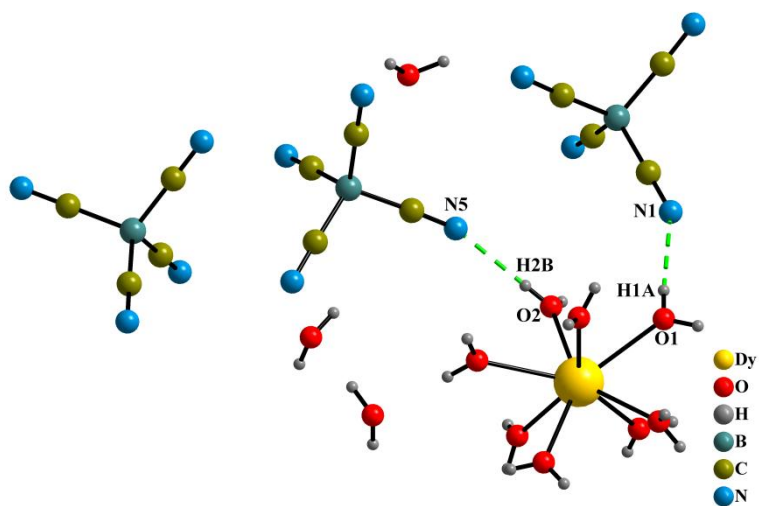


Figure 8.1.5. View of hydrogen bonds in $[\text{Dy}(\text{H}_2\text{O})_8][\text{B}(\text{CN})_4]_3 \cdot 3\text{H}_2\text{O}$ (5).

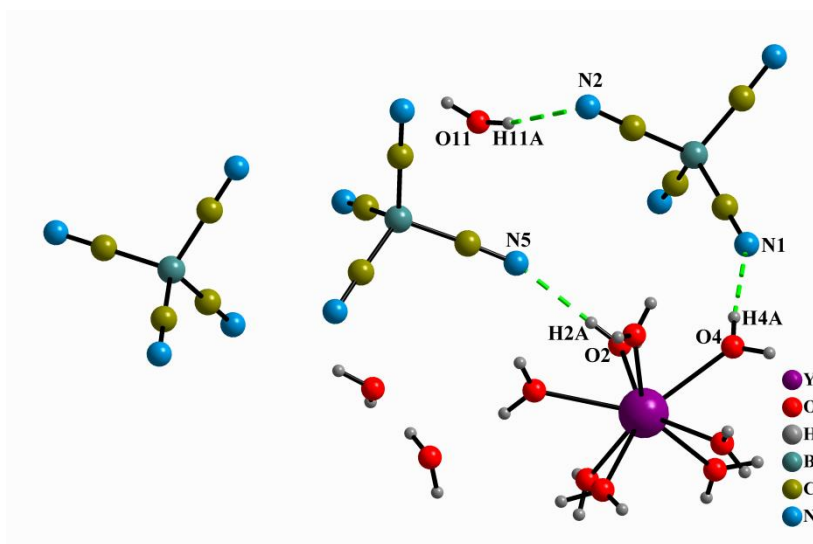


Figure 8.1.6. View of hydrogen bonds in $[\text{Y}(\text{H}_2\text{O})_8][\text{B}(\text{CN})_4]_3 \cdot 3\text{H}_2\text{O}$ (**6**).

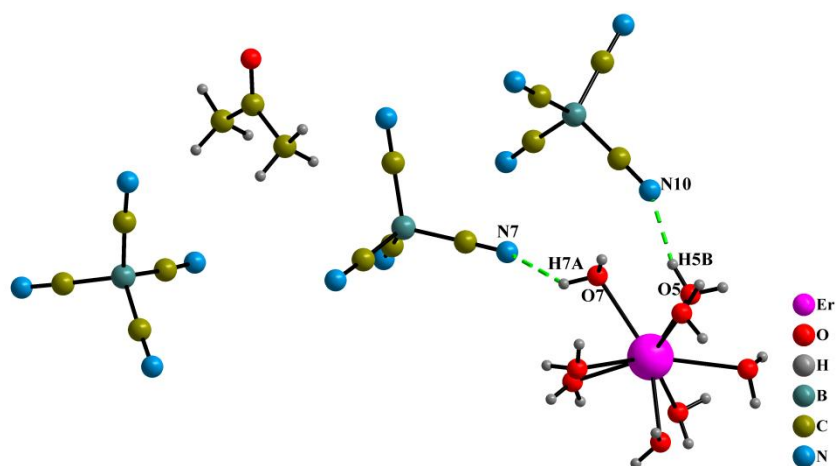


Figure 8.1.7. View of hydrogen bonds in $[\text{Er}(\text{H}_2\text{O})_8][\text{B}(\text{CN})_4]_3 \cdot \text{CH}_3\text{COCH}_3$ (**8**).

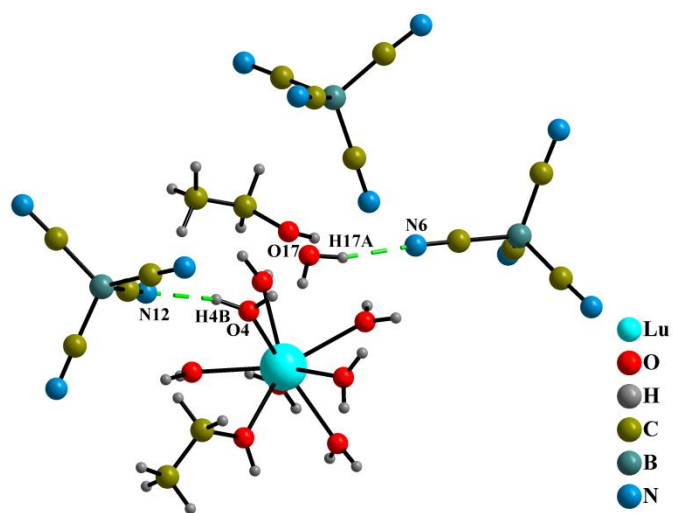


Figure 8.1.8. View of hydrogen bonds in $[\text{Lu}(\text{CH}_3\text{CH}_2\text{OH})(\text{H}_2\text{O})_7][\text{B}(\text{CN})_4]_3 \cdot \text{CH}_3\text{CH}_2\text{OH}, 0.5 \text{H}_2\text{O}$ (**9**).